# Stony Brook University

# Analysis of Principal Structural Orientation of Trabecular Bone Using Quantitative Ultrasound

A Dissertation Presented

by

**Liangjun Lin**

to

The Graduate School

in Partial Fulfillment of the

Requirements

for the Degree of

**Doctor of Philosophy**

in

**Biomedical Engineering**

Stony Brook University

**August 2014**

**Stony Brook University**

The Graduate School

**Liangjun Lin**

We, the dissertation committee for the above candidate for the

Doctor of Philosophy degree, hereby recommend

acceptance of this dissertation.

**Yi-Xian Qin, Ph.D. – Dissertation Advisor**
**Professor, Department of Biomedical Engineering**

**Wei Lin, Ph.D. - Chairperson of Defense**
**Associate Professor, Department of Biomedical Engineering**

**F. Avraham Dilmanian, Ph.D.**
**Professor, Department of Biomedical Engineering**

**Baosheng Li, Ph.D.**
**Research Professor, Mineral Physics Institute**

**Jonathan Kaufman, Ph.D.**
**Assistant Professor, Department of Orthopaedics**
**The Mount Sinai School of Medicine**

This dissertation is accepted by the Graduate School

Charles Taber

Dean of the Graduate School

Abstract of the Dissertation

**Analysis of Principal Structural Orientation of Trabecular Bone Using Quantitative Ultrasound**

by

**Liangjun Lin**

**Doctor of Philosophy**

in

**Biomedical Engineering**

Stony Brook University

**2014**

Quantitative ultrasound (QUS) has been accepted widely as a non-invasive, economic, non-radioactive and portable modality for assessing bone heath status. This technology utilizes the basic physical mechanism of interaction between ultrasound wave and bone structure to provide mechanical and structural information of bone. Instead of only evaluating the quantity of bone like other traditional techniques such as duel energy X-ray absorptiometry (DXA), QUS is also capable of measuring the quality of bone such as anisotropy, microarchitecture and microfracture. This advantage of QUS is beneficial for treating the patient suffering from osteoporosis or other bone health deterioration, long term bed-rest patient and astronaut experiences low gravity environment. To improve the current QUS technology for bone mechanical properties assessment and fracture risk prediction, the focuses of this study are: 1) to develop a novel QUS measurement protocol to predict the principal structural orientation (PSO) of spherical trabecular bone model; 2) to use finite element analysis (FEA) to evaluate the mechanical properties in the PSO predicted by QUS; 3) to apply this novel QUS measurement on human calcaneus as an improved evaluation for the mechanical properties. It is shown that the PSO predicted by QUS is highly close to the PSO predicted by micro computed tomography

(μCT), and the average angle difference is less than 5° using prediction of ultrasound velocity. The FEA simulation based on the μCT images showed the mechanical strength in the PSO predicted by QUS is significantly higher than the anatomical orientations and highly close to the value in longest vector of MIL tensor measured by μCT. By applying the same QUS measurement of PSO on bovine cubic bone samples and human calcaneus, the correlations between the QUS parameters and the mechanical and structural properties of trabecular bone were significantly improved ($p<0.05$), suggesting that such QUS measurement can be applied to human calcaneus evaluation and improves the reliability and accuracy for bone strength measurement and fracture risk assessment.

## Table of Contents

## List of Figures

## List of Tables

**Acknowledgments**

My thanks first go to my advisor Dr. Yi-Xian Qin, without whose help and guidance this work could not have been possible. His academic support and inspiration is much appreciated. Dr. Qin introduced me to this field of biomedical ultrasound imaging and guided me through all the adventures and challenges. He saw the potential in me and gave me confidence, set a strict and high academic standard for me because he believed that I have the ability to meet it. Dr. Qin gave me his caring and advice on matters not only in research, but also in life. I have often considered him as a father figure. I owe my achievement as a Ph.D. to him gratefully.

My gratitude also goes to my dissertation committee members: Dr. Wei Lin, Dr. Baosheng Li, Dr. F. Avraham Dilmanian and Dr. Jonathan Kaufman. Their valuable comments and suggestions significantly improved the quality of this disseatation. Special thanks go to Dr. Lin, who has been so nice to me since I became a student in this lab. He spent so much of his time to discuss my dissertation with me, gave me warm-hearted help on Matlab, LabView and all other technical skills.

Special thanks to Dr. Jiqi Cheng, Dr. Frederick Serra-Hsu and Dr. Jesse Muir for spending numerous hours discussing experiment and data with me and sharing your broad knowledge and experience in medical ultrasound research. I enjoyed all the inspiring discussion with them and learned extraordinary amount from them. Their enthusiasm and ability to ask the right questions to me or give perfect answer to my questions have motivated me greatly. I'm proud to be working with you side by side as colleagues; it is my honor and pleasure.

Certainly, thank you to all the lab mates and friends in the Department of Biomedical engineering. Their help for preparing this dissertation and the enjoyable working environment they created made this academic experience joyful and memorable. The focus of my research does not overlap with theirs vastly, but the biology and physiology I have learned from them have significantly improved the quality of my research. And that is exactly the beauty and core inter-disciplinary spirit of this Department of Biomedical Engineering, of which I am proud to be a member.

I would also like to thank Mr. Chris Lin, Mr. Ram Ghosh and Miss Vihitaben Patel for their generous assistance in conducting the ultrasound measurement. They spent so many hours with me to perform the ultrasound measurement on bone samples. The work we did together was tedious, but they brought fun into it, and I enjoyed working with them so much. Same gratitude goes to Miss Yingying Zhang from Beihang University. She was so generous to spend so many hours helping for the μCT scanning.

Last but not least, thanks to my family for giving me the support, love and caring. They have kept me motivated and confident from the beginning of these six years. There is nothing compared to family, especially for a student spending years for his doctoral degree. I have turned to my family to share all my ups and downs, and they have always been there when I needed them. I met my beautiful wife, Ping Lee, in Stony Brook. For my years pursuing the doctoral degree, she has been my lover, best friend and family. She deserves the credit, because she has been the closest witness for my journey. I consider myself the luckiest person in the world to be husband and wife with her.

# 1 Introduction

## 1.1 Osteoporosis

Osteoporosis is a condition of generalized skeletal fragility in which even loading such as routine daily activity can cause fracture due to the insufficient strength of bone (Marcus et al., 2009). This progressive, systematic metabolic disease is usually characterized by a decrease in bone density and strength that increases that chance of fracture. Osteoporosis is a major public health threat for United States of America that 10 million Americans, in which eight million are women and two million are men, are estimated to already have the disease. It is also estimated that another 30 million of Americans are having low bone mass, which makes them highly susceptible for osteoporosis. Osteoporosis is also responsible for more than 1.5 million fractures annually. It is predicted that about one in every two women and one in four men of age over 50 will have an osteoporosis-related fracture in her/his remaining life time. The financial burden came along with these fractures is reported to be 18 billion U.S. dollars annually and keeps rising (Foundation, 2010).

As a living, vital and dynamic connective tissue, the structure and composition of bone reflect a balance between its main functions: (1) sustaining loads from external actions (gravity) or from muscular insertion (movement); (2) protecting the vital organs; (3) maintaining the mineral and lipids homeostasis; (4) and producing blood cells. The main components of bone are cortical (or compact) and trabecular (or cancellous) bones, between which the distinction is mainly porosity. The porosity of cortical bone ranges only 5-20%, while the porosity of trabecular bone ranges from 40% to 95%. Cortical bone composes the external envelope of all bones: long bones such as femur or tibia, short bones such as vertebra or calcaneus and flat bones such as the skull. Cortical bone presents a dense structure of low porosity that seems compact at the macroscopic level. Cortical bone consists mainly of secondary osteons and circumferential lamellae that ring the outer surface of the diaphysis and a type of lamellar bone known as interstitial bone. Trabecular bone is usually found in the inner parts of bones. It looks like a porous sponge with a 3-dimensional network of rod- and plate-shape trabeculae surrounding an interconnected pore space filled with bone marrow (Martini and Ober, 2006, Marcus et al., 2009, Laugier and Haļat, 2011, Njeh et al., 1999, Martin et al., 1998).

The material properties of trabecular bone are influenced by many factors. The most influential determinants are considered apparent density and the microstructural arrangement of the trabecular network. For example, a 25% decrease in trabecular density, approximately equivalent to 15 years of age-related bone loss, can cause a 44% decrease in stiffness and strength of trabecular bone (Marcus et al., 2009). At the same time, it is also shown that for the same decrease in bone mass, loss of trabecular elements can cause 2 to 5 times of loss of bone strength more than decrease of trabecular thickness (Silva and Gibson, 1997). Other clinical studies also demonstrated the importance of trabecular bone microarchitecture that re-oriented trabecular network after adjusting to fractures could lead to weakening withstanding ability to unusual sideway loading conditions (Aaron et al., 2000, Link et al., 2000, Legrand et al., 2000, Ciarelli et al., 2000).

Table 1 - T-score values according to four groups of subjects. BMD is the Bone Mineral Density assessed by dual X-ray absorptiometry.

| | |
|---|---|
| Normal | BMD T-score $\geq$ -1.0 |
| Low bone mass or osteopenia | -1.0 $\geq$ BMD T-score > -2.5 |
| Osteoporosis | -2.5 $\geq$ BMD T-score |
| Established osteoporosis | -2.5 $\geq$ BMD T-score and at least one osteoporotic fracture |

There is still no found cure for osteoporosis (Foundation, 2010), which makes early diagnosis of osteoporosis extremely important. Currently, the most adopted diagnosis for osteoporosis in clinical practice heavily relies on bone mineral density (BMD) measured by dual energy X-ray absorptiometry (DXA). This diagnostic method is based on the T-score concept that the measured BMD value of an individual subject is compared to the mean value of a healthy young reference population, then the difference is normalized by the standard deviation of the reference population distribution as a T-score (Units and Bethesda, 2009). This T-score falls into one of the four categories defined by World Health Organization (WHO) as diagnosis for BMD (Kanis et al., 2005) (Table 1).

## 1.2 Quantitative ultrasound

Despite of its widely acceptance, the current DXA-based BMD measurement only focus on the quantification of bone mass, failing to take the other factors of bone quality into consideration for osteoporosis diagnosis. For example, BMD measurement is insensitive to measuring orientation, unable to provide information regarding to the spatial network architecture of trabecular structure. As National Institute of Health (NIH) defined that, "Bone quality refers to architecture, turnover, damage accumulation (e.g., microfractures) and mineralization" (2000). Complementary diagnostic methods to asses fracture risk are in urgent need. The rise of quantitative ultrasound (QUS) suggested an economic, fast, non-radioactive, portable and promising alternative for the task.

Compared to other imaging methods, ultrasound is non-invasive, radiation free, low cost, repeatable, safe, easy to operate and can provide immediate results. The currently used MRI and bone scintigraphy diagnostic methods are non-specific and frequently overlook the early symptoms of stress fracture, and the excellent results in the ultrasonography studies in the recent years have shown the high potential that ultrasound imaging method is capable of overcoming these drawbacks. QUS, utilizing the fundamental theory of wave propagation, has been more and more used in diagnosing bone health and characterizing bulk material and mechanical properties of bone (Njeh et al., 1997, Kilappa et al., 2010, Zheng et al., 2009, Zheng et al., 2007, Njeh and Langton, 1997, Nicholson, 2008, Lin et al., 2009, Xia et al., 2007, Xia et al., 2005, Gluer, 1997). As ultrasonic wave propagates through different mediums, both the velocity and the amplitude of the wave are modified. Properties of different mediums can thus be characterized based on the way ultrasonic wave is modified. The existing commercial QUS devices usually use the measurement of velocity and attenuation recorded by the device for such characterizing. And based on attenuation, another ultrasound parameter broadband ultrasound attenuation (BUA), the linear slope of the frequency-dependent spectrum of the ultrasound attenuation, is often used as indicator of bone health (Njeh et al., 1999).

The velocity of ultrasonic wave propagating through a certain medium is closely associated with the material properties of the medium. For example, an ultrasonic wave

propagating through a straight, uniform, solid bar with small cross-sectional dimensions compared to the wavelength, the ultrasound velocity UV is defined as following equation:

$$UV = \sqrt{\frac{E}{\rho}} \tag{6.1}$$

where $\rho$ is the density and $E$ is the Young's modulus of the medium (Kolsky, 1963). When the wavelength is small compared to the dimensions of the cross-section of the medium, the equation to calculate UV is given as:

$$UV = \sqrt{\frac{E(1-\upsilon)}{\rho(1+\upsilon)(1-2\upsilon)}} \tag{6.2}$$

where υ is the Poisson ratio of the medium.

As ultrasound wave propagates through the medium, some of its energy is inevitably lost due to the reflection, absorption and scattering, and this phenomenon is known as attenuation. Ultrasound attenuation (ATT) is usually reported in decibels (dB),measured using the substitution method developed by Langton et al. (Langton et al., 1984):

$$ATT = 20\log_{10}\left(\frac{A_1}{A_2}\right) \tag{6.3}$$

where $A_1$ is the amplitude of the ultrasound wave transmitted through the sample and $A_2$ is the amplitude of the reference ultrasound wave transmitted through the water. Or:

$$ATT = 10\log_{10}\left(\frac{I_1}{I_2}\right) \tag{6.4}$$

where $I_1$ is the intensity of the ultrasound wave transmitted through the sample and $I_2$ is the intensity of the reference ultrasound wave transmitted through the water.

By using Fourier transformation, the attenuation as a function of the ultrasound frequency f can be mathematically derived in a frequency-dependent spectrum. The attenuation curve over

a certain range of frequency is quasi-linear, and the attenuation is approximately linearly proportional to frequency:

$$ATT(f) = \alpha f \tag{6.5}$$

where $\alpha$ is the slope of the attenuation as a function of frequency in dB/MHz, known as broadband ultrasound attenuation (BUA). In some applications, BUA is also normalized to sample thickness ans reported in db/MHz/cm.

## 1.3 QUS measurement for trabecular bone architecture

Since its introduction to bone health assessment almost 30 years ago (Langton et al., 1984), QUS has been considered to be able to measure not only bone quantity, but also bone quality (Cortet et al., 2004, Nicholson et al., 2001, Grimm and Williams, 1997, Laugier et al., 1997, Gluer, 1997). Despite its technical immaturity and lack of standardization between different technical approaches, QUS has shown its promising ability in early screening for osteoporosis, and National Institute of Arthritis and Musculoskeletal and Skin Diseases (NIAMS) has justified QUS as an imaging tool for evaluating and assessing bone quality (Health, 2007).

Not only QUS has the ability to characterize the bulk material properties of bone, the propagation of ultrasound wave is also sensitive to the internal microstructure. Theoretically, Haïat *et al.* used finite-difference time-domain simulation to show that degree of anisotropy (DA) affects the time separation between the fast and slow ultrasound waves in trabecular model (Haïat et al., 2008). The same observation was found by Hosokawa et al. in a stratified trabecular bone model as well (Hosokawa, 2009a). This difference in separation time is in agreement with the finding that fast waves are more closely related to the material properties and microarchitecture of bone phase in the bone/marrow composite material, whereas the slow waves are more related to the marrow phase (Hosokawa and Otani, 1997, Mizuno et al., 2010, Mizuno et al., 2009, Yamamoto et al., 2009, Mizuno et al., 2008, Hosokawa, 2006, Hosokawa and Otani, 1998). These researchers all agree that when the ultrasound wave propagates along the principal orientation of trabecular bone, the fast wave velocity is the fastest. And it is commonly known that, this principal structural orientation is heavily associated with the mechanical loading environment. According to "Wolff's law" published by Julius Wolff, bone continually remodels and adapts its structure in response to the mechanical milieu (Wolff, 1896). Although it is still unknown that how exactly this adaptation process occurs, it has been shown by many researcher's work that the interaction between QUS and bone can provide useful information about the anisotropic microstructure and mechanical properties of trabecular bone (Cowin and Cardoso, 2011, Cardoso and Cowin, 2011, Cardoso and Cowin, 2012, Lee et al., 2007, Mizuno et al., 2010, Mizuno et al., 2009, Mizuno et al., 2008, Hosokawa and Otani, 1998, Hosokawa, 2011b, Han and Rho, 1998).

For the past few years, many researchers have been investigating extensively on the interaction between ultrasound wave propagation and the anisotropic structure of trabecular bone. Cardoso and Cowin (Cowin and Cardoso, 2011, Cardoso and Cowin, 2011, Cardoso and Cowin, 2012) studied the relation between fabric tensor – a measurement of the degree of anisotropy of the trabecular bone – and the wave propagation equations in anisotropic porous media. An angle-dependent model to the classic Biot's theory (Biot, 1956b, Biot, 1956a) to predict the ultrasound velocity in an anisotropic trabecular bone model was also introduced (Lee et al., 2007). Mizuno et al. reported in vitro studies on the different effects of the structural anisotropy of trabecular bone on the velocity of the fast wave and slow wave components of the broadband ultrasound signal (Mizuno et al., 2010, Mizuno et al., 2009, Mizuno et al., 2008). These data strongly suggests that it is feasible to use QUS to predict the principal structural orientation (PSO) of trabecular bone.

With the current technology, it is estimated that nearly 80% of the variation of QUS parameters can be explained by bone quantity with an additional 8-17% contributed by bone architectural parameters (Nicholson et al., 2001, Cortet et al., 2004), which means 50-70% of the variation of bone elasticity and strength can be predicted by QUS parameters (Langton et al., 1996, Han et al., 1997, Bouxsein and Radloff, 1997, Hakulinen et al., 2005, Toyras et al., 2002), leaving a big margin for technical improvement. As the most popular site for *in vivo* QUS measurement, human calcaneus is easily accessible and constituted by 90% trabecular bone, which can display bone metabolic changes before cortical bone due to a higher metabolic turnover rate (Njeh et al., 1999). The relatively flat and parallel lateral surfaces and thin overlaying soft tissue are ideal for transmission mode of QUS measurement. The commonly used QUS devices for calcaneus scan adapt a transmission configuration in which a transmitter and a receiver are placed on the medial and lateral sides of the calcaneus, respectively. In this configuration, the calculation of ultrasound attenuation, as introduced by Langton *et al*. as the classic substitution method (Langton et al., 1984), utilizes a reference wave signal obtained through water to compare to the wave signal received with the human foot positioned between the two ultrasound transducers. Since BMD measured by DXA is the current gold standard for the diagnosis of osteoporosis, research has been performed to evaluate the relationship between QUS parameters and calcaneal BMD measured by DXA. The correlation coefficient (R) varied between 0.49 and 0.81 (Laugier and Haḷat, 2011). To improve the ability of QUS to correlate

with BMD, mechanical properties of calcaneus, one possible solution is to take the microstructure of trabecular bone into consideration for the scanning orientation.

## 2 Hypotheses and Specific Aims

In this research, it is expected that a new QUS measurement protocol based on 3-dimensional circumferential scanning can be developed to predict the principal structural orientation (PSO) of trabecular. This development will utilize an ideal spherical bone model for QUS measurement, and the results of the PSO will be compared to the current gold standard – micro computed tomography (μCT). This prediction will be based on the interaction between the ultrasound wave and the trabecular alignment, and multiple QUS parameters such as ultrasound velocity and attenuation will be used for the prediction. The prediction for the PSO serves the purpose of analyzing the mechanical properties of trabecular bone. Therefore, an analysis on the mechanical properties according to the PSO prediction will be performed in the second part of the study. Given the spherical nature of the trabecular bone model used in the experiment and repeatability of the mechanical testing, finite element analysis (FEA) based on μCT imaging will be utilized to characterize the mechanical properties in different orientation of the same spherical bone model. This FEA simulation can also provide insights of the possible angle difference of the PSO prediction by QUS when compared to μCT data. It is hypothesized that this novel QUS method can achieve the same accuracy as μCT in predicting the PSO of trabecular bone. After the successful development of the new QUS measurement of finding the PSO, such method will be applied to trabecular bone cubes as an interim study between ideal spherical model to realistic human calcaneus with complex and irregular geometry. A more practical and realistic QUS protocol will be developed using the bone cube model before the final stage of the study – apply the novel QUS measurement on whole human calcaneus to verify the improvement in predicting the structural and mechanical properties. Given that this new QUS method was developed based on ideal spherical bone model, certain modification and compromise were needed to be made to apply the measurement on human calcaneus with irregular geometry. The experiment will be initiated with the circumferential QUS measurement on the transverse plane within a limited angle range. This QUS measurement is consisted of both transmission and reflection modes. The purpose of using reflection mode is to correct the signal difference induced by the variance of sample thickness—instead variance of microstructure—in different scanning angles in transmission mode. It is proposed by using this combined QUS measurement, the correlation between the QUS parameters and the mechanical properties of trabecular bone can be improved.

The overall objective of this work is to develop a novel non-invasive ultrasonic imaging method to predict the principal structural orientation (PSO) of trabecular bone, and furthermore correlate such ultrasonic evaluation with the mechanical and structural properties of trabecular bone. Following specific aims are designed in accordance to the hypotheses for the purpose of the global objection.

**Hypothesis 1: QUS measurement in a 3-dimensional and rotational manner on trabecular bone can provide enough information to reconstruct a 3-dimensional ultrasound profile to predict the PSO of trabecular bone.**

The propagation of ultrasound wave in trabecular bone is substantially influenced by the anisotropy of the trabecular structure. Previous studies have shown that both ultrasound velocity and amplitude is dependent on the scanning angle of the ultrasound signal into the bone sample. In order to perform rotational QUS scanning of the bone sample to measure the difference induced by the anisotropic structure, instead of the difference induced by altered thickness in different orientations, a spherical bone ball model is used in this aim. To show the accuracy of the prediction, MIL tensor based on μCT images will be used for comparison.

**Specific Aim 1: Perform 3D rotational QUS measurement on bovine spherical trabecular bone samples to predict the PSO, compare the results to the MIL tensor based on the μCT images of the samples.** The work in this aim will be completed in the following steps:

1. Prepare seven bovine spherical trabecular bone samples from distal femur for QUS measurement using lathe machine, and mark the anatomical orientations on the bone balls.
2. Perform μCT scan on the spherical bone samples, and obtain the structural parameters including mean intercept length (MIL) tensor from the evaluation.
3. Use QUS to scan the spherical bone samples in an incremental, 3-dimensional and rotational manner and obtain the raw ultrasound wave data to reconstruct an ultrasonic responsive profile for each sample.
4. Reconstruct the ultrasonic profile for each sample and predict the PSO with two ultrasound parameters (velocity and attenuation) in a coordinates system based on the anatomical orientations.

5. Compare the PSO prediction of QUS with the longest vector of MIL tensor from μCT.

**Hypothesis 2: The PSO predicted by QUS is associated with the anisotropic mechanical properties of trabecular bone, and such PSO should align with the orientation with the highest mechanical strength.**

The microarchitecture and alignment of trabecular bone is intended to adapt to the particular mechanical milieu applied to it. Due to this anisotropic mechanical property, assessment for trabecular bone quality and fracture risk prediction has to take the measurement orientation into consideration. In this aim, finite element models will be generated based on the μCT images of the spherical bone samples used in S.A. 1. Compressive loading will be applied to the models in simulation to evaluate the mechanical properties in different orientations. *In vitro* mechanical testing will be used as validation for the FEA.

**Specific Aim 2: Determine the mechanical strength in different orientations of finite element models based on the μCT images of spherical trabecular bone samples and validate the models by *in vitro* mechanical testing.** The work in this aim will be completed in the following steps:

1. Generate seven finite element models based on the μCT images of the bovine spherical trabecular bone samples obtained in S.A. 1.
2. Apply compressive loading to the models in different orientations, including the anatomical orientations, longest vector of MIL tensor and the PSOs predicted by QUS parameters in S.A. 1.
3. Determined the mechanical strength of the bone models in different orientations based on the FEA results.
4. Validate the FEA determined bone strength by performing in vitro mechanical testing on the spherical bone samples obtained in S.A. 1.

**Hypothesis 3: Ultrasound scanning in the principal structural orientation can significantly improve the correlations with the structural and mechanical properties of trabecular bone with a cubic model.**

Due to the geometry of cubic trabecular bone model, fully 3-dimensional measurement would be unrealistic and extremely difficult to achieve at this stage. Therefore, instead of the fully 3-dimensional ultrasound measurement, simplified 2-dimensionally rotational measurement in the frontal and transverse planes will be employed to test the hypothesis. To take the irregular geometry of bone cube into consideration for the measurement, surface topology with aid of the reflection mode of ultrasound measurement will be utilized to measure the sample thickness in difference scanning orientations. Additionally, the ultrasound measurement normalized by the sample thickness in the PSO will be used to correlate with the structural and mechanical parameters of the sample.

**Specific Aim 3: Combine the transmission and reflection modes of ultrasound measurements of trabecular bone cubes in the principal structural orientation, and correlate the ultrasound results with the structural and mechanical parameters.** The work in this aim will be completed in the following steps:

1. Use transmission mode ultrasound to measure the attenuation and ultrasound velocity of trabecular bone cubes in various angles in the frontal and transverse planes.
2. Use reflection mode ultrasound to perform surface topology of the trabecular bone cubes and calculate the sample thickness in different scanning orientations.
3. Combine the data from the transmission and reflection modes to predict the principal structural orientation of the sample.
4. Correlate the ultrasound parameters in the principal structural orientation and the structural and mechanical parameters of the sample, and compare this correlation with the conventional ultrasound scanning method.

**Hypothesis 4: Ultrasound scanning in the principal structural orientation can significantly improve the correlations with the density, structural and mechanical properties of human calcaneus.**

As the final stage of the study, bone mineral density, structural and mechanical properties of human calcaneus samples will be obtained, and the same QUS measurement used in S.A. 3 will be applied to them. Improved correlations between QUS and the material properties of calcaneus are expected.

**Specific Aim 4: Combine the transmission and reflection modes of ultrasound measurements of human calcaneus in the principal structural orientation, and correlate the ultrasound results with the density, structural and mechanical parameters.** The work in this aim will be completed in the following steps:

1. Use transmission mode ultrasound to measure the attenuation and ultrasound velocity of human calcaneus in various angles in the frontal plane.
2. Use reflection mode ultrasound to perform surface topology of human calcaneus and calculate the sample thickness in different scanning orientations.
3. Combine the data from the transmission and reflection modes to predict the principal structural orientation of the sample.
4. Correlate the ultrasound parameters in the principal structural orientation and the density, structural and mechanical parameters of the sample, and compare this correlation with the conventional ultrasound scanning method.

# 3 Prediction of Trabecular Bone Principal Structural Orientation using Quantitative Ultrasound Scanning

## 3.1 Introduction

According to the Wolff's law, bone has the ability to adapt its structure in response to the mechanical environment, and the alignment of trabecula is heavily influenced by the stress applied to it (Martin et al., 1998). This internal structural anisotropy of trabecular bone substantially affects its mechanical properties in different orientations, and the anisotropic deterioration of the trabecular structure increases the risk of fracture. Therefore, simply measuring the "quantity" of bone such as bone mineral density (BMD) by using dual-energy x-ray absorptiometry (DXA) is not sufficient to fully characterize the "quality" of bone. Since being introduced by Langton et al., quantitative ultrasound (QUS) has been widely used for bone health status assessment (Ashman et al., 1987, Nicholson et al., 1994, Gluer, 1997, Njeh et al., 1997, Cardoso et al., 2003, Lin et al., 2006, Kaufman et al., 2007, Qin et al., 2007). Compared to the current gold standard, DXA, QUS has the advantages such as safe, low cost, portable, radiation-free and easy to operate. As ultrasound wave propagates through bone, both the velocity and the amplitude of the wave are modified. This modification can provide useful information of the mechanical properties of bone, i.e., the elastic modulus (Njeh et al., 1999).

For the past few years, many researchers have been investigating extensively on the interaction between ultrasound wave propagation and the anisotropic structure of trabecular bone. Cardoso and Cowin (Cowin and Cardoso, 2011, Cardoso and Cowin, 2011, Cardoso and Cowin, 2012) studied the relation between fabric tensor – a measurement of the degree of anisotropy of the trabecular bone – and the wave propagation equations in anisotropic porous media. An angle-dependent model to the classic Biot's theory (Biot, 1956b, Biot, 1956a) to predict the ultrasound velocity in an anisotropic trabecular bone model was also introduced (Lee et al., 2007). Mizuno et al. reported in vitro studies on the different effects of the structural anisotropy of trabecular bone on the velocity of the fast wave and slow wave components of the broadband ultrasound signal (Mizuno et al., 2010, Mizuno et al., 2009, Mizuno et al., 2008). Hosokawa and Otani investigated the same subject (Hosokawa and Otani, 1998), and later on

computational simulation work was also reported by Hosokawa (Hosokawa, 2011b). Han and Rho (Han and Rho, 1998) reported that a combination of BMD and elastic anisotropy of the bone resulted in an enhanced correlation with broadband ultrasound attenuation, a spectrum of ultrasound attenuation in frequency domain.

Although those investigations mentioned above have shown how ultrasound wave propagation in trabecular bone is influenced by the anisotropic structural property of trabecular bone in both computation simulations and in vitro experiments, some basic and fundamental questions remained unanswered: if ultrasound wave can be used to characterize the anisotropy of the porous structure of trabecular bone, can we use quantitative ultrasound to predict such principal alignment of trabecula, and to what degree? Which quantitative ultrasound parameter has the better ability to provide information to characterize the anisotropy of the trabecular structure? The objective of this presented study is to employ quantitative ultrasound to non-invasively predict the principal structural orientation of trabecular bone, and use the longest vector of MIL tensor, the current gold standard, to validate the accuracy of such prediction.

## 3.2 Materials and methods

### 3.2.1 3-D volumetric trabecular sample preparation

Seven trabecular bone cylinders (Ø 38.1 mm) were cut from distal bovine femurs using cylindrical cutting bit. Then seven trabecular bone balls (Ø 25.4 mm) were machined from the bone cylinders using lathe machine. Anatomical orientations were first marked on the surface of the cylinder. Then one half of the bone ball was machined, and the orientation markers were extended to the newly machined semi-spherical surface before the other half of the bone ball is machined. Anatomical poles were marked on the surfaces of the bone balls to indicate the three principal anatomical orientations – anterior-posterior (AP), medial-lateral (ML) and proximal-distal (PD). The bone marrow inside the trabeculae was flushed out using dental water-pick. For preservation, the bone balls were wrapped in gauze soaked with saline and 70% ethanol "half-and-half" solution and stored in 4°C refrigerator. Before quantitative ultrasound measurement, the bone balls were put into a vacuum chamber for three hours to remove the air bubbles trapped among the trabeculae.

### 3.2.2 Quantitative ultrasound measurement

Quantitative ultrasound measurement was performed by using a scanning confocal acoustic diagnostic (SCAD) system (Xia et al., 2007), consisted of a computer-controlled 2-dimensional scanner unit and a pair of focused transducers (V302-SU-F2.00IN, Olympus NDT Inc., Waltham, MA) with a center frequency of 1 MHz. The diameter of the transducers is 25.4 mm, and the confocal length of the transducers is 50.8 mm. Therefore, the transducers were coaxially installed 101.6 mm away from each other, aligning with the center of the bone ball which is placed in a rotation stage at the midpoint of the two transducers. The rotation stage is consisted of a holder for the bone ball and a base with angular calibration (Figure 1). For ultrasound measurement, ultrasonic pulses transmitted through the center of the bone ball, and the bone ball was rotated 10 degrees around the long axis of the rotation stage between every two scans. For every bone ball, ultrasound measurement was performed around all three anatomical axes, resulting 36 scans around each axis and 108 scans in total for each trabecular bone ball. Because of the shape of the bone ball sample, for each measurement in different scanning angles

of a bone ball, the distance that ultrasound wave traveled in the bone sample should be the same. Therefore, the difference of amplitude and signal arrival time among the received signals in different scanning angles of a bone ball was induced by the anisotropic material property. The ultrasound results were then processed and visualized in a custom written MATLAB program. For each measurement, ultrasound attenuation and velocity were calculated using the classic substitution method (Langton et al., 1984). Based on the previous work showing that the speed of fast wave is more related with the change of the incident angle than the speed of slow wave, and that the amplitude of both the fast wave and slow wave are influenced by the incident angle (Mizuno et al., 2010, Hosokawa and Otani, 1998), the fast wave of the ultrasound pulse was chosen for the velocity calculation via the following equation:

$$c_b = \frac{c_w d}{d - c_w \Delta t} \tag{3.1}$$

Here, $c_b$ is the ultrasound velocity in the bone sample, $c_w$ is the ultrasound velocity in the water, $d$ is the diameter of the bone ball, and $\Delta t$ is the phase difference of the same signal landmark of the reference signal and the sample signal. In this study, 1480 m/s was used for the velocity of ultrasound in water (Langton et al., 1990).

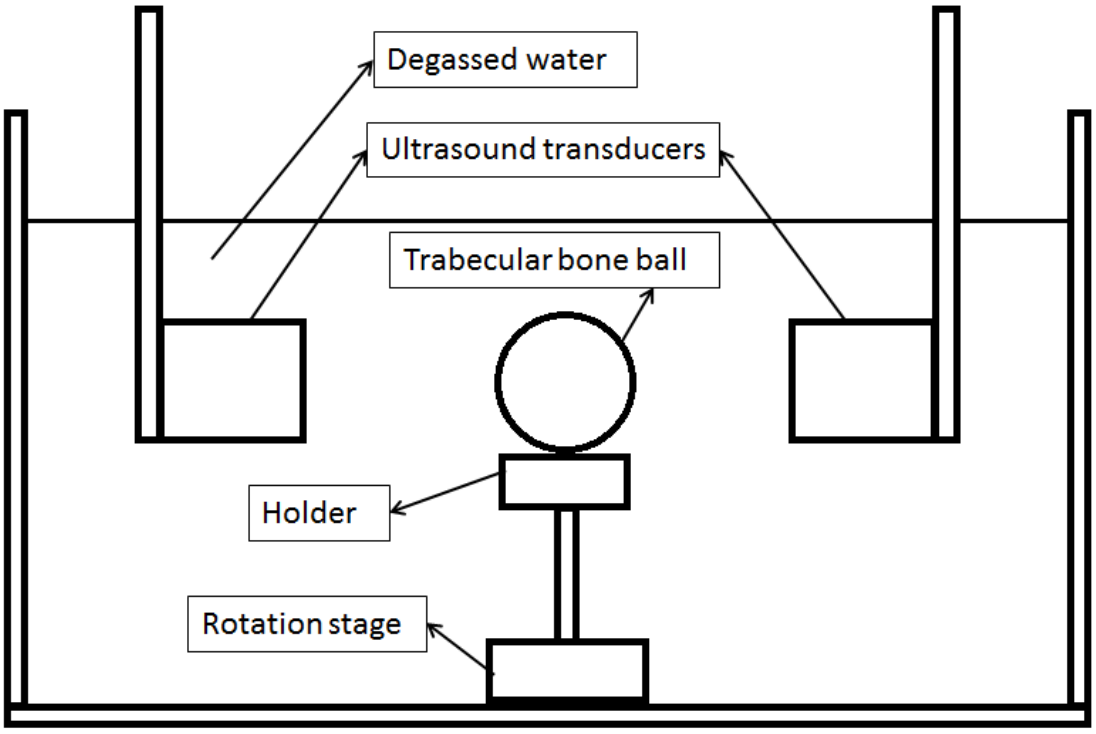


Figure 1 - Schematic representation of the ultrasound measurement experiment set up. A trabecular bone ball is placed onto a holder with a rotation stage. The stage was placed in a water tank filled with degassed water. Two ultrasound transducers used for the measurement were placed on both sides of the bone ball, with the bone ball at the confocal point. The ultrasound signal was transmitted from one of the transducers and received by the other one after propagating through the bone ball sample and the water between the sample and transducers.

### 3.2.3 µCT scanning and imaging

µCT with a resolution of 18 µm was performed on each trabecular bone ball by using a *µCT 40* system (SCANCO Medical AG, Brüttisellen, Switzerland). In order to eliminate the influence from the surface condition induced by the machining of the bone ball, a cubic volume ($15 \times 15 \times 15$ mm$^3$) of trabecular bone in the center of the bone ball was used for evaluation. The longest vector of the MIL tensor **H** was obtained from the µCT system. Currently, MIL is the gold standard of quantifying the structural anisotropy (Whitehouse, 1974). When straight lines in an arbitrary direction intercept with a medium, the average value of the intercept lengths is defined as MIL, and the degree of anisotropy is defined as the ratio of the longest MIL in the principle direction of the medium to the shortest MIL in the orthogonal direction. By the

definition of MIL tensor, the longest vector indicates the direction in which smallest number of intercepts occurs. According the equation:

$$MIL(\theta,\varphi) = \frac{L_{TOT}}{N(\theta,\varphi)} \tag{3.2}$$

Where $MIL(\theta, \varphi)$ is the length of a MIL vector in a certain direction, $L_{TOT}$ is the total length sectors of lines in that certain direction and $N(\theta, \varphi)$ is the number of intersections, the number of intersections and MIL vector length is inversely proportional to each other; a long MIL vector indicates small number of intercepts (Tabor, 2011). Therefore, the longest MIL vector indicates the smallest number of intersections, which should be the main direction of trabeculae.

A piece of rubber foam was used to fix the sample in certain orientation during the CT scanning, and a screw was inserted in the foam and included in the CT scanning as the reference of the sample's orientation. The MIL tensor was computed in a cube volume within the sample. Based on the μCT data, the average trabecular thickness for all the samples was 189 μm, about 10 times of the scanning resolution 18 μm. This resolution should be fine enough to characterize the geometrical information of the sample. To binarize the images, a threshold value of 138 was used and it was based on triangularization of surfaces.

### 3.2.4 Calculation of the principal structural orientation of bone ball

A Cartesian coordinates system (*x*-, *y*- and *z*-axes) with the origin set at the center of the bone ball was defined to calculate the principal structural orientation. The quantitative ultrasound parameters were plotted against the scanning incident angle on the corresponding orthogonal plane in the Cartesian coordinates system. Based on the ultrasound parameter around three different axes (AP, ML and PD), a specific angle in which the ultrasound with the peak measurement was chosen for calculation for the specific orthogonal plane. In the 3-dimensional Cartesian coordinates system, a plane normal to the orthogonal plane was determined based on that angle, and the three normal planes of all three corresponding measuring anatomical planes can be denoted as the following 3 equations:

$$\begin{aligned} a_1x + b_1y + c_1z &= 0 \\ a_2x + b_2y + c_2z &= 0 \\ a_3x + b_3y + c_3z &= 0 \end{aligned} \tag{3.3}$$

The normal vectors of these planes, ($a_1$,$b_1$,$c_1$), ($a_2$,$b_2$,$c_2$) and ($a_2$,$b_2$,$c_2$), were used to calculate the 3 intersecting lines between every two planes using the following equations:

$$\begin{aligned} \mathbf{I_{12}} &= (a_1, b_1, c_1) \times (a_2, b_2, c_2) \\ \mathbf{I_{13}} &= (a_1, b_1, c_1) \times (a_3, b_3, c_3) \\ \mathbf{I_{23}} &= (a_2, b_2, c_2) \times (a_3, b_3, c_3) \end{aligned} \tag{3.4}$$

Theoretically, these three vectors should represent the same direction because all three planes intersect at the same line. This is based on the assumption that there is one principle orientation in the bone ball sample, and the ultrasound measurement in the direction along this orientation should have the highest values. The peak values recorded in the rotational measurements around three anatomical axes were in the direction which is the projection of the principal orientation on the orthogonal planes. For example, the peak value in the measurements rotating around x-axis was in the direction of the projected vector of the principal orientation on the y-z plane. Therefore, when using the intersections of every two normal planes to determine the principal orientation, the results should be the same line, because there can be only one intersecting line between every two planes.

Due to the inevitable measurement error, intersection vectors of every two planes differed from each other. Therefore, a center vector **I**($x$, $y$, $z$) is calculated from the intersection vectors (**$\mathbf{I_{12}}$**, **$\mathbf{I_{13}}$** and **$\mathbf{I_{23}}$**). The three intersection vectors were converted from Cartesian coordinates system ($x$, $y$, $z$) to Spherical coordinates system ($r$, $\theta$, $\varphi$). Then the angular components of the vectors were averaged as the angular components of the center vector. The magnitude of the center vector was arbitrarily decided as 1. The center vector was then converted back to Cartesian coordinates system to compare to the longest vector of the MIL tensor, **H**($x_H$, $y_H$, $z_H$) by using the following equation:

$$\varphi = \cos^{-1}\left(\frac{\mathbf{H} \bullet \mathbf{I}}{|\mathbf{H}||\mathbf{I}|}\right) \tag{3.5}$$

An illustration of the mathematic approach of the calculation for the principal orientation was shown in Figure 2.

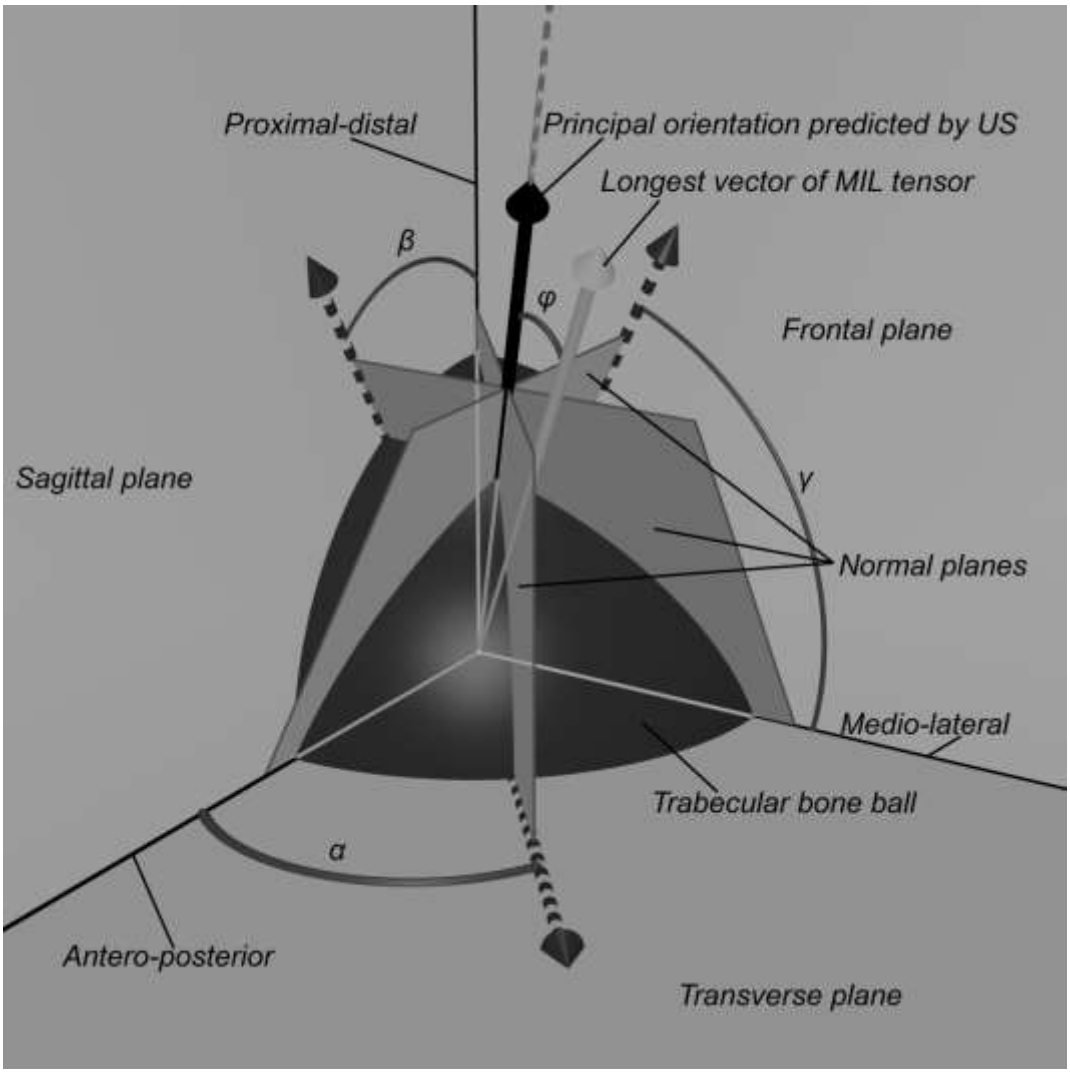


Figure 2 - The trabecular bone ball (dark sphere) was placed in a Cartesian coordinates system defined by the orthogonal anatomical planes (frontal, sagittal and transverse planes) with the center of the ball placed at the origin of the coordinates. Based on the rotational ultrasound measurement around 3 anatomical axes, the angles α, β and γ were determined. These are the angles in which the ultrasound measurements obtained peak values. According to these angles, three vectors (dash arrows) on the corresponding orthogonal anatomical planes were determined, i.e., the vector on the transverse plane is determined by the ultrasound measurements around proximal-distal axis. Along the direction of each of these 3 vectors, a plane was defined normal to the corresponding anatomical plane. These normal planes (gray planes) intersect at one line (dash line). The normal vectors of these normal planes were used to define the intersection line using Equation (3.3) and Equation (3.4). A vector (dark arrow) along the direction of that intersection line is defined as the principal orientation predicted by ultrasound, and the angle

difference φ compared to the longest vector of MIL tensor (light arrow) was calculated using Equation (3.5).

## 3.3 Results

The received ultrasound wave from all incident angles for the same bone ball showed angle-dependent pattern in both amplitude and signal arrival time (Figure 3).

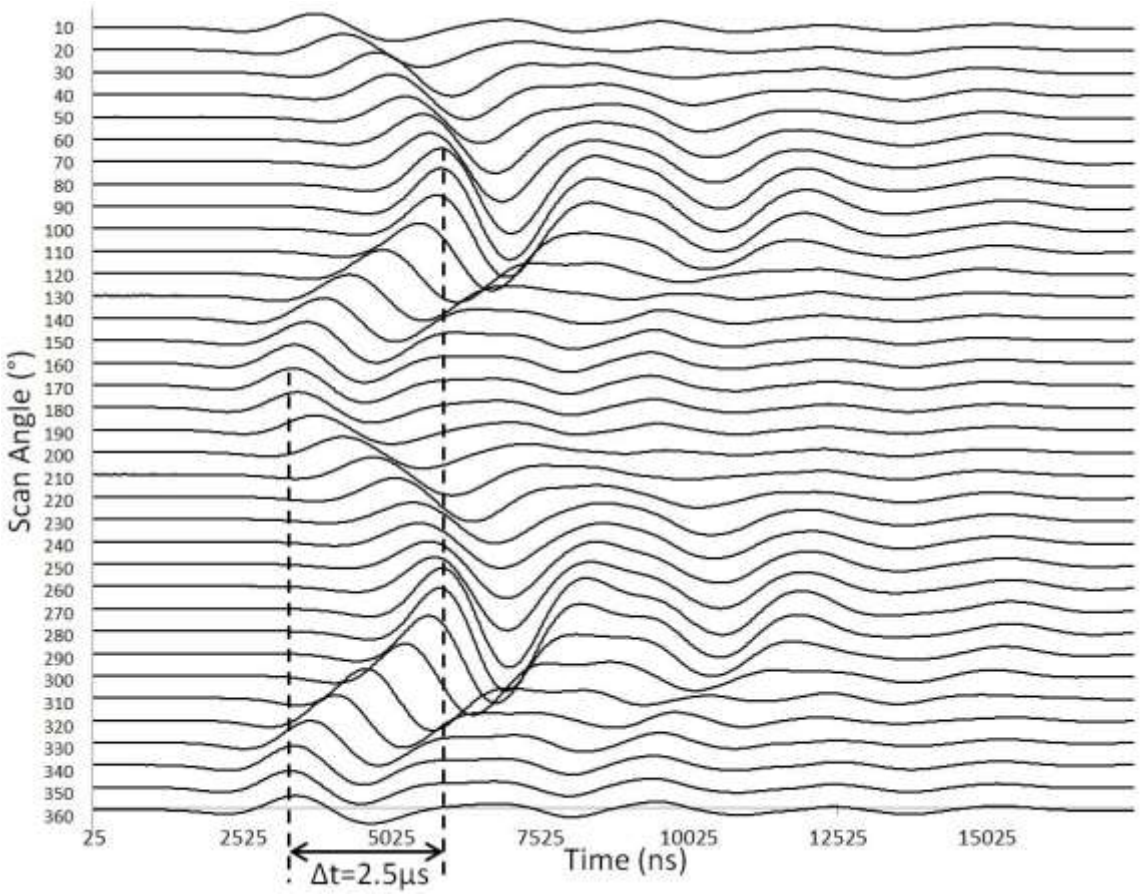


Figure 3 - Typical ultrasound waves transmitted through the trabecular bone ball in 36 different incident angles around one anatomical axis. Both amplitude (value on y-axis) and arrival time (value on x-axis) of the ultrasound waves showed angle-dependent pattern.

To further analyze this pattern, the x-axis value (arrival time) and the y-axis value (amplitude) of the first high peaks of all the 36 received ultrasound signals in different incident angles around one anatomical axis of a trabecular bone ball are plotted in Figure 4.

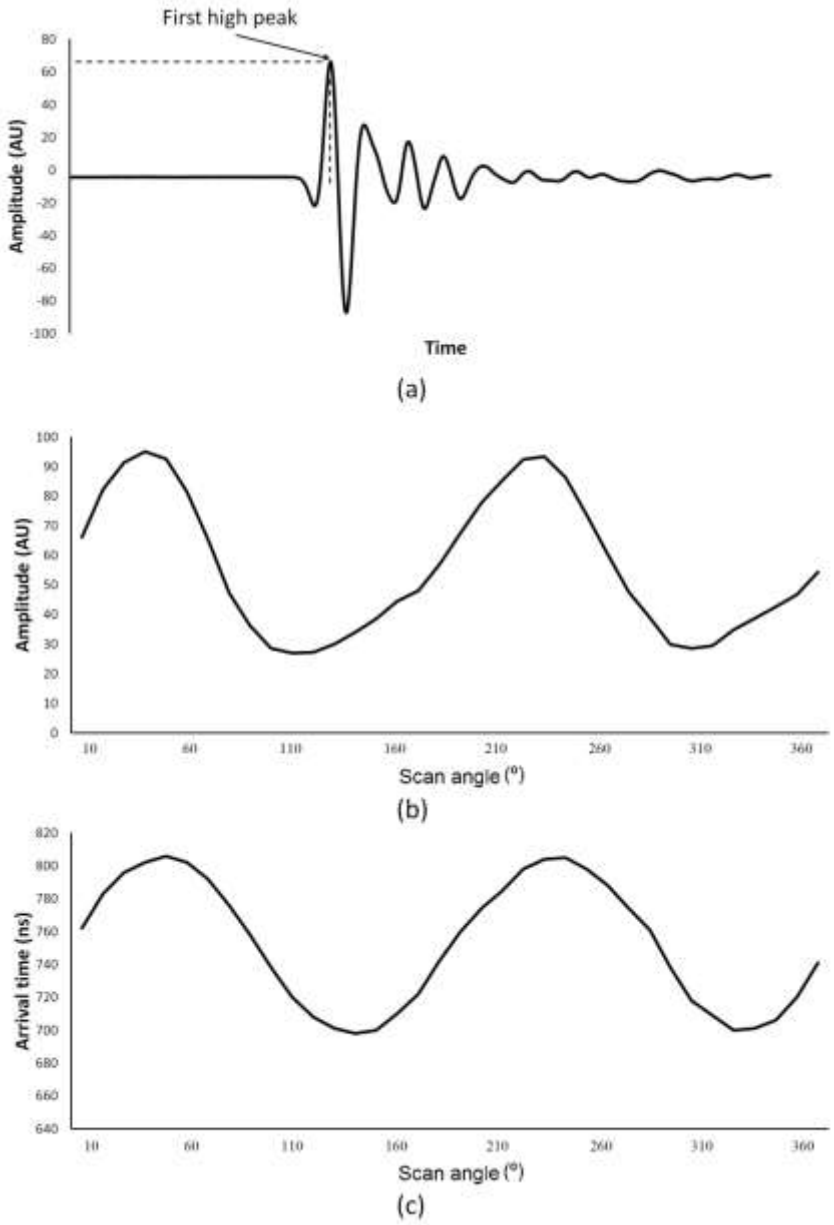


Figure 4 - By tracing the first high peaks of the 36 received ultrasound signals around 1 anatomical axis of a trabecular bone ball (a), similar angle-dependent patterns between the incident angle and the amplitude of the signal (b) and signal arrival time (c) can be observed. The high peaks and low valleys in these curves indicate that both amplitude and arrival time are affected by the anisotropy of the trabecular structure. These peaks and valleys also showed geometrical symmetry: the two peaks/valleys are located approximately 180 ° away from each other, indicating that they come from the same ultrasound propagating pathway, only in opposite directions.

The high peaks and low valleys in these curves indicate that both amplitude and arrival time are affected by the anisotropy of the trabecular structure. These peaks and valleys also

showed geometrical symmetry: the two peaks/valleys are located approximately 180° away from each other, indicating that they come from the same ultrasound propagating pathway, only in opposite directions. The peak values of the 180° apart measurements were averaged. 4 consecutive scans are plotted in Figure 5, in which both fast and slow wave components of the ultrasound pulses can be observed. It is demonstrated that, as the scan angle changes, the signal arrival time of the fast wave components changes gradually. On the other hand, little change in arrival time can be observed for the slow wave components.

According to the μCT data, the average porosity of the samples was 0.67. Of all 21 rotational measurements (3×7), the phenomenon that the fast wave amplitude is larger than the slow wave amplitude was observed in 14 measurements. And in the other 7 measurements, the slow wave amplitude was larger than the fast wave amplitude. Due to the certain existence of overlapping between the fast wave and slow wave components, the first high peak of the whole ultrasound pulse signal was chosen as the landmark to calculate the ultrasound velocity in Equation (3.1), and the amplitude of the whole ultrasound pulse signal was used to calculate the attenuation of the signal.

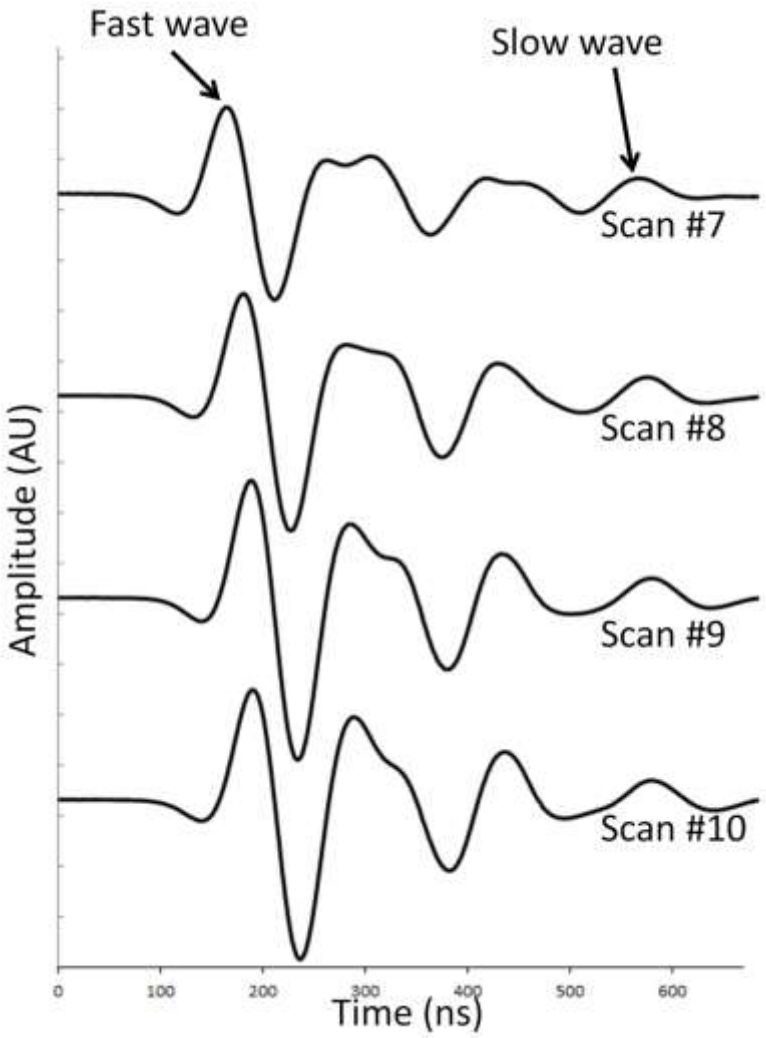


Figure 5 - The fast wave and slow wave components of the received ultrasound pulses in 4 consecutive incident angles. The arrival time of the fast wave component gradually altered as the scanning angle changed, while the arrival time of the slow wave component remained relatively unaffected.

Similar to the amplitude and arrival time curves in Figure 4, the ultrasound attenuation and velocity curves from 36 scans around each anatomical axis of a bone ball showed similar trends with adjacent peak and valley positions (Figure 6). The ultrasound velocity measured from all 7 bone balls ranged from 1700 m/s to 2300 m/s, and this range is in accordance to the velocity of the fast wave in bovine trabecular bones reported by other investigators' work (Hosokawa and Otani, 1997, Mizuno et al., 2010, Mizuno et al., 2008, Lee et al., 2007, Cardoso et al., 2003). Despite that these attenuation and velocity results showed high correlations for all 7 bone balls with an overall average $R^2$ value of 0.79 (

Table 2), certain phase shift can be observed. In Table 3, the angle difference between the principal structural orientations predicted by quantitative ultrasound and μCT is listed. Both ultrasound attenuation (ATT) and the velocity of the fast wave (UV) were used for the prediction. Here, $\mathbf{I}_{12}$, $\mathbf{I}_{13}$ and $\mathbf{I}_{23}$ are the vectors of the interception lines calculated from Equation (3.4) and $\mathbf{I}$ is the center vector calculated from $\mathbf{I}_{12}$, $\mathbf{I}_{13}$ and $\mathbf{I}_{23}$. For the prediction, the principal structural orientation predicted using ATT has an average angle difference of 11.67 ºfrom the **H** vector predicted by μCT, while the orientation predicted using UV has a difference of only 4.45 º. Statistically, a paired t-Test showed that the prediction from UV has a significantly smaller error than ATT ($p<0.05$).

Table 2 - Average Pearson correlation coefficient values ($R2 \pm$standard deviation) between ultrasound velocity and attenuation for all 7 bone balls around 3 different anatomical axes.

| | AP | ML | PD | Average |
|---|---|---|---|---|
| $R^2$ | $0.77 \pm 0.11$ | $0.75 \pm 0.09$ | $0.83 \pm 0.08$ | $0.79 \pm 0.09$ |

Table 3 - Angle difference ( $^\circ$) between the principal structural orientations predicted by μCT and quantitative ultrasound calculated from Equation (3.5). In this table, $\mathbf{I_{12}}$, $\mathbf{I_{13}}$ and $\mathbf{I_{23}}$ are the vectors of the intersection lines calculated from Equation (3.4), and velocity of the fast wave (UV) results were used for the prediction. Overall, the orientation predicted by UV has less average angle difference, $4.45^\circ$, with the μCT orientation than the prediction of the ATT, whose average angle difference is $11.67^\circ$.

| | | Bone 1 | Bone 2 | Bone 3 | Bone 4 | Bone 5 | Bone 6 | Bone 7 | Average ± Standard deviation |
|---|---|---|---|---|---|---|---|---|---|
| ATT | $I_{12}$ | 5.45 | 9.48 | 21.34 | 9.86 | 13.01 | 7.59 | 1.77 | |
| | $I_{13}$ | 33.34 | 24.75 | 10.56 | 8.00 | 18.32 | 6.72 | 20.18 | $14.13 \pm 9.03$ |
| | $I_{23}$ | 29.44 | 16.73 | 9.88 | 2.72 | 25.46 | 17.76 | 4.33 | |
| | I | 20.52 | 16.06 | 10.74 | 3.13 | 18.61 | 5.03 | 7.65 | $11.67 \pm 6.83$ |
| UV | $I_{12}$ | 6.98 | 2.72 | 22.14 | 10.91 | 28.36 | 12.12 | 6.43 | |
| | $I_{13}$ | 8.26 | 1.24 | 9.43 | 18.53 | 5.35 | 15.54 | 22.98 | $11.59 \pm 7.02$ |
| | $I_{23}$ | 6.22 | 4.93 | 11.49 | 12.41 | 11.73 | 16.96 | 8.73 | |
| | I | 6.30 | 2.41 | 5.45 | 0.82 | 7.16 | 4.34 | 4.67 | $4.45 \pm 2.20$ |

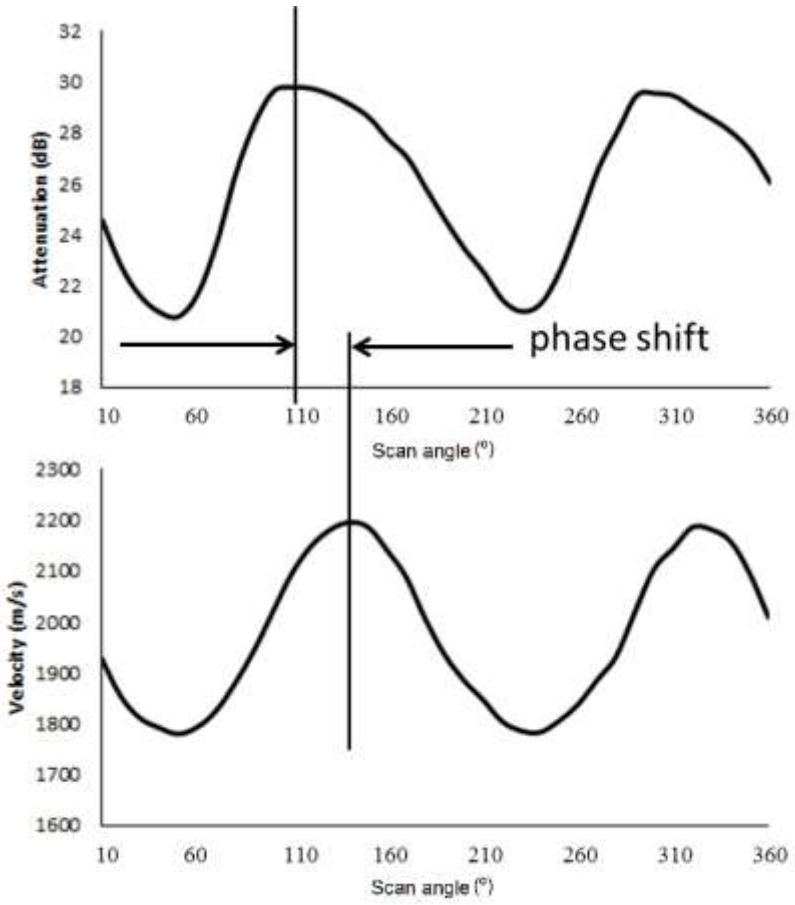


Figure 6 - Typical ultrasound attenuation and fast wave velocity curves of all the ultrasound scans around 1 anatomical axis of the same bone ball. Similar trends with adjacent peak/valley positions can be observed, while certain phase shift also exists between two curves.

## 3.4 Discussion

This work presented a non-invasive quantitative ultrasound method to predict the principal structural orientation of trabecular bone. Both attenuation and fast wave velocity of the ultrasound signal were used for independent predictions, and these predictions were evaluated by comparing to the current gold standard – the longest vector of the MIL tensor. For the ultrasound velocity calculation, the velocity of the fast wave component was chosen based on the previously reported phenomenon that fast waves are more related to the material properties of the solid phase in a porous medium, whereas the slow waves are more related to the liquid phase (Hosokawa and Otani, 1997, Mizuno et al., 2010, Mizuno et al., 2009, Yamamoto et al., 2009, Mizuno et al., 2008, Hosokawa, 2006, Hosokawa and Otani, 1998). These investigators all agreed that when the ultrasound wave propagates along the direction of the trabecular bone alignment, the phase velocity of the fast wave is the fastest. The explanation for this phenomenon is that the ratio of trabecular structure along its alignment is the highest and the compression velocity of ultrasound in bone material is much higher than in water.

Table 4 - Angle difference between the predicted trabecular structural orientation by UV and ATT.

| | Bone 1 | Bone 2 | Bone 3 | Bone 4 | Bone 5 | Bone 6 | Bone 7 | Average ± Standard deviation |
|---|---|---|---|---|---|---|---|---|
| Angle difference between UV and ATT (°) | 21.48 | 14.19 | 5.57 | 3.22 | 13.35 | 1.06 | 3.89 | 8.96±7.48 |

By definition, the longest vector of the MIL tensor is the direction in which a straight line intercepts with the most bone content. Therefore, a pathway along this direction, in which the "solid/liquid" or "bone/water" ratio is the highest, is expected to give rise to the greatest fast wave velocity – as presented in this study. Although certain bone-water or water-bone interfaces still exist along the trabecular structural orientation, their effect on the velocity of ultrasound wave is much smaller than that on the attenuation. Besides the energy absorption, the scattering and refraction caused by these interfaces substantially contribute to the measurement of ultrasound attenuation. This difference represents itself as the phase shift we observed in the ultrasound velocity and attenuation curves around 1 anatomical axis of a bone ball (Figure 6), and eventually resulted in the angle difference between the predictions for the principal

orientations (Table 4). The overall average angle difference is 8.96 ºwith the maximum of 21.48 º and the minimum of 1.06 º.

The prediction of fast wave velocity has a smaller angle difference (4.45 º) with the MIL vector than the prediction of the attenuation (11.67 º). This finding is in agreement with the work of Mizuno et al. (Mizuno et al., 2010), in which the velocity of fast wave was shown to have a higher correlation with the MIL tensor than the ultrasound attenuation. The prediction of fast wave ultrasound velocity is not only better than attenuation by the average angle difference, but also by the angle variance of the interception vectors $\mathbf{I_{12}}$, $\mathbf{I_{13}}$ and $\mathbf{I_{23}}$. As shown in Table 3, the average angle difference for these individual interception vectors from the ATT prediction was 14.13 °, with a standard deviation of 9.03 °. On the other hand, the average angle difference for the individual interception vectors from the UV prediction was 11.59 °, with a standard deviation of 7.02 °. The variance of individual interception vectors were reduced by the introduction of the center vector $\mathbf{I}$. The calculation of $\mathbf{I}$ was based on assumption that, theoretically the magnitudes of $\mathbf{I_{12}}$, $\mathbf{I_{13}}$ and $\mathbf{I_{23}}$ are the same, and the angle variance came from the error of measurement and interpretation of the ultrasound attenuation and velocity curves. Therefore, these individual vectors were normalized and converted into a spherical coordinates system to calculate the center vector by averaging the angular components of the coordinates of the individual vectors.

This center vector approach lowered the error in calculating the predicted orientations from both ultrasound attenuation and velocity by reducing the prediction error from 14.13 ° to 11.67 ° for ATT and from 11.59 ° to 4.45 ° for UV. Considering that the increment of the rotational ultrasound scan was 10 º, an angle error of 4.45 º for the prediction is promising and satisfactory. Such small error demonstrated the feasibility of using quantitative ultrasound to non-invasively predict the principal structural orientation. Although, as shown in this study, ultrasound velocity has a better prediction for the MIL tensor than attenuation, future study should take combining the predictions from ATT and UV as a comprehensive method into consideration. Ultrasound velocity can provide reliable information of the structural alignment of the trabecular bone, but the mechanical properties in such alignment direction is yet to be tested. It is very crucial to verify the mechanism behind the difference between the predictions for the structural orientation by different ultrasound parameters. By integrating the potential angle-dependent mechanical information carried by ultrasound attenuation with the existing prediction

protocol, a more precise and extensive method to provide information of both structural and mechanical anisotropy of the trabecular bone tissue is expected to be established.

# 4 Principal Trabecular Structural Orientation Predicted by Quantitative Ultrasound is Strongly Correlated with μFEA Determined Anisotropic Apparent Stiffness

## 4.1 Introduction

One important observation about trabecular bone is its ability to adapt its structure according to the specific mechanical environment, as commonly defined as "Wolff's law" (Wolff, 1896, Martin et al., 1998). This anisotropic nature of trabecular bone indicates that the "quality" of bone cannot be simply characterized by using dual-energy x-ray absorptiometry (DXA) to quantify some global parameters of bone, such as bone mineral density (BMD). As the National Institutes of Health specifies, "Bone quality refers to architecture, turnover, damage accumulation (e.g., microfractures) and mineralization" (2000). To overcome the limitation of the current bone imaging techniques, researchers have developed alternative modalities to assess bone quality and predict fracture risk (Cody et al., 1999, Link, 2012, Tommasini et al., 2012, Krug et al., 2010, Burghardt et al., 2011). Quantitative ultrasound (QUS), a safe, low cost, portable, radiation-free and noninvasive imaging tool, has been widely used for bone quality assessment since it was introduced (Ashman et al., 1987, Cardoso et al., 2003, Gluer, 1997, Haiat et al., 2008, Njeh et al., 1997, Langton et al., 1984, Lin et al., 2006, Qin et al., 2007).

The propagation of ultrasound waves through trabecular bone is heavily influenced by the macroarchitecture and alignment of trabeculae (Mizuno et al., 2010). Recently, many researchers have been investigating the interaction between the anisotropic trabecular macroarchitecture and the quantitative ultrasound propagation (Cardoso and Cowin, 2011, Cardoso and Cowin, 2012, Cowin and Cardoso, 2011, Lee et al., 2007, Mizuno et al., 2009, Mizuno et al., 2008, Mizuno et al., 2010, Hosokawa and Otani, 1998, Han and Rho, 1998, Hosokawa, 2009b, Hosokawa, 2010, Hosokawa, 2011b, Hosokawa, 2011a). In a 3-dimensional volumetric trabecular structure, not only the alignment of the trabeculae but also the "solid/liquid" or "bone/marrow" interfaces play a very important role in scattering, refracting and attenuating the ultrasound wave. It has been recognized by researchers that the microstructure of trabecular bone has a substantial effect on the measurement of QUS that generalizing the bone quality by using any global measurement value may lose information about anisotropic material properties of trabecular bone. Our

previous work successfully demonstrated a noninvasive quantitative ultrasonic method to predict the principal structural orientation (PSO) of trabecular bone (Lin et al., 2012). Such prediction using both ultrasound attenuation and velocity showed highly correlated results compared to the current gold standard—the longest vector of mean intercept length (MIL) tensor measured using micro computed tomography (μCT). Finite element analysis (FEA) based on μCT has been used as a noninvasive tool to evaluate the mechanical properties of bone (Keaveny, 2010, Eswaran et al., 2009, Wald et al., 2011, Yeni et al., 2008, Kim et al., 2007, Liu et al., 2009, Bevill et al., 2006).

Although it is commonly accepted that trabecular architecture is aligned against loading through remodeling, and it has been shown that such principal direction in trabecular bone can be predicted by the QUS, certain angle differences still exist between QUS prediction and μCT measurement. It remains unknown whether this angle difference can induce significant differences in mechanical properties or not. It is hypothesized that the principal trabecular structural orientation predicted by QUS is strongly correlated with μCT-based μFEA determined anisotropic mechanical strength. The objective of this study is then to evaluate the mechanical properties in different principal structural orientations predicted using different methods, i.e., QUS and μCT validated by mechanical testing, thus to investigate the ability of QUS as a means to predict the principal structural orientation and principal strength of trabecular bone noninvasively. By validating the ability of QUS in predicting the PSO with the highest mechanical properties of trabecular bone, it is beneficial for future QUS applications in a way that QUS measurement in the PSO can provide information more correlated with the mechanical properties than in other orientations.

## 4.2 Materials and methods

### 4.2.1 3-D volumetric trabecular sample preparation and μCT imaging

Seven spherical trabecular bone samples (Ø 25.4 mm) were machined from seven distal bovine femurs using a lathe machine. Three principal anatomical orientations were marked on the surfaces of the bone samples as anterior-posterior (AP), medial-lateral (ML) and proximal-distal (PD). The bone marrow inside the trabeculae was flushed out using a dental water-pick.

μCT imaging with resolution of 18 μm was performed on each trabecular bone ball by using a *μCT 40* system (SCANCO Medical AG, Brüttisellen, Switzerland) to obtain the 3-dimensional geometry of the bone ball samples. The longest vector of the mean intercept length (MIL) tensor—the current gold standard of quantifying the structural anisotropy—was calculated using the μCT system (Whitehouse, 1974). The calculation function for MIL tensor is provided by the software of the μCT system. Then the 3-dimensional images of bone ball samples were converted into digital imaging and communications in medicine (DICOM) format images for later analysis using information processing language (IPL) in the μCT system.

### 4.2.2 Quantitative ultrasound measurement and prediction for the principal structural orientation

A scanning confocal acoustic navigation (SCAN) system (Xia et al., 2007) was used for the quantitative ultrasound measurement. The center frequency of the two focused transducers (V302-SU-F2.00IN, Olympus NDT Inc., Waltham, MA) is 1 MHz; the diameter of the transducers is 25.4 mm; and the confocal length of the transducers is 50.8 mm. The transducers were coaxially installed 101.6 mm away from each other, aligning with the center of the bone ball which is placed in a rotation stage at the midpoint of the two transducers. For ultrasound measurement, the spherical bone sample is placed on a rotational stage, and rotational QUS measurement was performed on three orthogonal planes perpendicular to the three anatomical axes of the bone specimen. During each scan, broadband ultrasound pulses with center frequency of 1 MHz were repeatedly transmitted through the center of the bone ball, and the average product of these 400 pulses was used for analysis. For the measurement on each orthogonal plane, the increment between every two QUS scan was 10 degrees, generating a total of 36 scans on each plane and 108 scans for every bone sample. This rotational QUS measurement method is based on the assumption that QUS measurement in the PSO has the highest result, and the peak measurement on each orthogonal plane is the projection of the measurement in PSO on that plane, and therefore can be used to back-calculate the 3-dimensional vector of PSO. Two QUS parameters, Ultrasound attenuation (ATT) and ultrasound velocity (UV) were calculated using the classic substitution method (Langton et al., 1984). ATT is calculated using the following equation:

$$ATT = 10\log_{10}\left(\frac{I_1}{I_2}\right) \tag{4.1}$$

Where $I_1$ and $I_2$ are the intensity of reference and sample wave, calculated by integrating the amplitude of the received pulse over time. UV is calculated using the following equation:

$$UV = \frac{C_r d}{d - C_r \Delta t} \tag{4.2}$$

Where $C_r$ is the velocity of ultrasound in water, $\Delta t$ is the arrival time difference between reference and sample wave and $d$ is the diameter of the bone sample. In this study, the first high peak of the fast wave is used as the landmark to calculate the time difference $\Delta t$.

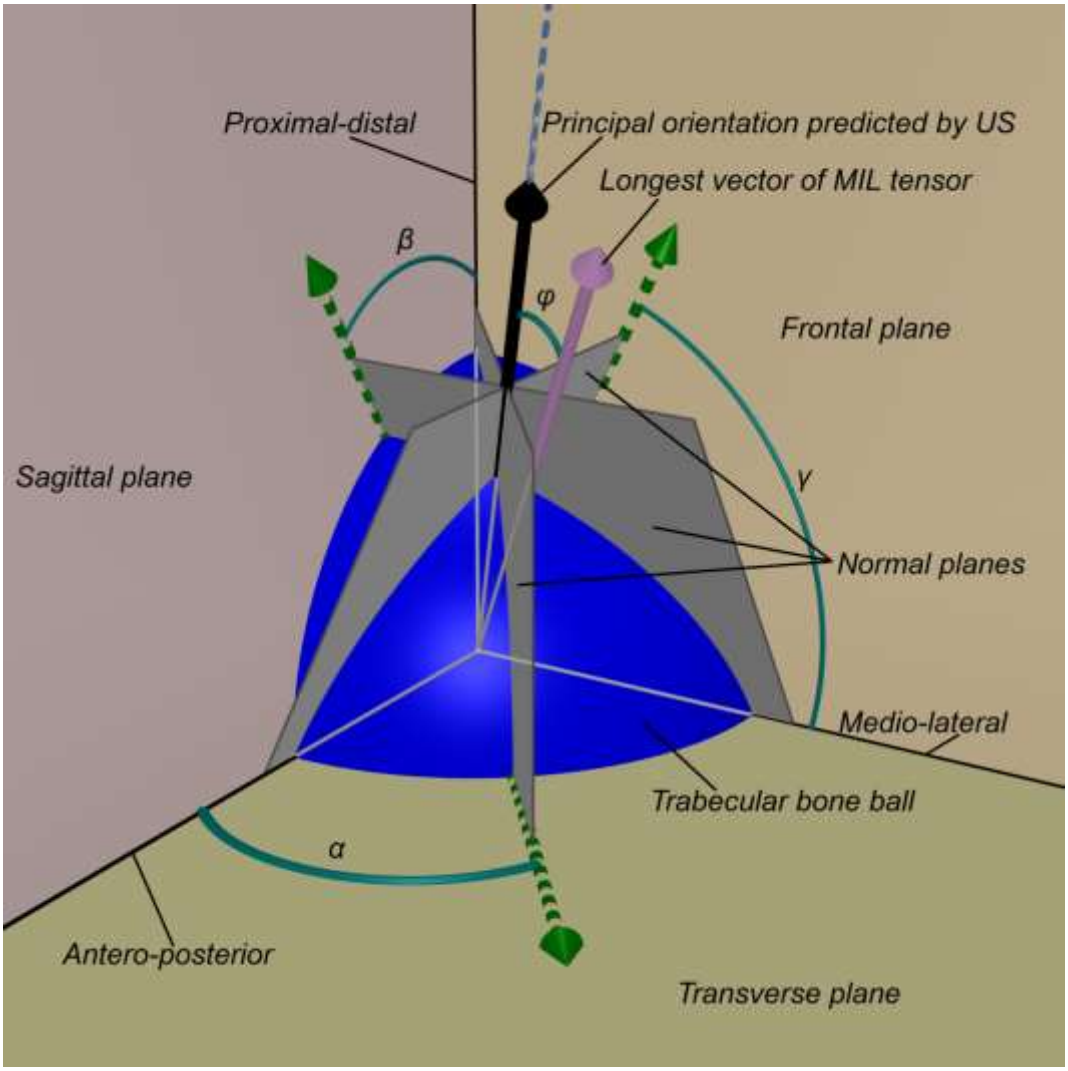


Figure 7 - The trabecular bone ball (blue sphere) was placed in a Cartesian coordinates system defined by the orthogonal anatomical planes (frontal, sagittal and transverse planes) with the center of the ball placed at the origin of the coordinates. Based on the rotational ultrasound measurement around 3 anatomical axes, the angles α, β and γ were determined. These are the angles in which the ultrasound measurements obtained peak values. According to these angles, three vectors (green arrows) on the corresponding orthogonal anatomical planes were determined, i.e., the vector on the transverse plane is determined by the ultrasound measurements around proximal-distal axis. Along the direction of each of these 3 vectors, a plane was defined normal to the corresponding anatomical plane. These normal planes (gray planes) intersect at one line (blue dash line). The normal vectors of these normal planes were used to define the intersection line using Equation (4.3) and Equation (4.4). A vector (black arrow) along the direction of that intersection line is defined as the principal orientation predicted by ultrasound, and the angle difference φ compared to the longest vector of MIL tensor (pink arrow) was calculated.

As shown in Figure 7, a Cartesian coordinate system (x-, y- and z-axes) with the origin set at the center of the bone ball was defined in accordance to the anatomical orientations (AP,

ML and PD) to calculate the PSO. The QUS parameters were plotted against the scanning angle on the corresponding orthogonal plane in the Cartesian coordinates system. A specific angle was determined based on the peak measurement of the QUS parameters for the measurement around a specific anatomical axis. In the 3-dimensional Cartesian coordinates system, a plane normal to the orthogonal plane was determined based on that angle, and the three normal planes of all three corresponding measuring anatomical planes can be denoted as the following 3 equations:

$$\begin{aligned} a_1x + b_1y + c_1z &= 0 \\ a_2x + b_2y + c_2z &= 0 \\ a_3x + b_3y + c_3z &= 0 \end{aligned} \tag{4.3}$$

The normal vectors of these planes, ($a_1$,$b_1$,$c_1$), ($a_2$,$b_2$,$c_2$) and ($a_2$,$b_2$,$c_2$), were used to calculate the 3 intersecting lines between every two planes using the following equations:

$$\begin{aligned} \mathbf{I_{12}} &= (a_1, b_1, c_1) \times (a_2, b_2, c_2) \\ \mathbf{I_{13}} &= (a_1, b_1, c_1) \times (a_3, b_3, c_3) \\ \mathbf{I_{23}} &= (a_2, b_2, c_2) \times (a_3, b_3, c_3) \end{aligned} \tag{4.4}$$

Theoretically, these three vectors should represent the same direction because all three planes intersect at the same line. Again, this is based on the assumption that QUS measurement in the PSO should have the highest values and the peak values recorded in the rotational measurements around three anatomical axes were in the projected vector of PSO of the principal orientation on the orthogonal planes. For example, the peak value in the measurements rotating around x-axis was in the direction of the projected vector of the PSO on the y-z plane. Therefore, when using the intersections of every two normal planes to determine the principal orientation, the results should be the same line, because there can be only one intersecting line between every two planes. Due to the inevitable measurement error, intersection vectors of every two planes differed from each other. Therefore, a center vector **I**($x$, $y$, $z$) is calculated from the intersection vectors ($\mathbf{I_{12}}$, $\mathbf{I_{13}}$ and $\mathbf{I_{23}}$). The three intersection vectors were converted from Cartesian coordinate system ($x$, $y$, $z$) to Spherical coordinate system ($r$, $\theta$, $\varphi$). After that, the angular components of the vectors were averaged as the angular components of the center vector. The magnitude of the center vector was arbitrarily decided as 1. The center vector was then converted back to

Cartesian coordinates system to compare to the longest vector of the MIL tensor, $\mathbf{H}(x_H, y_H, z_H)$ by using the following equation:

$$\varphi = \cos^{-1}\left(\frac{\mathbf{H} \bullet \mathbf{I}}{|\mathbf{H}||\mathbf{I}|}\right) \tag{4.5}$$

### 4.2.3 Finite element analysis of μCT-based trabecular bone ball models

The implementation of the spherical trabecular bone model gave rise to the feasibility of repeating the mechanical testing on the same bone specimen in different orientations, besides the anatomical orientations which were the only available options in the traditional bone cube model. FEA based on μCT images usually consists of the following steps: convert the gray-scale Hounsfield Unit data in the standard DICOM format into calibrated and segmented values; convert the calibrated DICOM image into finite element model and assign local material property to it; apply loading and boundary conditions to the finite element model; validate the finite element model using *in vitro* mechanical testing. The unfiltered DICOM format μCT images of each bone ball were processed and converted into a 3-D tetrahedral meshing structure. To eliminate the effect induced by the surface condition, a smaller spherical subvolume of trabecular bone with a diameter of 12 mm from the center of each bone ball image was cropped out for analysis. For image segmentation, global optimum threshold values were chosen by visual observation to include all trabeculae of the bone sphere. For some models, manual modifications of the threshold values were implemented by visually comparing the segmented image and the underlying original image for all μCT images by only one observer.

The segmented spherical sub-volumes of the bone samples were then used for mesh generation (Mimics V. 16.0, Meterialise NV, Plymouth, MI). Filters were applied to the volume of voxels to close small holes, filter small isolated parts, smooth the surface and improve connectivity of the model. Then a mesh of tetrahedral 4-point elements (C3D4) was created by grouping every two neighbor voxels together. The 3-dimensional mesh model was exported to ABAQUS version 6.10EF (Dassault Systemes, Inc., Providence, RI) (Figure 8). Certain notable changes can be observed between finite element model and the μCT image. These changes due to the filters applied and the grouping of voxels can induce differences between the mechanical properties between FEA and *in vitro* experiments. These differences are considered uniform

throughout each model and independent of any tested orientation; therefore, do not affect the comparison between mechanical properties in different tested orientations.

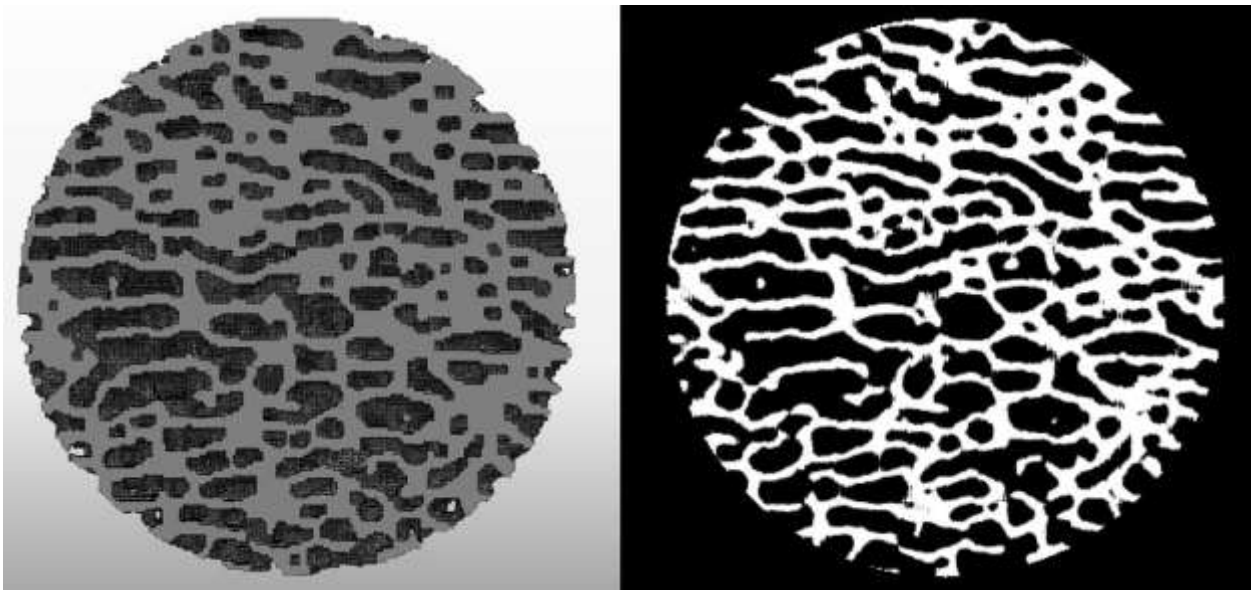

Figure 8 - Typical cross-section of the spherical bone model in ABAQUS (left) and the binarized μCT image of the same section (right). After converted from the DICOM image from μCT using Mimics, the finite element mesh models used in the simulation were able to capture most of the geometrical features of the bone samples and reproduce the original structure of the samples.

In the simulation, all seven bone ball models were loaded compressively in six orientations, AP, ML, PD, ATTmax (PSO predicted by ultrasound attenuation), UVmax (PSO predicted by ultrasound velocity) and MIL (PSO predicted by the longest vector of MIL tensor). Trabecular bone tissue in the models was assumed as homogenous and linear elastic isotropic. Density of 1739 kg/m$^3$ (Ashman and Rho, 1988) and Poisson's ratio of 0.3 (Wirtz et al., 2000) were assigned to the material properties of the models. The Young's modulus assigned to each bone ball model was back-calculated from *in vitro* validation mechanical testing. The average Young's modulus of seven bone balls is 15.9 GPa. As shown in Figure 9, along the loading direction, two reference points (RP1, RP2) were defined 12 mm away from the center of the bone ball, on opposite sides. Two sets of nodes (NS1, NS2) were defined in accordance to the two reference points by using the following procedure: 1) two parallel planes perpendicular to the loading direction axis were defined; 2) one of the planes was tangent to the bone ball surface, and the other one was 0.2 mm into the bone ball; 3) the nodes between these two planes were included in the node set. The node sets were generated through a custom MATLAB program.

The nodes in NS1 and NS2 were applied coupling with RP1 and RP2 in all six degrees of freedom. The introduction of RP1, RP2, NS1 and NS2 is to make sure that the compression loading is normal to the surface of the spherical model and through the center of the model. For the compressive loading, RP1 was pinned in all six degrees of freedom, while RP2 translated towards to center of the bone ball along the loading direction coupling with all the nodes in NS2 for 2,000 μstrain, namely 0.024 mm. This loading was done over the duration of 1 second. The reaction force of the whole model under the loading and the von Mises stress were recorded for analysis. Based on the reaction force of the bone ball models, the apparent stiffness of the bone samples in different loading orientations can be calculated by dividing the reaction force by the loading displacement. To focus on the stiffness difference between different orientations, and to eliminate the stiffness variance between different samples, the stiffness results in 6 orientations of each model were normalized to the stiffness value in the MIL orientation.

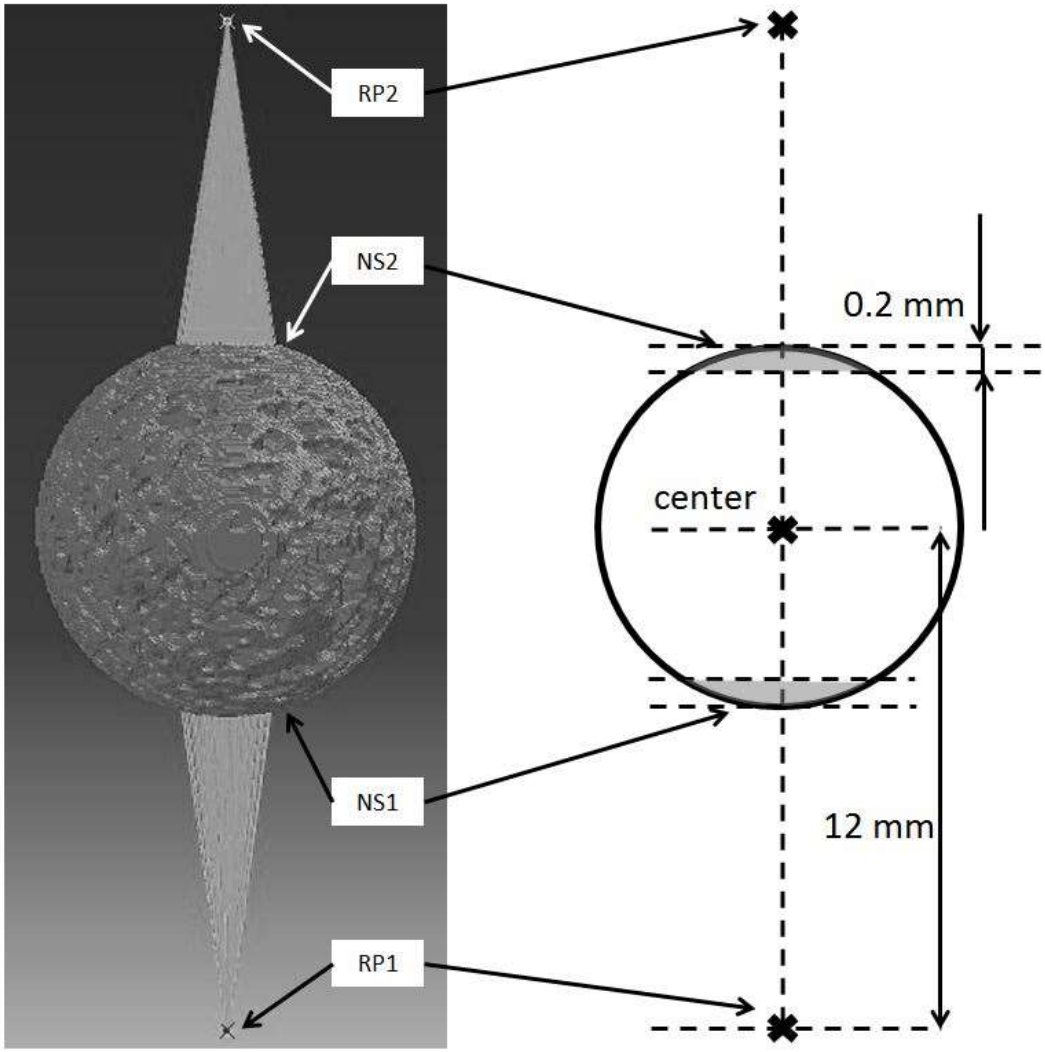


Figure 9 - For the boundary condition of the model, two sets of nodes (NS1, NS2) were defined to couple with two reference points (RP1, RP2). RP1 and RP2 were both 12 mm away from the center of the bone ball. The nodes in NS1 and NS2 (grey region in the schematic figure on the right) were respectively coupling constrained with RP1 and RP2 in all six degrees of freedom. During the loading, RP1 was encastred in all six degrees of freedom, and RP2 translated towards the center of the bone ball along the loading direction coupling with all the nodes in NS2 for 2,000 μstrain.

### 4.2.4 *In vitro* mechanical testing of the trabecular bone balls

*In vitro* mechanical testing for the bone balls was performed to validate the model used in FEA. All seven bone balls were thoroughly thawed for 3 hours before the mechanical testing. Axial compressive loading was performed on a MTS MiniBionix 858 (MTS Corporation, Minneapolis, MN) axial load frame with TestStar II control software and a 5 kN MTS 19F-01

load cell. Two cylindrical holders were made of self-curing acrylic material to provide an interface between the bone sample and the loading piston (Serra-Hsu et al., 2011). One surface of the holder was polished flat with sand paper, and the other surface was made as a concave surface with a spherical wax mode, which had the same diameter as the bone balls. This concave surface created a bowl shape contact area about 1 mm deep to provide stable and uniformly distributed loading over the contact interface between the holder and the bone balls (Figure 10). The loading protocol began with a 50 N preload to make sure full contact between all the interfaces and eliminate the effect caused by the surface conditions of the samples. The loading then proceeded for 2,000 μstrain, namely 0.05 mm at the rate of 0.005 mm/s. The loading piston retreated back after the compressive loading, and the same loading cycle was repeated for 5 times. Force applied to the bone sample and displacement of the loading piston were recorded to calculate the apparent stiffness of the bone balls. For each bone ball sample, the compressive loading was performed in three anatomical orthogonal orientations, AP, ML and PD.

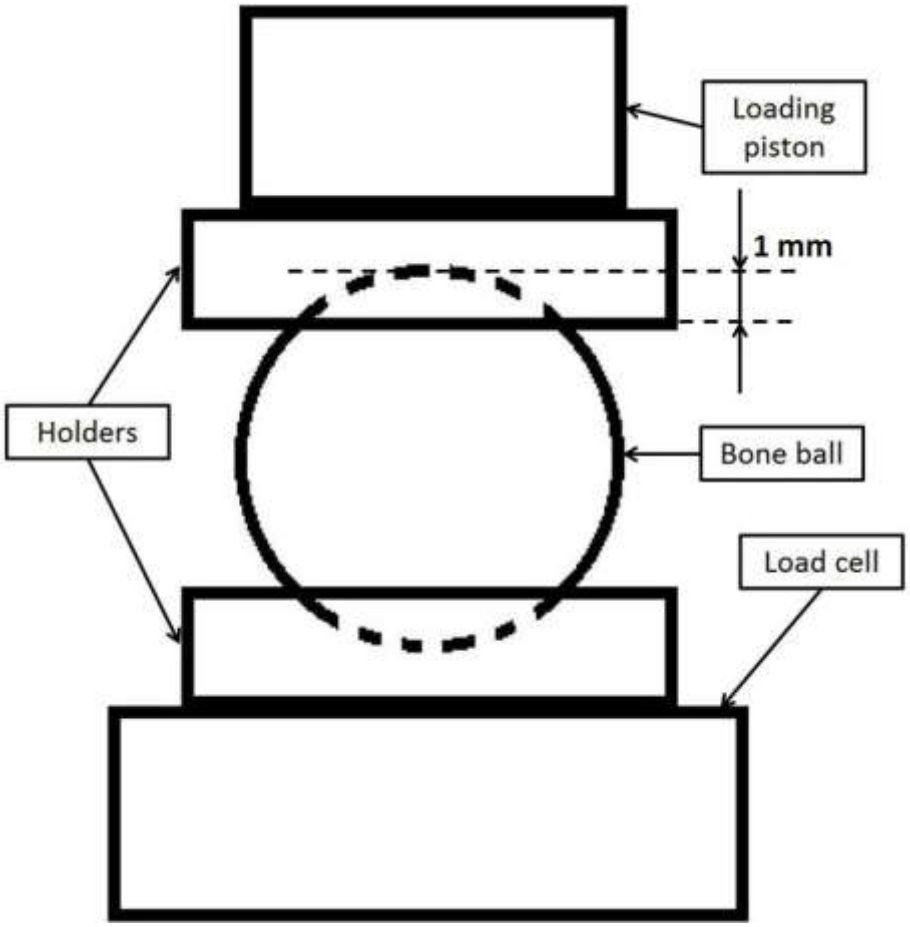


Figure 10 - Schematic representation of the *in vitro* mechanical testing set up. The bone ball was placed between two cylindrical holders with concave surfaces. The holders are made of self-curing acrylic, and each has one flat surface and one concave surface. The concave surfaces created a bowl shape area about 1 mm in depth and provided stable and uniformly distributed loading between the bone ball and the holder; the flat surface secured the stable and solid contact between the holders and the loading piston or load cell.

### 4.2.5 Data analysis

All values are reported as mean ± standard deviation. To confirm the normality of the data, Shapiro-Wilk test was performed, and normality was determined at significance of $W<0.05$. Repeat measures analysis of variance (ANOVA) and Tukey's post-hoc test were used to detect statistically significant differences between the normalized stiffness in different orientations. The same statistics test was also performed to compare the normalized von Mises stress in different tested orientations. Significance was determined at $p<0.05$, $p<0.001$ and $p<0.0001$. Correlations between stiffness in the PSOs predicted by QUS parameters and microCT and between FEA and

*in vitro* mechanical loading were determined by using multiple linear regressions and Pearson's correlation coefficient.

## 4.3 Results

As reported in previous publication (Lin et al., 2012), the average angle difference between the PSOs predicted by ultrasound attenuation (ATTmax) and μCT is 11.67±6.83°; the angle difference between prediction by ultrasound velocity (UVmax) and μCT is 4.45±2.20°. The predictions from ATTmax and UVmax have an average angle difference of 8.96±7.48°. While stiffness in UVmax direction had the highest value out of all tested orientations, ML direction had the lowest value, 36.6% less than the stiffness in UVmax direction ($p<0.001$). The other two anatomical orientations, AP and PD, were 14.6% and 27.6% ($p<0.05$), which is lower than UVmax. Stiffness in ATTmax and MIL directions were only 2.9% and 3.8% lower than UVmax (Figure 11). No statistical significance was found between the stiffness in the PSOs predicted by ATTmax, UVmax and MIL. With further analysis, highly significant correlations were also found between stiffness in the PSOs predicted by QUS parameters versus the longest vector of MIL tensor: ATTmax vs. MIL, $R^2=0.98$, $p<0.001$; UVmax vs. MIL, $R^2=0.92$, $p<0.001$ (Figure 12). Von Mises stress was also reported from the FEA in the same normalized manner as stiffness. Similar to stiffness, the Von Mises stress in the PSO predicted by UVmax has the highest value, only 1% and 1.1% higher than ATTmax and MIL, but 6.4%, 21.8% ($p<0.001$) and 14.7% ($p<0.05$) higher than the values of AP, ML and PD, respectively (Figure 13).

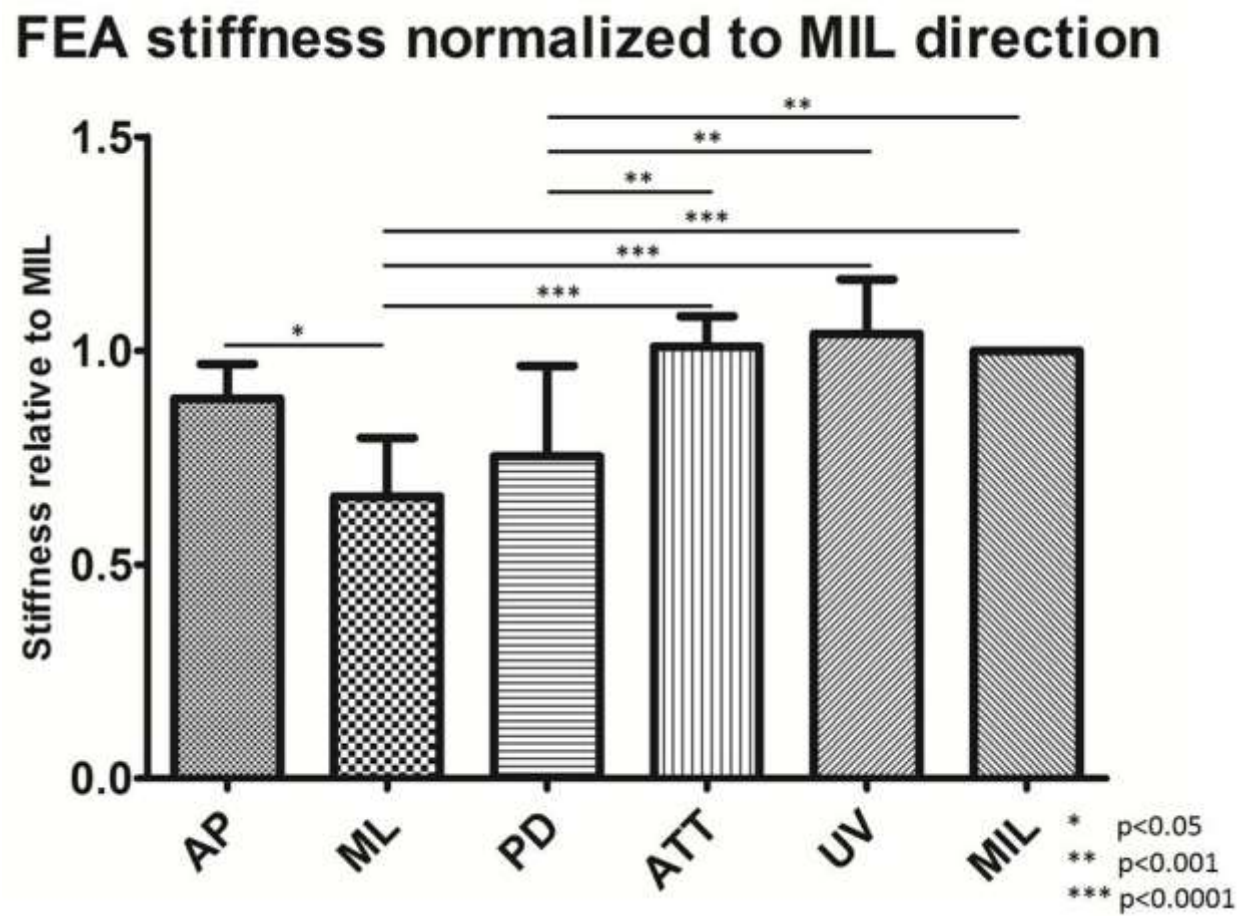


Figure 11 - The stiffness data from FEA was normalized to the values in the MIL orientations. Significant difference was observed: AP vs. ML, $p<0.05$; ML vs. ATTmax, $p<0.0001$; ML vs. UVmax, $p<0.0001$; ML vs. MIL, $p<0.0001$; PD vs. ATTmax, $p<0.001$; PD vs. UVmax, $p<0.001$; PD vs. MIL, $p<0.001$. No significant difference was observed between the stiffness in the PSOs predicted by ultrasound parameters and μCT.

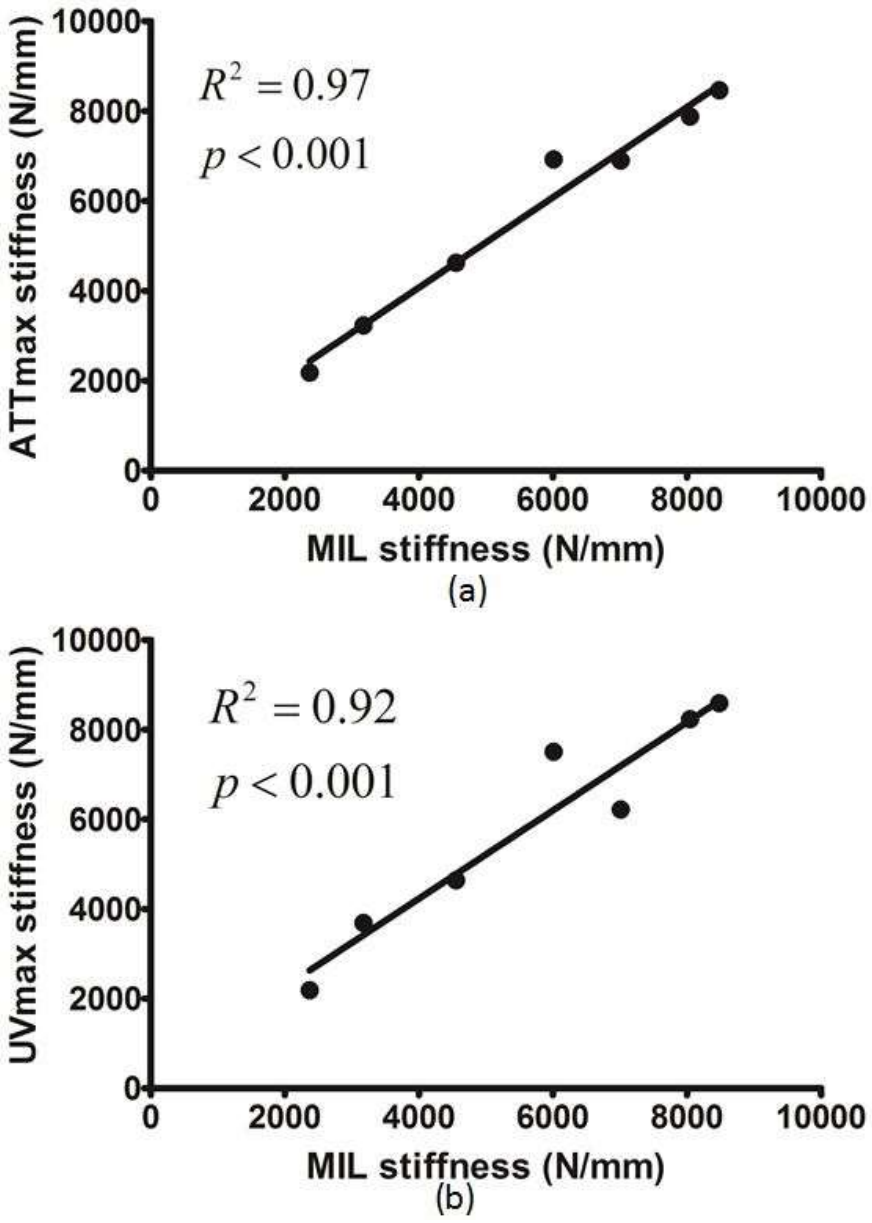


Figure 12 - When comparing the stiffness from FEA of all seven bone ball models, highly significant correlations were found between the stiffness in the PSOs predicted by QUS and μCT. (a) ATTmax vs. MIL, $R^2$=0.98, p<0.001; (b) UVmax vs. MIL, $R^2$=0.92, p<0.001.

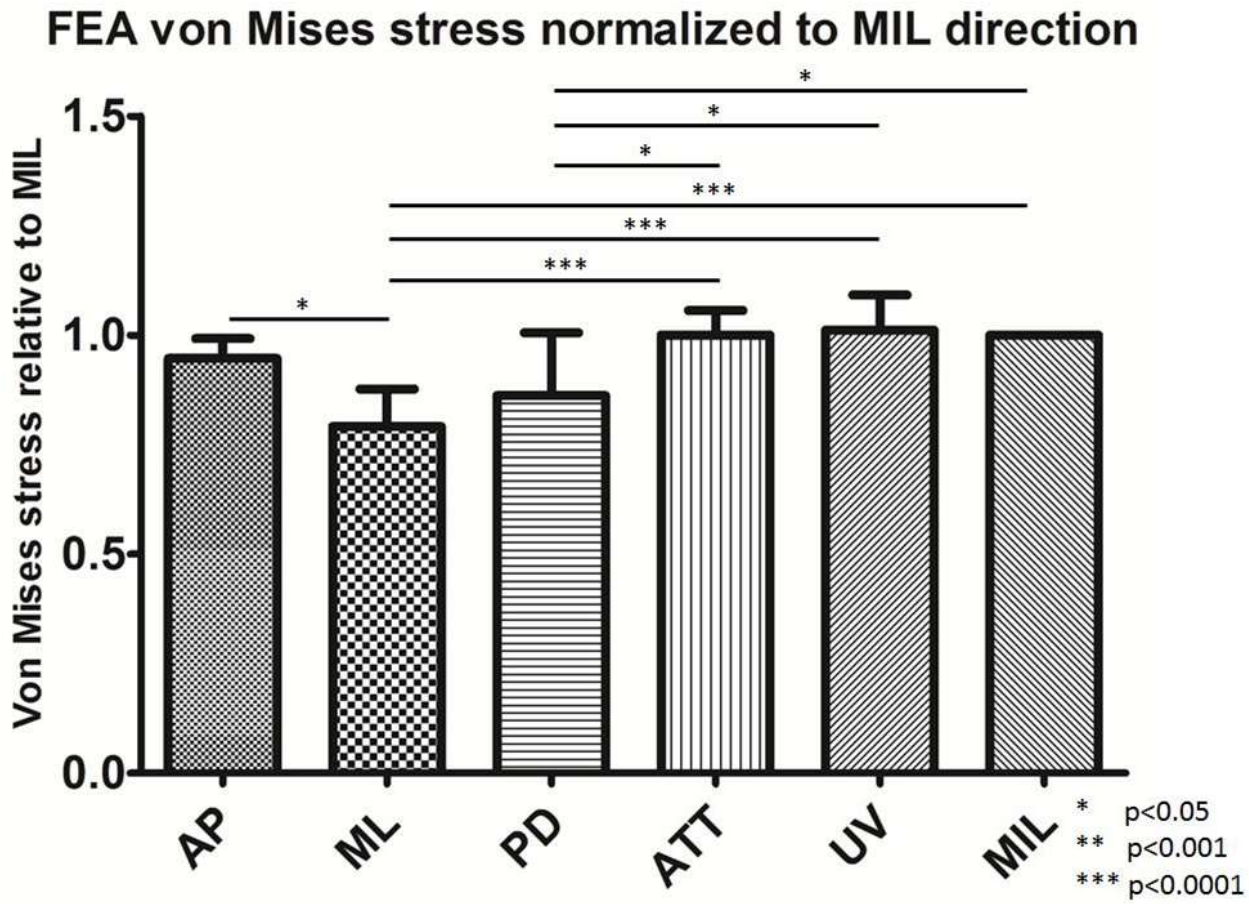


Figure 13 - The von Mises stress data was also normalized to the values in the MIL orientations. Significant difference was observed: AP vs. ML, $p<0.05$; ML vs. ATTmax, $p<0.0001$; ML vs. UVmax, $p<0.0001$; ML vs. MIL, $p<0.0001$; PD vs. ATTmax, $p<0.05$; PD vs. UVmax, $p<0.05$; PD vs. MIL, $p<0.05$. No significant difference was observed between the von Mises stress in the PSOs predicted by ultrasound parameters and μCT.

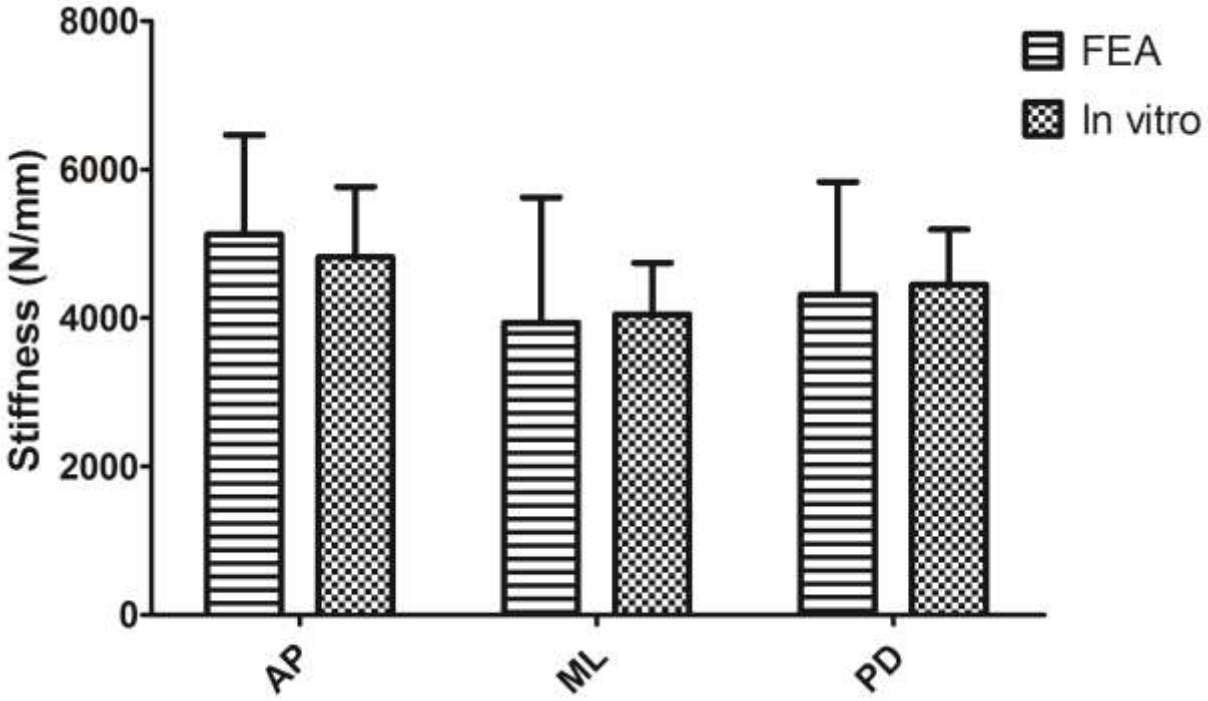


Figure 14 - Comparison between the stiffness from both *in vitro* mechanical testing and FEA. The stiffness data from two different tests followed the same trend. The average difference percentage between the stiffness of two tests in the same orientation is 4.0%, and there is no significant difference found.

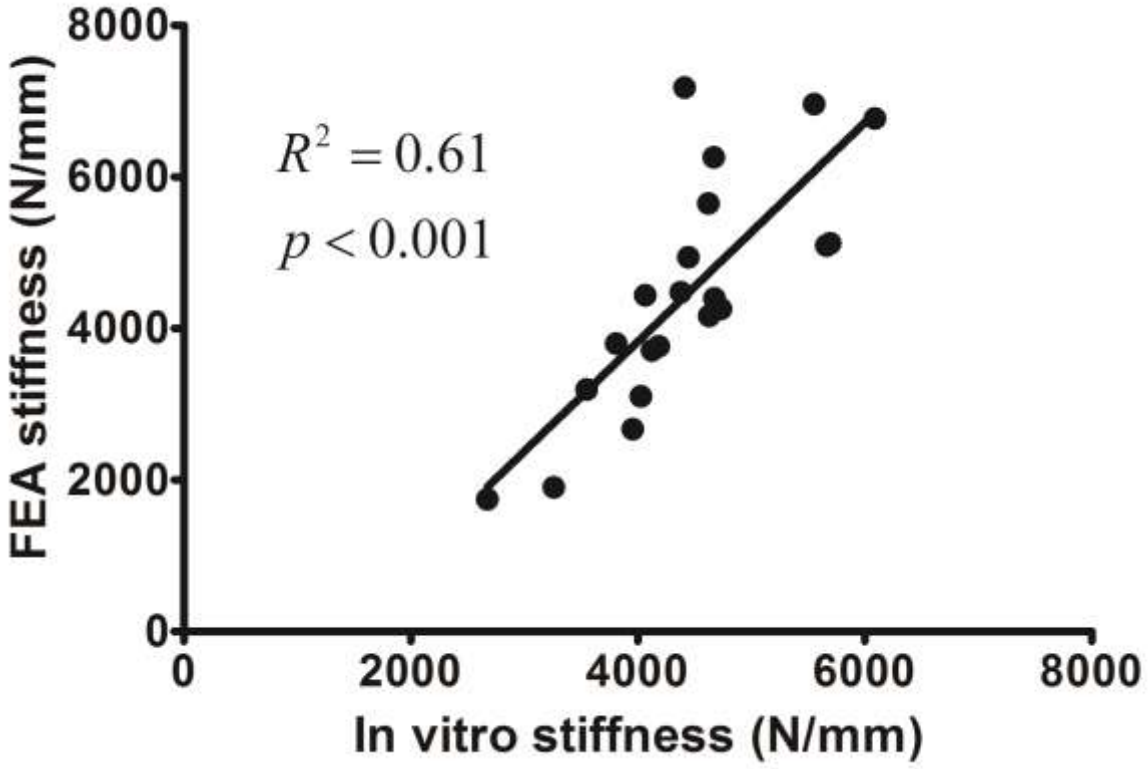


Figure 15 - Highly significant correlation was found between the stiffness data for all anatomical orientations of all seven bone balls in FEA and in vitro mechanical testing ($R^2$=0.61, p<0.001).

Similar to the data analysis of FEA, the slope of the loading force vs. loading displacement curve was calculated as the stiffness of the bone sample from the *in vitro* mechanical tests. The stiffness data from *in vitro* mechanical loading shows the same AP>PD>ML trend as the FEA data. Stiffness in ML direction is 16.0% and 9.0% lower than AP and PD. By comparing the stiffness from FEA and *in vitro* mechanical testing of the same loading direction, no significant difference was found in all three orientations (Figure 14). By pooling the stiffness data points of all anatomical orientations together, a highly strong and significant correlation ($R^2$=0.61, p<0.001) exits between the FEA and *in vitro* mechanical testing (Figure 15).

## 4.4 Discussion

This study evaluated the mechanical properties of trabecular bone in various orientations by using μCT-based FEA method. The seven spherical trabecular bone samples were the same

samples used in a previous study (Lin et al., 2012) to demonstrate the ability of QUS in detecting the principal structural orientation. Therefore, performing the μFEA on the same bone specimens not only served the purpose of validating such QUS prediction for PSO, but also helped to provide new insights on the correlation between QUS prediction and the anisotropic mechanical properties and microarchitecture of trabecular bone.

Previous studies (Hosokawa and Otani, 1997, Mizuno et al., 2010, Mizuno et al., 2009, Yamamoto et al., 2009, Mizuno et al., 2008, Hosokawa, 2006, Hosokawa and Otani, 1998) all suggested that when ultrasound waves propagate along the direction of the trabecular bone alignment, ultrasound velocity is the fastest and the attenuation is the highest. The explanation for this phenomenon is that the ratio of trabecular structure along its alignment is the highest and the compression velocity of ultrasound in bone material is much higher than in water, and the ultrasound attenuation coefficient of bone material is also much higher than water or marrow. These findings all support our QUS prediction of PSO using either ATT or UV. The prediction of UV has a smaller angle difference (4.45 °) with the MIL vector than the prediction of ATT (11.67 °). This finding is in agreement with the work of Mizuno et al. (Mizuno et al., 2010), in which the velocity of fast wave was shown to have a higher correlation with the MIL tensor than the ultrasound attenuation. This study didn't focus on separation of the overlapping fast and slow waves. From the previous work, while the overlapping is observed, it didn't affect distinguishing the first high peak for the analysis of the signal arrival time. While the analysis of the ultrasound velocity is based on the fast wave, the attenuation calculation takes both fast and slow waves into consideration. This difference could be accountable for the angle difference between the PSO predictions of UV and ATT. The prediction of fast wave ultrasound velocity is not only better than attenuation by the average angle difference, but also by the angle variance of the interception vectors $\mathbf{I_{12}}$, $\mathbf{I_{13}}$ and $\mathbf{I_{23}}$. For the ease of comparing the angle difference of PSOs predicted by QUS and μCT and investigating the effect of the trabecular orientation on the mechanical properties, mean intercept length values of the PSOs predicted by ATTmax, UVmax and the maximum MIL from μCT are listed in Table 5.

Table 5 - Tensor coordinates values of the maximum MIL orientation from the μCT system and QUS measurement and the length of the vector in the MIL orientation |**H2**| in mm. The values of the QUS parameters, ATTmax and UVmax are converted from the spherical coordinates system.

These values are used in the calculation of the angle difference between the PSOs predicted by μCT and QUS.

| | | Bone 1 | Bone 2 | Bone 3 | Bone 4 | Bone 5 | Bone 6 | Bone 7 |
|---|---|---|---|---|---|---|---|---|
| MIL | x | -0.04 | 0.70 | -0.71 | 0.54 | -0.04 | -0.39 | 0.70 |
| | y | 0.42 | -0.04 | -0.02 | -0.04 | -0.78 | -0.12 | -0.08 |
| | z | 0.50 | 0.33 | 0.25 | -0.23 | 0.16 | 0.83 | 0.25 |
| ATTmax | x | -0.12 | 0.81 | -0.89 | 0.93 | -0.31 | -0.34 | 0.88 |
| | y | 0.34 | -0.31 | -0.19 | -0.11 | -0.88 | -0.12 | -0.14 |
| | z | 0.93 | 0.50 | 0.41 | -0.35 | 0.37 | 0.93 | 0.45 |
| UVmax | x | -0.16 | 0.89 | -0.93 | 0.92 | -0.09 | -0.35 | 0.91 |
| | y | 0.65 | -0.07 | -0.12 | -0.08 | -0.94 | -0.14 | -0.16 |
| | z | 0.74 | 0.46 | 0.36 | -0.39 | 0.32 | 0.93 | 0.39 |
| |**H2**| (mm) | | 0.65 | 0.77 | 0.75 | 0.59 | 0.79 | 0.93 | 0.75 |

In our study, the average material elastic modulus assigned to the model, 15.9 GPa, was in the range of the reported data of the previous studies (Ashman and Rho, 1988, Hosokawa and Otani, 1997, Isaksson et al., 2010). This value was back-calculated based on the biomechanical testing results, further proving the validity of the FEA model. According to the our previous work (Lin et al., 2012), there are certain angle differences between PSOs predicted by QUS parameters and μCT. Although these angle differences are relatively small, before this study, it was unknown how much of a difference in mechanical properties this angle difference can induce. It is very important to address that the PSO predicted by QUS not only has the highest value in QUS measurement, but also has the highest mechanical properties. The development of using QUS to predict PSO serves the purpose of finding the best orientation to perform QUS measurement in order to get the highest correlation with mechanical properties. The loaded volumes of the bone balls in the FEA model are the center subvolume of the real bone balls and are smaller than the bone balls used in the mechanical test. This alteration resulted in the variation of the structural orientation of the outer layer of the trabecular bone ball not being analyzed in the FEA model. For the ROI of the QUS measurement, the ultrasound pulse propagates through the center of the bone ball, comparable to the ROI of the *in vitro* mechanical testing. In this study, due to the different ROIs used in the FEA model and QUS measurement, the *in vitro* mechanical testing also serves as a transition method to compare the results of FEA and QUS, besides validating the FEA model.

The main goal of this study is to find out how much the mechanical properties differentiate between the PSO predicted by QUS and the MIL orientation. Before the FEA, the angle difference between the PSO and MIL was quantified by QUS measurement. However, it is inappropriate to define whether this angle difference is “big” or “small” until the difference of the mechanical properties is determined. The stiffness in the PSOs predicted by ATTmax and UVmax are very close to the value in MIL orientation, with no significant differences. On the other hand, a significant difference can be found between the stiffness in the anatomical orientations and the QUS-predicted PSOs. These results lead to the conclusion that although the PSOs predicted by QUS and μCT have certain angle differences, the mechanical properties measured in these PSOs are of the same level, having no significant differences. The significant correlations between the stiffness in the PSO predicted by QUS parameters and MIL, in addition to the small difference of stiffness value, further demonstrated the ability of QUS in finding the principal orientation with the highest apparent stiffness.

It is noted that the correlation between the stiffness in the PSO predicted by UV and in the MIL orientation is lower than the correlation between the stiffness in the PSO predicted by the ATT and tin the MIL orientation, while the angle of the MIL orientation is more closer to the angle of the PSO predicted by UV than by ATT. In this study, we are more focus on relative comparison of mechanical properties in different orientations, the correlations between the stiffness in the PSOs predicted by QUS parameters and MIL directions can show us the validity of the FEA model in showing the relative relation of the mechanical properties in different orientations. We do not have any direct evidence to show a smaller angle difference between two orientations can lead to a higher correlation of mechanical properties in the two orientations. While the difference of mechanical properties in two close orientations can be small because of the small variation in structure, the correlations between the mechanical properties in these orientations could be affected by many factors, e.g., the two outliers in the UVmax stiffness vs. MIL stiffness graph. What we can conclude from the data presented in this paper is that the stiffness in the PSO predicted by QUS is not significantly different from the stiffness in the MIL direction. Further research on the geometrical distribution of the PSOs and MIL orientations could provide more insight on the relation between the proximity of orientations and the correlations of mechanical properties in the orientations.

The aim of both loading conditions in the FEA and in vitro was to make sure the compressive loading was normal to the sample surface, through the center of the bone ball and aligned with the desired tested orientation. The introduction of the concave holder used in the in vitro mechanical testing was able to stabilize the spherical bone sample during the compressive loading, and apply the loading uniformly over the concave surface along the orthogonal anatomical orientation of the bone ball sample. The linear translation of the reference point and the coupling between it and the node group was also able to simulate the same loading condition as the *in vitro* testing.

From our FEA analyses, von Mises stress was used to measure the equivalent stress to predict local tissue failure. The von Mises stress which takes into consideration principal and shear stresses of our bone model can predict the onset of bone yielding and indicate an increased propensity for local stress concentrations which could lead to local tissue failure. Displacement controlled compression loading protocol was used to ensure the same exertion of strain was applied on all bone models in every tested orientation. Our data clearly indicates that under the same compressive loading protocol, the distribution of von Mises stresses when loaded in the PSOs predicted by QUS is similar to that of MIL orientation and significantly higher than other anatomical orientations. While it is indicated that the local concentration of stress is higher in those QUS orientations, it is also implied that it takes more work to deform the bone in these PSOs due to the higher resistant force. The apparent stiffness data, combined with von Mises stress data, comprehensively leads to the conclusion that QUS clearly predicts the geometrical anisotropy nature of our bone models, and the PSOs predicted by QUS parameters not only have the higher apparent stiffness, but also are more structurally stable and less likely to yield, compared to the anatomical orientations.

It should be recognized that the essential methodologies and mechanisms of predicting such PSO are different when using QUS and μCT (Whitehouse, 1974). Researchers have shown that there is a certain angle difference between the trabeculae alignment and the orthogonal anatomical orientations (Pidaparti and Turner, 1997), between the loading milieu applied and the force distribution pattern (Biewener et al., 1996), and between the principal orientation of the loading environment and the principal alignment of the trabeculae (Gefen and Seliktar, 2004). These findings all remind us of the fact that simply investigating the geometric parameters

cannot provide a comprehensive understanding of how the microarchitecture of trabecular bone is affected by the mechanical environment and react to it in return.

As a successive study of the previous work (Lin et al., 2012), this paper evaluates the mechanical properties in the PSO predicted by QUS, thus validated the ability of QUS in predicting such orientations. Future studies should take a step back and use this angle-dependent mechanical information to understanding the mechanism of such QUS modality. One limitation of this study is that successive compressive loading tests were performed on one sample in the in vitro testing. Residual effects such as microcrack induced by the previous compressive loading can affect the results of the latter testing in different orientation. To minimize such effect, the compressive loading was controlled at 2000 μstrain, which is within the elastic deformation range of trabecular bone and reported as the peak strain experienced by human in daily vigorous activities (Burr et al., 1996, Burr et al., 1998, Rubin and Lanyon, 1984). With this study, it is shown that although there is a certain angle difference between the PSOs predicted by QUS and μCT, the mechanical properties in these orientations are very close. A further study in the details of the propagation of ultrasound wave in trabecular bone, combined with the comprehensive information of the geometrical parameters, should be able to take us one step closer to the answer of the very question: can we use quantitative ultrasound to find the principal structural orientation of trabecular bone, and why?

# 5 Enhanced correlation between quantitative ultrasound parameters and structural and mechanical properties using combined transmission-reflection measurement

## 5.1 Introduction

It is widely accepted that quantitative ultrasound (QUS) can quantify fracture risk (Bauer et al., 1997, Hadji et al., 2000, Huopio et al., 2004), as well as predict fracture type (Drozdzowska and Pluskiewicz, 2002). When ultrasound waves travel through trabecular bone, a porous media, information regarding material properties, such as density, elastic modulus and anisotropy can be calculated by evaluating two main ultrasound parameters, velocity and attenuation (Njeh et al., 1999, Laugier, 2006). These two parameters are heavily influenced by not only the quantity of bone mass, but also the macroarchitecture and alignment of trabeculae (Mizuno et al., 2010). The anisotropic structure of trabecular bone is the result of adaptation to its mechanical environment, according to "Wolff's Law" (Wolff, 1896). Recent studies describe the interaction between trabecular bone structural alignment and ultrasound wave (Cardoso and Cowin, 2011, Cardoso and Cowin, 2012, Cowin and Cardoso, 2011, Lee et al., 2007, Mizuno et al., 2009, Mizuno et al., 2008, Mizuno et al., 2010, Hosokawa and Otani, 1998, Han and Rho, 1998, Hosokawa, 2009b, Hosokawa, 2010, Hosokawa, 2011b, Hosokawa, 2011a, Liu et al., 2014). These researchers all came to the same conclusion; that quantitative ultrasound is sensitive enough to pick up the difference of structural and mechanical properties of trabecular bone in different orientations, and generally provide more comprehensive information of bone "quality" than simply bone "quantity".

Our group and others reported a novel QUS method using a 3-dimensional rotational ultrasound scan to predict the principal structural orientation (PSO) of spherical trabecular bone specimens (Lin et al., 2012, Mizuno et al., 2010). This work demonstrated that ultrasound has the ability to predict the trabecular structural orientation just as accurately as the current gold standard—the longest vector of mean intercept length (MIL) tensor measured using micro computed tomography (μCT). Further study utilized a finite element model of spherical trabecular bone validated the QUS prediction of PSO (Lin et al., 2014). The mechanical

properties in the PSO predicted by QUS are significantly higher than the anatomical orientations and comparatively close to the longest vector of MIL tensor.

While traditional QUS measurement, especially of the human calcaneus, is performed in medial-lateral orientation, the results of our previous work indicate that QUS measurement can determine the structural alignment of trabecular bone and correlate strongly with mechanical properties of the trabecular bone. By performing ultrasound scan in the critical orientations, the prediction of mechanical properties can be improved from simply performing QUS measurement conventionally in the anatomical orientations. This present study aims to improve the correlations between QUS parameters and structural and mechanical properties of trabecular bone by performing QUS measurement in the PSO determined by QUS. To progress from an ideal spherical bone model used in the previous work, trabecular bone specimens with more practical cubic geometry are tested. To eliminate the samples thickness difference in different QUS scanning angles, reflection mode QUS as described by Xia et al. (Xia et al., 2007) is performed to measure the sample thickness in different scanning orientations. The sample thickness measured by reflection mode is combined with the transmission mode QUS scan to evaluate the structural and mechanical properties.

## 5.2 Materials and methods

### 5.2.1 Trabecular bone cubes preparation

24 trabecular bone cubes were harvested from the distal end of bovine femurs. The samples were cut into 15-20 mm cubes using a slow speed diamond saw (Microslice, Metals Research Limited, Cambridge, England) with constant water irrigation. The principal anatomical orientations were marked on the surfaces of the bone samples as anterior-posterior (AP), medial-lateral (ML) and proximal-distal (PD). The fat marrow among the trabeculae was flushed out using dental water-pick. For preservation, the bone specimens were soaked in saline and 70% ethanol "half-and-half" solution and stored in a 4℃ refrigerator. Before quantitative ultrasound measurement, the bone cubes were put into a vacuum chamber while in solution for three hours to remove the air bubbles trapped among the trabeculae.

### 5.2.2 Quantitative ultrasound measurement

Quantitative ultrasound measurements were performed by using a scanning confocal acoustic navigation (SCAN) system (Xia et al., 2007), consisted of a computer-controlled 2-dimensional scanner unit and a pair of focused transducers (V302-SU-F2.00IN, Olympus NDT Inc., Waltham, MA) with a center frequency of 1 MHz. The diameter of the transducers is 25.4 mm, and the confocal length of the transducers is 50.8 mm. The transducers were coaxially installed 101.6 mm away from each other on a rotational stage, aligning with the center of the bone cube which was wrapped in acoustic-wave-proof foam at the midpoint of the two transducers. QUS measurements were performed in two orthogonal anatomical planes, frontal plane and transverse plane, in a defined range of angle utilizing the rotational stage. As shown in Figure 16, for QUS measurement on transverse plane, an angle range of 60° was defined with the medial-lateral axis as the neutral axis. The QUS scans were performed in this 60° range with an interval of 5°, namely a total of 13 scans on frontal plane for each sample. As for the QUS scan on frontal plane, a similar angle range of 60° was also defined for the measurement with the medial-lateral axis as the neutral axis. For each scanning angle on each anatomical plane, the QUS measurement was performed in 2 different modes; transmission and reflection.

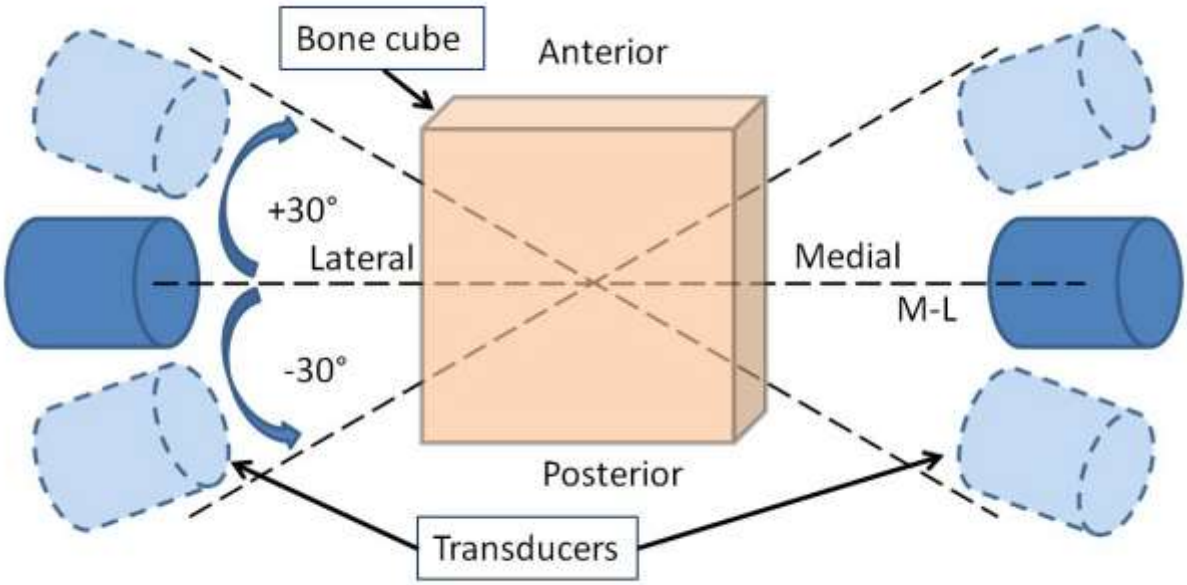


(a)

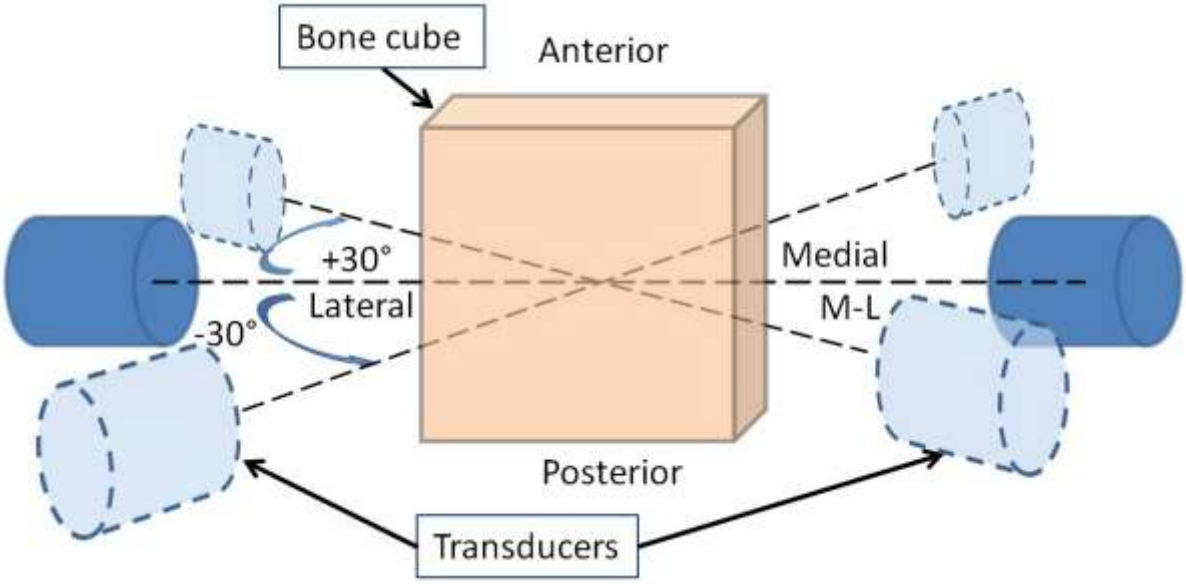


(b)

Figure 16 - Schematic representations of the QUS measurement configuration on (a) transverse plane and (b) frontal plane. For both planes, medial-lateral axis is used as the neutral axis, and the QUS measurement is performed is a 60° angle range, ±30° from the medial-lateral axis.

Within the 60° angle scanning range, the interval between every two scans is 5°, resulting 13 scanning angles on each plane of each sample.

#### 5.2.2.1 Transmission mode QUS measurement

The transmission mode QUS measures the interaction between the ultrasound wave and trabecular bone, and therefore material properties of trabecular bone can be derived from the received ultrasound wave after propagating through the bone sample. As shown in Figure 17 (a), in transmission mode, an ultrasound wave was emitted by one transducer and received by another after traveling through the trabecular bone cube sample. Two QUS parameters, ultrasound attenuation (ATT) and ultrasound velocity (UV) were calculated using the classic substitution method (Langton et al., 1984). ATT is calculated using the following equation:

$$ATT = 10\log_{10}\left(\frac{I_1}{I_2}\right) \tag{5.1}$$

Where $I_1$ and $I_2$ are the intensity of reference and sample wave, calculated by integrating the amplitude of the received pulse over time. UV is calculated using the following equation:

$$UV = \frac{C_r d}{d - C_r \Delta t} \tag{5.2}$$

Where $C_r$ is the velocity of ultrasound in water, $\Delta t$ is the arrival time difference between reference and sample wave and $d$ is the diameter of the bone sample. In this study, the first high peak of the fast wave is used as the landmark to calculate the time difference $\Delta t$.

#### 5.2.2.2 Reflection mode QUS measurement

The reflection mode ultrasound scan was utilized to measure the thickness of trabecular bone for each scanning angle. In this mode, the echo of the ultrasound wave off of the surface of the bone cube sample is picked up by the same transducer which emitted the ultrasound wave. The same measurement was repeated using both transducers to calculate the distance between the transducers and bone cube, $d_1$ and $d_2$:

$$d_1 = C_r t_1$$
$$d_2 = C_r t_2 \tag{5.3}$$

Where $C_r$ is the velocity of ultrasound in water, $t_1$ and $t_2$ are the time taken for the ultrasound pulses from both transducers to bounce back off the surface of the bone cube and return to the transducers. With $d_1$ and $d_2$, the thickness of the bone cube $d$ was calculated:

$$d = D - d_1 - d_2 \tag{5.4}$$

Where $D$ is the distance between the two transducers, 101.6 mm. Figure 17 (b) illustrates the relation of the measuring of the distances. Then, the calculated bone cube thickness $d$ was used in equation (5.2) to calculate the ultrasound velocity and normalize the ultrasound attenuation calculated using equation (5.1).

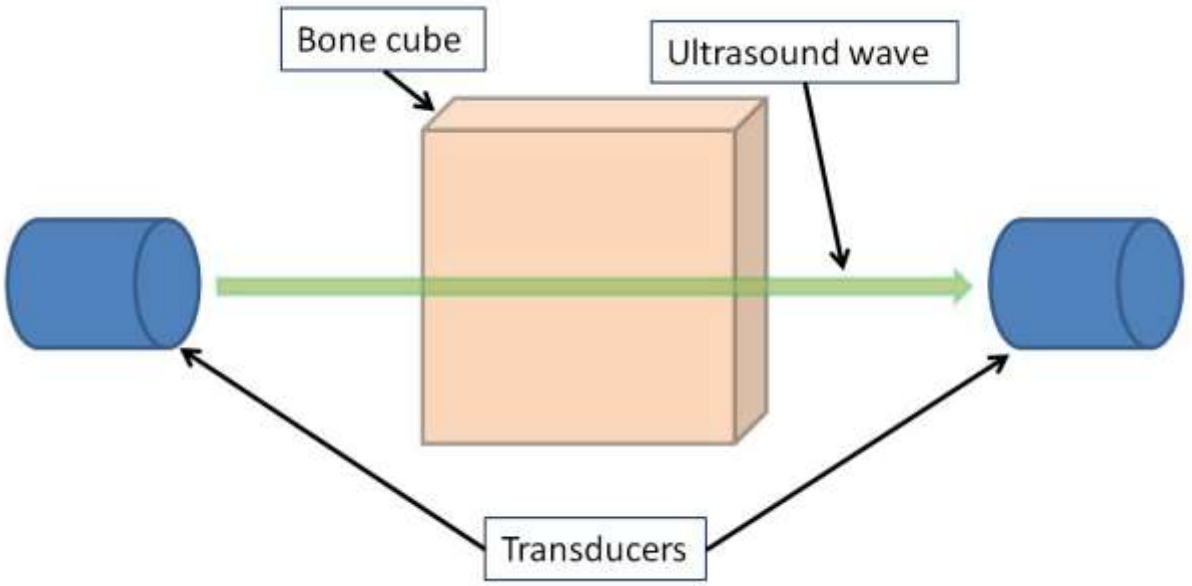


(a)

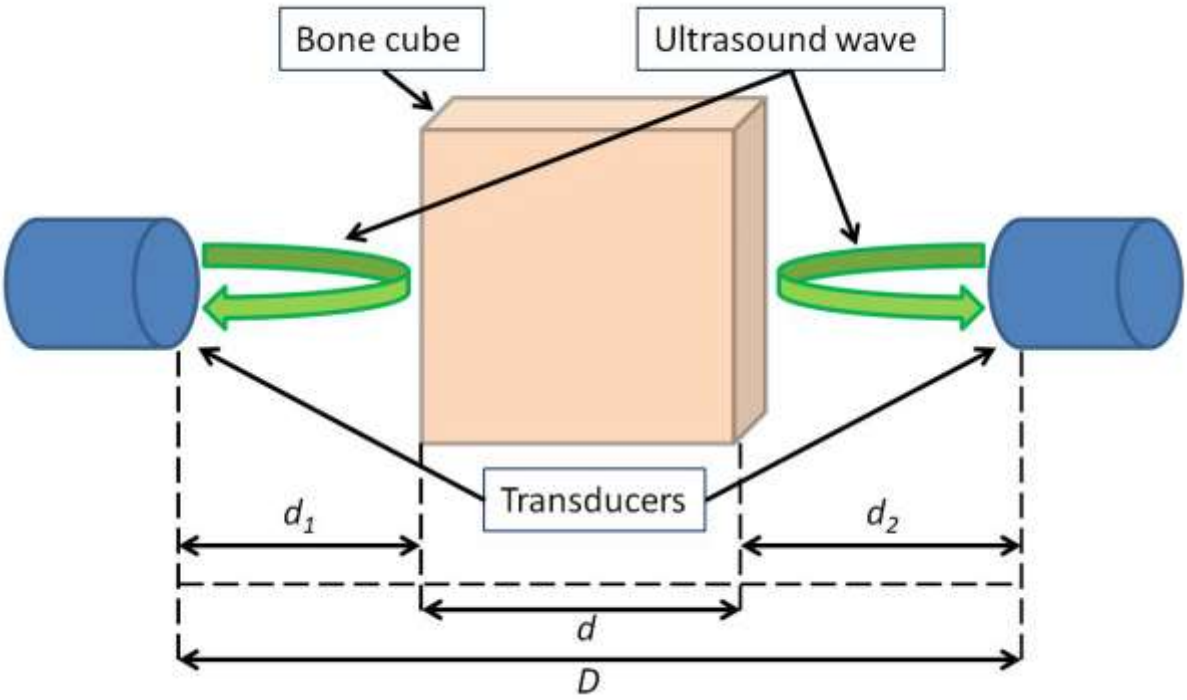


(b)

Figure 17 - Schematic representation of (a) transmission mode QUS measurement and (b) reflection mode measurement. For transmission mode, ultrasound wave is emitted by one transducer and received by the other transducer on the side of the sample after propagating through the sample. For reflection mode, each transducer emits its own ultrasound wave signal and picks up the echo bounced back off the surface of the sample. Based on the time of flight of the echo, the distances between the sample surface and the transducer, $d_1$ and $d_2$, can be determined. The sample thickness can also be calculated, given the distance between two transducers $D$.

5.2.2.3 Combination of transmission and reflection modes of QUS measurement

The attenuation data from the transmission mode QUS measurement was normalized to the sample thickness in the corresponding scanning angle, which was obtained from the reflection mode QUS measurement. Ultrasound velocity in transmission mode was also calculated based on the sample thickness from reflection mode measurement. For attenuation, the angle with the highest normalized attenuation value was considered to be along the structural orientation of the trabecular architecture. The normalized attenuation value was denoted as $ATT_{T\text{-}R}$, while the conventional attenuation value in the medial-lateral orientation was denoted as $ATT_{M\text{-}L}$. The same calculation was also applied to the ultrasound velocity data. The highest

normalized velocity value among all scanning angles was denoted as $ATT_{T-R}$, and the velocity value in the medial-lateral orientation was denoted as $UV_{M-L}$.

### 5.2.3 μCT imaging

μCT imaging with a resolution of 30 μm was performed on each trabecular bone cube using a *μCT 40* system (SCANCO Medical AG, Brüttisellen, Switzerland) to analyze the structural properties, such as structural model index (SMI), bone volume fraction (BV/TV), bone surface density (BS/BV), trabecular bone number (Tb.N), trabecular thickness (Tb.Th), trabecular spacing (Tb.Sp) and degree of anisotropy (DA).

### 5.2.4 Compressive mechanical loading

Compressive mechanical loading was performed on a MTS MiniBionix 858 (MTS Corporation, Minneapolis, MN) axial load frame with TestStar II control software and a SMT2-2000N load cell (Interface Inc., Scottsdale, AZ). A smooth curved nail head was placed on the top surface of the bone cube to guide the loading force from the loading piston along the normal orientation of the bone cube surface. This method overcame the slight deviation from the parallelism between the top and bottom surfaces of the bone cube (Mittra et al., 2008). The loading protocol began with a 50 N preload to make sure full contact between interfaces and eliminate effects caused by the surface conditions of the samples. The loading then proceeded for 2,000 μstrain at the rate of 0.005 mm/s to minimize the effect caused by the viscosity of bone material. The loading piston retreated back after the compressive loading, and the same loading cycle was repeated for 5 times. The force and displacement data recorded by the system was then used to calculate the Young's modulus ($E$) of the bone cube using the following equation:

$$E = \frac{Fd}{lA} \tag{5.5}$$

Where $F$ is the loading force of the piston, $l$ is the displacement of the loading piston, $d$ is the thickness of the sample and $A$ is the cross section area perpendicular to the loading orientation.

### 5.2.5 Data analysis

Linear correlation analysis was performed between the ultrasound parameters and the structural parameters, and between the ultrasound parameters and the mechanical property. Further analysis of covariance (ANCOVA) was made between the correlations of conventional QUS scan in medial-lateral orientation and the combined transmission-reflection method to evaluate the improvement of adapting the new QUS method. ANCOVA was performed using SPSS, in which p-value less than 0.05 was considered significant.

## 5.3 Results

The thickness of the bone cubes in medial-lateral orientation was measured using a caliper to validate the accuracy of the reflection mode ultrasound scan. The reflection mode QUS demonstrated significant agreement with the thickness determined by caliper with correlation coefficient $R^2$=0.87 (Figure 18). The mean, standard deviation, range and the 95% confidence interval of the structural, mechanical and QUS parameters are listed in Table 6.

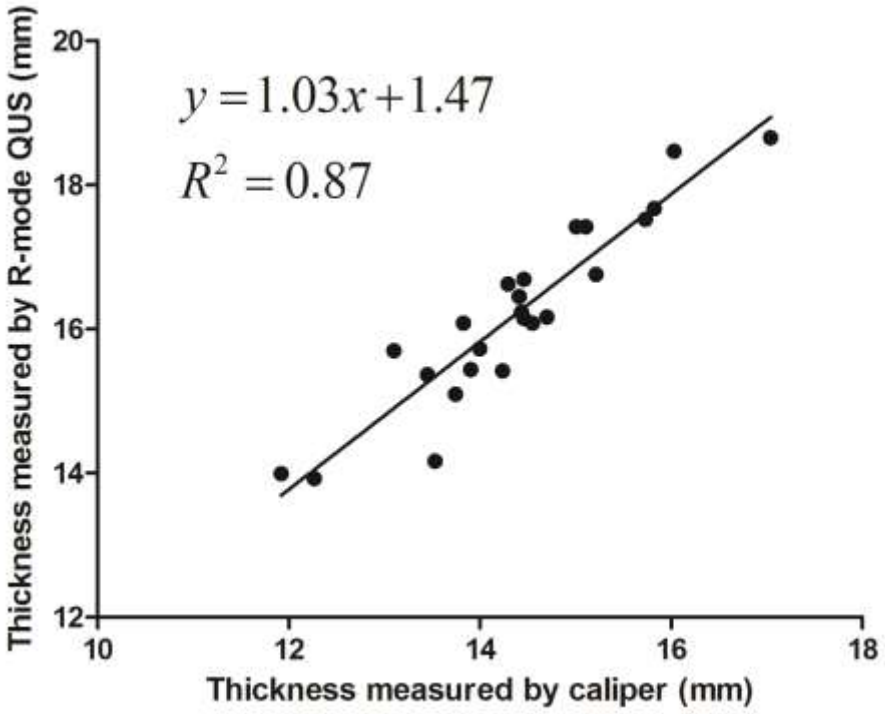


Figure 18 - Linear regression analysis of the sample thickness measured by caliper and reflection mode QUS shows high linear correlation ($R^2$ = 0.87). This high correlation between two measurements validates the accuracy of the reflection mode QUS measurement.

Table 6 - Mean, standard deviation, maximum, minimum and the 95% confidence interval of the measured structural, mechanical and QUS parameters.

| | Mean | SD | Maximum | Minimum | 95% CI |
|---|---|---|---|---|---|
| Structural | | | | | |
| SMI | -0.43 | 1.06 | 1.51 | -2.12 | -0.85 - 0.00 |
| BV/TV | 0.39 | 0.10 | 0.54 | 0.18 | 0.35 - 0.43 |
| BS/BV (1/mm) | 10.01 | 2.27 | 14.77 | 6.71 | 9.11 - 10.92 |

| | | | | | |
|---|---|---|---|---|---|
| Tb.N (1/mm) | 1.85 | 0.20 | 2.24 | 1.33 | 1.77 - 1.93 |
| Tb.Th (mm) | 0.21 | 0.05 | 0.30 | 0.14 | 0.19 - 0.23 |
| Tb.Sp (mm) | 0.34 | 0.09 | 0.62 | 0.23 | 0.30 - 0.38 |
| DA | 1.69 | 0.29 | 2.39 | 1.32 | 1.57 - 1.81 |
| Mechanical Modulus (MPa) | 304.16 | 73.07 | 444.86 | 120.06 | 274.92 - 333.39 |
| QUS (transverse) | | | | | |
| $ATT_{M-L}$ (dB/mm) | 0.83 | 0.16 | 1.15 | 0.60 | 0.77 – 0.90 |
| $ATT_{T-R}$ (dB/mm) | 0.95 | 0.19 | 1.30 | 0.60 | 0.87 - 1.02 |
| $UV_{M-L}$ (mm/s) | 1566.84 | 67.28 | 1728.80 | 1454.13 | 1539.93 - 1593.76 |
| $UV_{T-R}$ (mm/s) | 1600.28 | 76.87 | 1777.05 | 1484.87 | 1569.53 - 1631.04 |
| QUS (frontal) | | | | | |
| $ATT_{M-L}$ (dB/mm) | 0.86 | 0.18 | 1.25 | 0.58 | 0.79 - 0.93 |
| $ATT_{T-R}$ (dB/mm) | 0.96 | 0.19 | 1.33 | 0.61 | 0.89 - 1.04 |
| $UV_{M-L}$ (mm/s) | 1577.41 | 75.42 | 1731.35 | 1446.00 | 1547.23 - 1607.58 |
| $UV_{T-R}$ (mm/s) | 1626.40 | 86.27 | 1779.96 | 1487.80 | 1591.88 - 1660.91 |

### 5.3.1 QUS measurement on transverse plane

The transmission ATT data was normalized to the sample thickness obtained from reflection mode measurement. On transverse plane, the average of $ATT_{M-L}$ was $0.83 \pm 0.16$ dB/mm, significantly 12% lower than the average of $ATT_{T-R}$, $0.94 \pm 0.19$ dB/mm ($p<0.05$). The linear correlation between $ATT_{M-L}$ and $ATT_{T-R}$ was significant ($R^2=0.79$, $p<0.001$). For ultrasound velocity, the average of $UV_{M-L}$ $1566.84 \pm 67.28$ m/s was only 2% lower than the average of $UV_{T-R}$, $1600.28 \pm 76.87$ m/s, and the linear correlation between them was also significant ($R^2=0.86$, $p<0.001$).

The correlation between ultrasound parameters and both structural and mechanical parameters are listed in Table 7. No significant correlation was found between QUS parameters and degree of anisotropy. All other structural or mechanical parameters have significant correlation with at least one QUS parameter, either ATT or UV.

Table 7 - Linear correlation coefficient (R) between QUS parameters on transverse plane and structural and mechanical parameters. All structural or mechanical parameters have significant correlations with at least one QUS parameters, except for DA.

| | $ATT_{M-L}$ (dB/mm) | $ATT_{T-R}$ (dB/mm) | $UV_{M-L}$ (mm/s) | $UV_{T-R}$ (mm/s) |
|---|---|---|---|---|
| SMI | -0.66*** | -0.70*** | -0.47* | -0.46* |

| | | | | |
|---|---|---|---|---|
| BV/TV | 0.68*** | 0.73*** | 0.44* | 0.45* |
| BS/BV (1/mm) | -0.62** | -0.73*** | -0.35 | -0.40 |
| Tb.N (1/mm) | 0.56** | 0.48* | 0.58** | 0.46* |
| Tb.Th (mm) | 0.59** | 0.72*** | 0.29 | 0.36 |
| Tb.Sp (mm) | -0.69*** | -0.71*** | -0.54** | -0.49* |
| DA | 0.12 | 0.24 | 0.02 | 0.13 |
| Modulus (MPa) | 0.61** | 0.69*** | 0.46* | 0.46* |

(* - $p<0.05$, ** - $p<0.01$, *** - $p<0.001$)

ANCOVA test showed that $ATT_{T-R}$ has significant higher correlations with BS/BV ($p<0.05$), Tb.Th ($p<0.01$) and DA ($p<0.05$), when compared to $ATT_{M-L}$ (

Table 8). As for ultrasound velocity measurement, $UV_{T-R}$ only showed significantly improved prediction for Tb.N ($p<0.05$) and Tb.Th ($p<0.001$), when compared to $UV_{M-L}$ (Table 9).

Table 8 - Comparison of the correlation coefficients (R) between ultrasound attenuation on transverse plane and structural and mechanical parameters shows that $ATT_{T-R}$ has significant better prediction for BS/BV, Tb.Th and DA than $ATT_{M-L}$.

| | $ATT_{M-L}$ | $ATT_{T-R}$ | p |
|---|---|---|---|
| SMI | -0.66 | -0.70 | N.S. |
| BV/TV | 0.68 | 0.73 | N.S. |
| BS/BV (1/mm) | -0.62 | -0.73 | <0.05 |
| Tb.N (1/mm) | 0.56 | 0.48 | N.S. |
| Tb.Th (mm) | 0.59 | 0.72 | <0.01 |
| Tb.Sp (mm) | -0.69 | -0.71 | N.S. |
| DA | 0.12 | 0.24 | <0.05 |
| Modulus (MPa) | 0.61 | 0.69 | N.S. |

Table 9 - Comparison of the correlation coefficients (R) between ultrasound velocity on transverse plane and structural and mechanical parameters shows that $UV_{T-R}$ has significant better prediction for Tb.N and Tb.Th than $UV_{M-L}$.

| | $UV_{M-L}$ | $UV_{T-R}$ | p |
|---|---|---|---|
| SMI | -0.47 | -0.46 | N.S. |
| BV/TV | 0.44 | 0.45 | N.S. |
| BS/BV (1/mm) | -0.35 | -0.40 | N.S. |
| Tb.N (1/mm) | 0.58 | 0.46 | <0.05 |
| Tb.Th (mm) | 0.29 | 0.36 | <0.001 |
| Tb.Sp (mm) | -0.54 | -0.49 | N.S. |
| DA | 0.02 | 0.13 | N.S. |
| Modulus (MPa) | 0.46 | 0.46 | N.S. |

### 5.3.2 QUS measurement on frontal plane

For QUS measurement in the frontal plane, the average of $ATT_{M-L}$ was $0.86 \pm 0.17$ dB/mm, 10.37% lower than the average of $ATT_{T-R}$, $0.96 \pm 0.19$ dB/mm. The linear correlation between $ATT_{M-L}$ and $ATT_{T-R}$ was significant ($R^2=0.87$, $p<0.001$). For ultrasound velocity, the average of $UV_{M-L}$ $1581.85 \pm 73.84$ m/s was 2.3% lower than the average of $UV_{T-R}$, $1619.72 \pm 81.62$ m/s, and the linear correlation between them was also significant ($R^2=0.91$, $p<0.001$).

The correlation between ultrasound parameters and both structural and mechanical parameters are listed in Table 10. No significant correlation was found between QUS parameters

and degree of anisotropy. All other structural or mechanical parameters had significant correlation with both ATT and UV. Furthermore, almost all correlation coefficient values from the measurement in frontal plane were higher than those from the measurement on transverse plane, excepting correlation between $ATT_{M-L}$ and Tb.N.

Table 10 - Linear correlation coefficient (R) between QUS parameters on frontal plane and structural and mechanical parameters. All structural or mechanical parameters have significant correlations with QUS parameters, except for DA.

| | $ATT_{M-L}$ (dB/mm) | $ATT_{T-R}$ (dB/mm) | $UV_{M-L}$ (mm/s) | $UV_{T-R}$ (mm/s) |
|---|---|---|---|---|
| SMI | -0.73*** | -0.81*** | -0.67*** | -0.75*** |
| BV/TV | 0.75*** | 0.83*** | 0.73*** | 0.79*** |
| BS/BV (1/mm) | -0.69*** | -0.81*** | 0.56** | -0.64*** |
| Tb.N (1/mm) | 0.56** | 0.58** | 0.59** | 0.62** |
| Tb.Th (mm) | 0.67*** | 0.80*** | 0.52** | 0.62** |
| Tb.Sp (mm) | -0.74*** | -0.79*** | -0.66*** | -0.73*** |
| DA | 0.19 | 0.35 | 0.28 | 0.24 |
| Modulus (MPa) | 0.61** | 0.73*** | 0.50* | 0.59** |

(* - $p<0.05$, ** - $p<0.01$, *** - $p<0.001$)

Combined transmission-reflection QUS measurement showed significantly improved correlation with mechanical and structural parameters in the frontal plane than transverse plane measurement. $ATT_{T-R}$ had significantly higher correlations with SMI ($p<0.01$), BV/TV ($p<0.01$), BS/BV ($p<0.001$), Tb.Th ($p<0.001$), DA ($p<0.05$) and Young's Modulus ($p<0.001$), when compared to $ATT_{M-L}$ (Table 11). As for ultrasound velocity measurement, $UV_{T-R}$ showed significantly improved prediction for SMI ($p<0.01$), BV/TV ($p<0.05$), BS/BV ($p<0.05$), Tb.Th ($p<0.01$), Tb.Sp ($p<0.05$) and Young's Modulus ($p<0.01$), when compared to $UV_{M-L}$ (Table 12).

Table 11 - Comparison of the correlation coefficients (R) between ultrasound attenuation on frontal plane and structural and mechanical parameters shows that $ATT_{T-R}$ has significant better prediction for SMI, BV/TV, BS/BV, Tb.Th, DA and Modulus than $ATT_{M-L}$.

| | $ATT_{M-L}$ | $ATT_{T-R}$ | p |
|---|---|---|---|
| SMI | -0.73 | -0.81 | <0.01 |
| BV/TV | 0.75 | 0.83 | <0.01 |
| BS/BV (1/mm) | -0.69 | -0.81 | <0.001 |
| Tb.N (1/mm) | 0.56 | 0.58 | N.S. |
| Tb.Th (mm) | 0.67 | 0.80 | <0.001 |
| Tb.Sp (mm) | -0.74 | -0.79 | N.S. |

| | | | |
|---|---|---|---|
| DA | 0.19 | 0.35 | <0.001 |
| Modulus (MPa) | 0.61 | 0.73 | <0.001 |

Table 12 - Comparison of the correlation coefficients (R) between ultrasound velocity on frontal plane and structural and mechanical parameters shows that $UV_{T-R}$ has significant better prediction for SMI, BV/TV, BS/BV, Tb.Th, Tb.Sp and Modulus than $UV_{M-L}$.

| | $UV_{M-L}$ | $UV_{T-R}$ | p |
|---|---|---|---|
| SMI | -0.67 | -0.75 | <0.01 |
| BV/TV | 0.73 | 0.79 | <0.05 |
| BS/BV (1/mm) | -0.56 | -0.64 | <0.05 |
| Tb.N (1/mm) | 0.59 | 0.62 | N.S. |
| Tb.Th (mm) | 0.52 | 0.62 | <0.01 |
| Tb.Sp (mm) | -0.66 | -0.73 | <0.05 |
| DA | 0.28 | 0.24 | N.S. |
| Modulus (MPa) | 0.50 | 0.59 | <0.01 |

## 5.4 Discussion

This study is designed to combine transmission and reflection modes of QUS measurement to improve the prediction for the structural and mechanical properties of trabecular bone. Our previous works have shown that the correlation between QUS measurement and mechanical strength of trabecular bone is highly orientation-dependent, in the manner that the orientation in which ultrasound attenuation and velocity peak has the highest mechanical strength (Lin et al., 2012, Lin et al., 2014). These previous results were obtained from ideal spherical trabecular bone specimens or models, of which sample thickness remained the same for all measuring orientations. To progress from ideal model to realistic bone geometry, this present study employs cubic trabecular bone sample as an interim model to explore the feasibility of applying QUS technique on real human bones. The cubic model gives rise to the need of taking the varying sample thickness in different scanning orientations into consideration. Reflection mode QUS is a well-established method of measuring the distance between an object and the ultrasound transducer, based on the time of flight of the reflected echo. The high linear correlation shown in Figure 18 between the medial-lateral thickness measured by caliper and reflection mode QUS validated the accuracy of such distance measurement.

The intended application of this technique is to scan clinically critical sites very rich in trabecular bone that have high fracture risk, such as the human calcaneus. As mentioned before, the current QUS protocol for calcaneus only includes scanning in the medial-lateral orientation, in which the results may not be the best predictor for the mechanical strength. Considering the physiological location of calcaneus and its surrounding structure, QUS in the frontal and transverse planes was performed to evaluate the efficacy of this combined QUS measurement and to develop the proper protocol to apply it. As shown in Table 8, Table 9, Table 11 and Table 12, linear correlations between QUS and structural and mechanical properties in the frontal plane are generally higher than those in the transverse plane. This trend is expected because the frontal plane is more aligned to the weight bearing orientation, provided that the samples used in this study are from bovine distal femur, and the future intended measuring site is human calcaneus. It is also observed that significant prediction of elastic modulus was only found in measurement in the frontal plane, not in the transverse plane. This finding supports that measurement in the

frontal plane is a better configuration and can provide information more relevant to the mechanical properties than the transverse plane.

Most structural and mechanical parameters have significant correlations with both QUS parameters and in both anatomical planes, except for DA. Degree of anisotropy, defined as the ratio of the longest vector of the mean intercept length (MIL) tensor over the shortest vector, is based on the calculation of MIL tensor (Whitehouse, 1974). Therefore to obtain a reliable prediction of degree of anisotropy using QUS, a complete 3-D measurement over the specimen is required. In this study, QUS measurement was only performed on 2 anatomical planes and within a 60° angle range, and was not able to ensure that the longest and shortest vector of MIL tensor were included in the scanning orientations. While this confined scanning range is a limitation of this QUS technique, it is also realistic, given the fact that full 360° QUS is not possible on any of the 3 anatomical planes for human calcaneus because of the existence of other bones like tibia and tarsal bones. Therefore, a confined 60° scanning angle range in the frontal and transverse plane is a practical approach to collect orientation-dependent QUS information in a physiologically feasible configuration.

The results show that combined transmission-reflection QUS significantly improves the ability to determine the structural and mechanical properties when compared to the conventional QUS measurement in medial lateral orientation. This improvement is achieved by taking additional consideration of the different sample thickness in different scanning orientations and the fact that QUS information more aligned to the weight bearing orientation is more correlated with the mechanical strength. Figure 19 (a) details the attenuation data in the frontal plane of a bone cube sample before being normalized to the samples thickness. From all the scanning orientations, medial-lateral (0°) has the lowest attenuation value (12.79 dB), whereas measurements in +30° and -30° orientations have relatively higher values (15.42 dB and 15.61 dB). The longer sample thickness in these orientations contributed to the higher ultrasound attenuation values. By normalizing the attenuation values to the corresponding sample thicknesses, the data in Figure 19 (b) shows that QUS measurements at +30° have the highest normalized attenuation value (0.86 dB/mm) and are chosen to represent this sample in the correlation analysis with structural and mechanical properties. As shown in Figure 20, this method significantly improved the correlation between ultrasound attenuation and BV/TV. The

same mechanism applies to the ultrasound velocity analysis, in which sample thickness plays an intrinsically important role in the calculation process, as indicated in equation (5.2). It has been reported by Xia et al. (Xia et al., 2007) that a subtle change in sample thickness can cause significant difference in ultrasound velocity calculation, which implies that simply assume a uniform sample thickness for ultrasound measurement can cause error that leads to inaccurate prediction for bone strength and fracture risk.

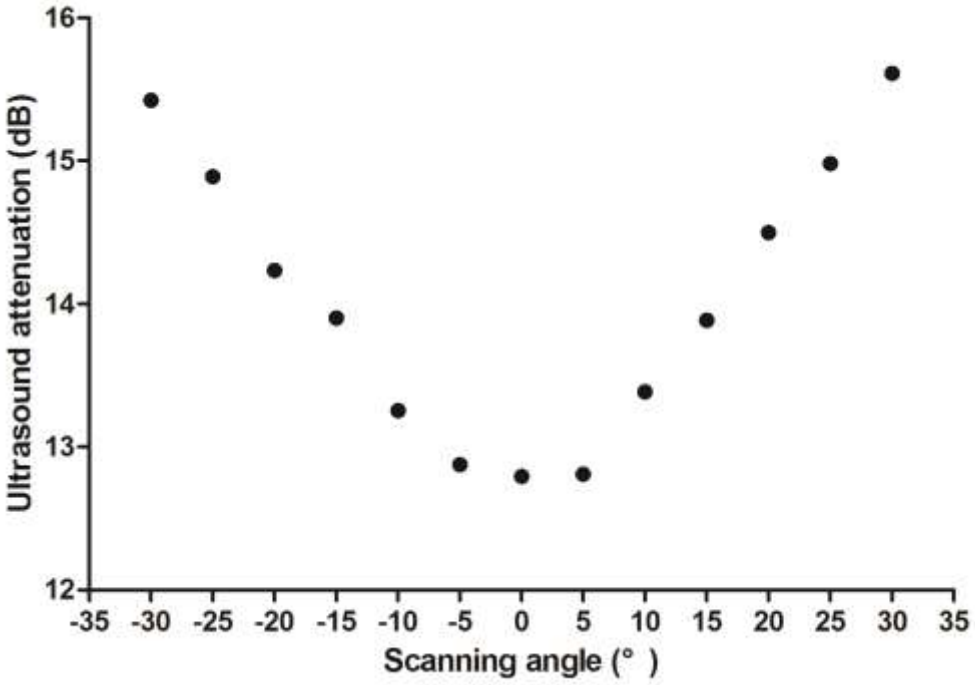


(a)

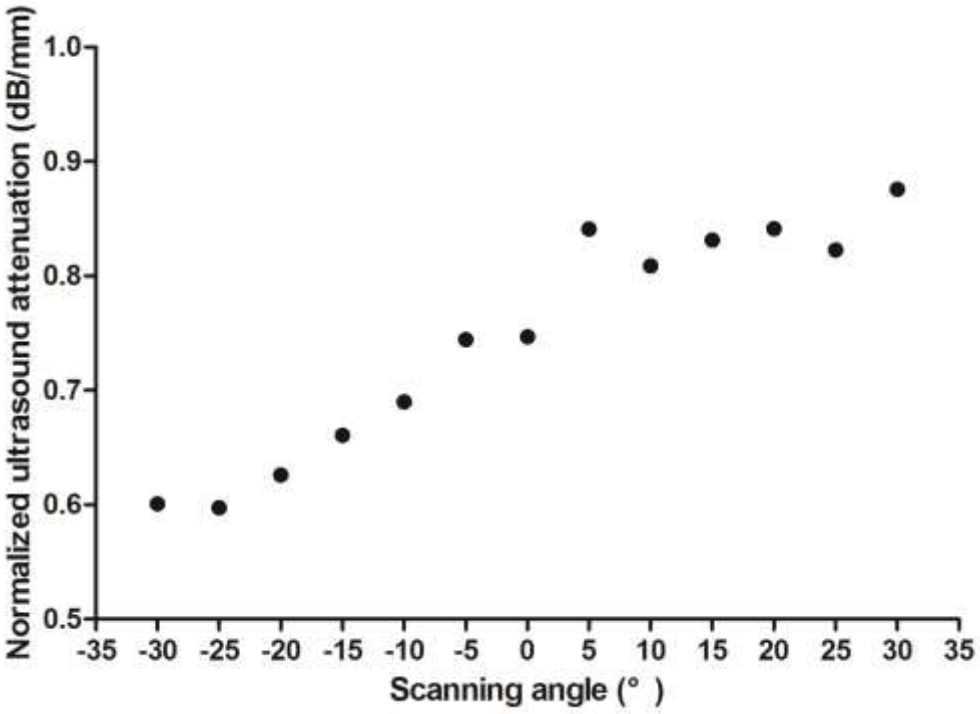


(b)

Figure 19 - Attenuation values of a bone cube sample in all scanning angles on frontal plane (a) before and (b) after normalization the sample thickness in each scanning angle. Before normalization, medial-lateral orientation (0°) has the loweat attenuation value (12.79 dB), whereas measurements in +30° and -30° orientations have relatively higher values (15.42 dB and 15.61 dB). After normalization, QUS measurement in +30° has the highest normalized attenuation value (0.86 dB/mm) and is chosen to represent this sample in the correlation analysis with structural and mechanical properties.

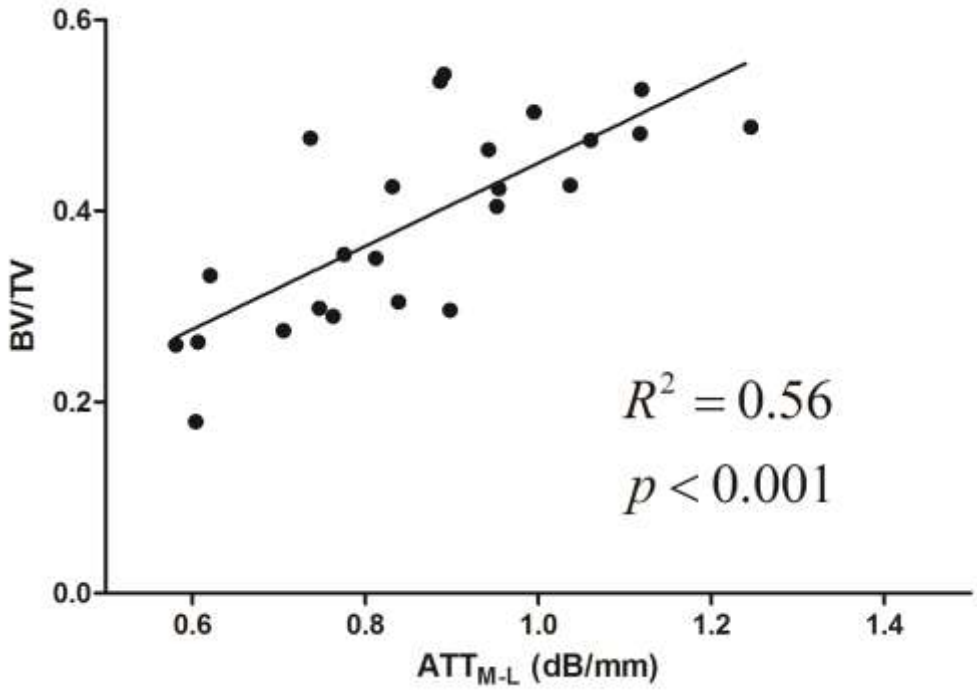


(a)

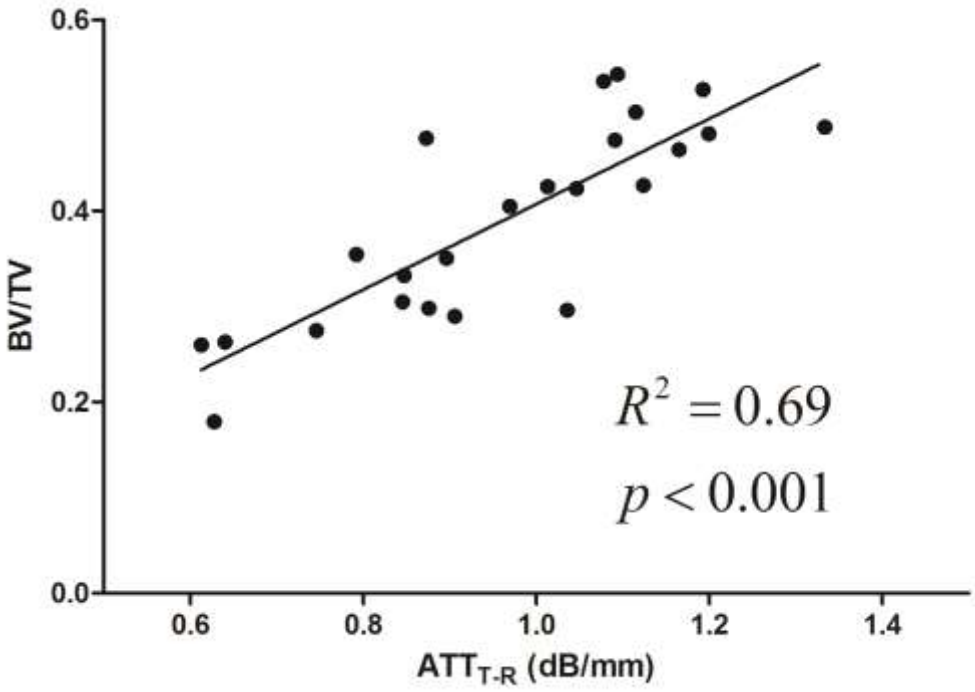


(b)

Figure 20 - Linear correlation between ultrasound attenuation (ATT) and bone volume fraction (BV/TV) using (a) traditional QUS ($ATT_{M-L}$) in medial-lateral orientation and (b) combined transmission-reflection QUS ($ATT_{T-R}$) in the frontal plane. Correlation of $ATT_{T-R}$ vs. BV/TV ($R^2 = 0.69$) is significantly higher than $ATT_{M-L}$ vs. BV/TV ($R^2 = 0.56$), $p<0.01$.

## 5.5 Conclusion

Reflection mode QUS scanning can accurately measure the sample thickness in different scanning orientations; such sample thickness can be used to normalize the transmission mode QUS data, thus to determine the peak normalized QUS parameters. The normalized QUS values demonstrate significantly improved correlations with structural and mechanical properties of trabecular bone, when compared to the QUS values obtained from current QUS measurement protocol. This improvement indicates that better prediction for bone strength and fracture risk can be achieved by applying this combined transmission-reflection QUS measurement in proper clinical environment.

# 6 Trabecular Bone Architectural and Strength Assessment with Angle Sensitive Transmission and Reflection Measurement in Human Calcaneus using Quantitative Ultrasound

## 6.1 Introduction

Quantitative ultrasound (QUS) is capable of quantifying fracture risk (Bauer et al., 1997, Hadji et al., 2000, Huopio et al., 2004), as well as predict fracture type (Drozdzowska and Pluskiewicz, 2002). Ultrasound velocity and attenuation are the two primary QUS parameters used in predicting structural and mechanical properties of bone, such as density, elastic modulus and anisotropy (Njeh et al., 1999, Laugier, 2006). These parameters are heavily influenced by not only the quantity of bone mass, but also the macroarchitecture and alignment of trabeculae (Mizuno et al., 2010). The anisotropic structure of trabecular bone is the result of adaptation to its mechanical milieu, according to "Wolff's Law" (Wolff, 1896). Recent studies describe the interaction between trabecular bone structural alignment and ultrasound wave (Cardoso and Cowin, 2011, Cardoso and Cowin, 2012, Cowin and Cardoso, 2011, Lee et al., 2007, Mizuno et al., 2009, Mizuno et al., 2008, Mizuno et al., 2010, Hosokawa and Otani, 1998, Han and Rho, 1998, Hosokawa, 2009b, Hosokawa, 2010, Hosokawa, 2011b, Hosokawa, 2011a, Liu et al., 2014). These data suggested that QUS is sensitive enough to pick up the difference of structural and mechanical properties of trabecular bone in different orientations, and generally provide more comprehensive information of bone "quality," such as architecture and strength of bone, than simply bone "quantity," e.g., bone density.

With the current technology, it is estimated that nearly 80% of the variation of QUS parameters can be explained by bone quantity with an additional 8-17% contributed by bone architectural parameters (Nicholson et al., 2001, Cortet et al., 2004), which means 50-70% of the variation of bone elasticity and strength can be predicted by QUS parameters (Langton et al., 1996, Han et al., 1997, Bouxsein and Radloff, 1997, Hakulinen et al., 2005, Toyras et al., 2002), leaving a big margin for technical improvement. As the most popular site for *in vivo* QUS measurement, human calcaneus is easily accessible and constituted by 90% trabecular bone, which can display bone metabolic changes before cortical bone due to a higher metabolic

turnover rate (Njeh et al., 1999). The relatively flat and parallel lateral surfaces and thin overlaying soft tissue are ideal for transmission mode of QUS measurement. The commonly used QUS devices for calcaneus scan adapt a transmission configuration in which a transmitter and a receiver are placed on the medial and lateral sides of the calcaneus, respectively. In this configuration, the calculation of ultrasound attenuation, as introduced by Langton *et al*. as the classic substitution method (Langton et al., 1984), utilizes a reference wave signal obtained through water to compare to the wave signal received with the human foot positioned between the two ultrasound transducers. Since BMD measured by DXA is the current gold standard for the diagnosis of osteoporosis, research has been performed to evaluate the relationship between QUS parameters and calcaneal BMD measured by DXA. The correlation coefficient (R) varied between 0.49 and 0.81 (Laugier and Haļat, 2011).

To improve the ability of QUS to correlate with BMD, mechanical properties of calcaneus, one possible solution is to take the microstructure of trabecular bone into consideration for the scanning orientation. Our group and others reported a novel QUS method using a 3-dimensional rotational ultrasound scan to predict the principal structural orientation (PSO) of spherical trabecular bone specimens (Lin et al., 2012, Mizuno et al., 2010). This work demonstrated that ultrasound has the ability to predict the trabecular structural orientation just as accurately as the current gold standard—the longest vector of mean intercept length (MIL) tensor measured using micro computed tomography (μCT). Further study utilized a finite element model of spherical trabecular bone validated the QUS prediction of PSO (Lin et al., 2014). The mechanical properties in the PSO predicted by QUS are significantly higher than the anatomical orientations and comparatively close to the longest vector of MIL tensor.

While traditional QUS measurement, especially of the human calcaneus, is performed in medial-lateral orientation, the results of our previous work indicate that QUS measurement can determine the structural alignment of trabecular bone and correlate strongly with mechanical properties of the trabecular bone. By performing ultrasound scan in the critical orientations, the prediction of mechanical properties can be improved from simply performing QUS measurement conventionally in the anatomical orientations. This present study aims to improve the correlations between QUS parameters and structural and mechanical properties of trabecular bone by performing QUS measurement in the PSO determined by QUS. To progress from an

ideal spherical bone model to a more clinically relevant configuration, human cadaver calcanei specimens are tested. To eliminate the effect caused by irregular geometry and samples thickness difference in different QUS scanning angles, reflection mode QUS as described by Xia et al. (Xia et al., 2007) is performed to measure the sample thickness in different scanning orientations. The sample thickness measured by reflection mode is combined with the transmission mode QUS scan to evaluate the structural and mechanical properties.

## 6.2 Materials and methods

### 6.2.1 Calcaneus sample preparation

55 human cadaver calcanei were harvested from the anatomical lab at Stony Brook University Medical School and were kept frozen at -40 C°. The age span of the cadavers ranged from 53 to 92. The soft tissue on the calcaneus was carefully cleaned off by using surgical scalpel. Anatomical orientations were marked on the surface of the bone samples using permanent marker.

### 6.2.2 DXA measurement

The 55 intact calcanei were scanned in a DXA machine (Hologic QDR 4500A) with the lumbar spine settings in array mode. For each sample, the volume of interested (VOI) being scanned was the posterior part where the lateral and medial surfaces are relatively flat and parallel. DXA instrument operation, data collecting and bone mineral density (BMD) calculation was all performed by certified technician from Stony Brook Osteoporosis Center.

### 6.2.3 VivaCT imaging

VivaCT imaging with a resolution of 39 μm was performed on each calcaneus using a *VivaCT 40* system (SCANCO Medical AG, Brüttisellen, Switzerland) to analyze the structural properties, such as connectivity density (Conn-Dens.), structural model index (SMI), bone volume fraction (BV/TV), bone surface density (BS/BV), trabecular bone number (Tb.N), trabecular thickness (Tb.Th), trabecular spacing (Tb.Sp) and degree of anisotropy (DA). The VOI being analyzed in the vivaCT is the same VOI in the DXA measurement for BMD.

### 6.2.4 Quantitative ultrasound measurement

Quantitative ultrasound measurements were performed by using a scanning confocal acoustic navigation (SCAN) system (Xia et al., 2007), consisted of a computer-controlled 2-dimensional scanner unit and a pair of focused transducers (V302-SU-F2.00IN, Olympus NDT Inc., Waltham, MA) with center frequency of 1 MHz. The diameter of the transducers is 25.4 mm, and the confocal length of the transducers is 50.8 mm. In order to infiltrate the calcanei with

degassed water to eliminate the air bubbles within the trabecular structure, a trabecular cylinder of 23 mm diameter was drilled out of the calcaneus along medial-lateral orientation at the relatively flat region of posterior part of the calcaneus, keeping the cortical bone plate on both ends of the bone cylinder (Figure 21). The fat marrow among the trabeculae was flushed out using dental water-pick. The trabecular bone cylinder was then put in degassed water bath in a vacuum chamber for 6 hours to ensure no air bubble is trapped in the bone cylinder.

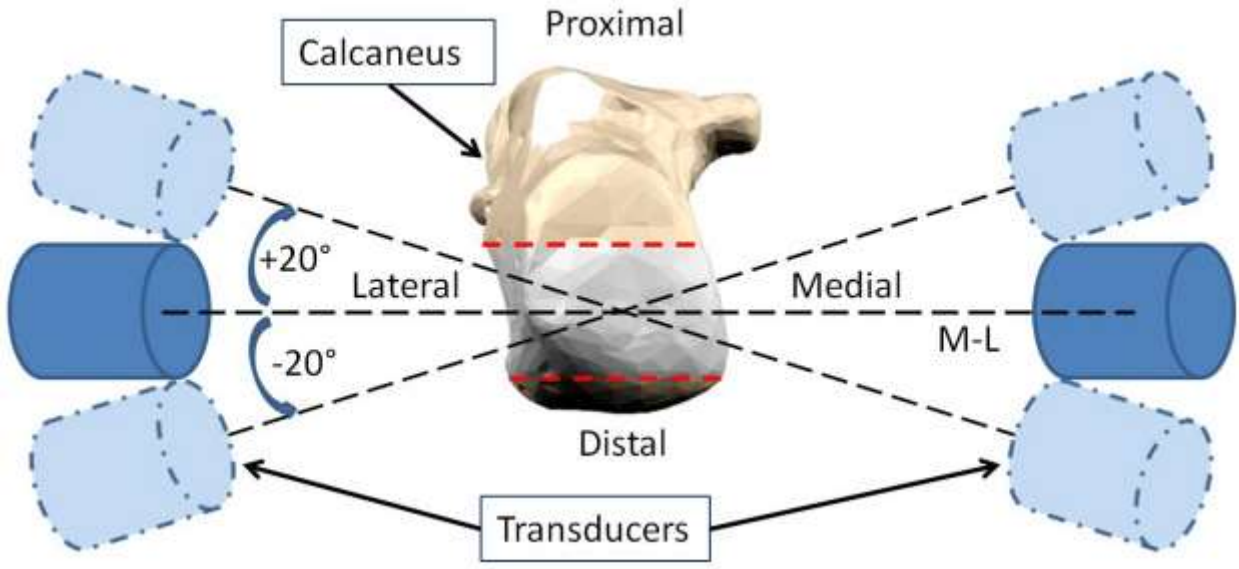


Figure 21 - Schematic representations of the QUS measurement configuration from the posterior view of the calcaneus. A cylinder of 23 was drilled out of the calcaneus along medial-lateral orientation at the relatively flat region of posterior part of the calcaneus, keeping the cortical bone plate on both ends of the bone cylinder. The cylinder is shown as the volume between two parallel dash lines in this figure. Medial-lateral (M-L) axis is used as the neutral axis, and the QUS measurement is performed is a 40° angle range, ±20° from the M-L axis. Within the 40° angle scanning range, the interval between every two scans is 5°, resulting 9 scanning angles for each sample.

During QUS measurement, the transducers were coaxially installed 101.6 mm away from each other on a rotational stage, aligning with the center of the bone cylinder which was wrapped in acoustic-wave-proof foam at the midpoint of the two transducers. QUS measurements were performed in the frontal in a defined range of angle utilizing the rotational stage. As shown in Figure 21, an angle range of 40 °, ±20 ° from medial-lateral axis, was defined with the medial-lateral axis as the neutral axis. The QUS scans were performed in this 40° range with an interval

of 5°, namely a total of 9 scans for each sample. For each scanning angle on each anatomical plane, the QUS measurement was performed in 2 different modes; transmission and reflection.

#### 6.2.4.1 Transmission mode QUS measurement

The transmission mode QUS measures the interaction between the ultrasound wave and trabecular bone, and therefore material properties of trabecular bone can be derived from the received ultrasound wave after propagating through the bone sample. As shown in Figure 22 (a), in transmission mode, an ultrasound wave was emitted by one transducer and received by another after traveling through the trabecular bone cylinder sample. Two QUS parameters, ultrasound attenuation (ATT) and ultrasound velocity (UV) were calculated using the classic substitution method (Langton et al., 1984). ATT is calculated using the following equation:

$$ATT = 10\log_{10}\left(\frac{I_1}{I_2}\right) \tag{6.1}$$

Where $I_1$ and $I_2$ are the intensity of reference and sample wave, calculated by integrating the amplitude of the received pulse over time. UV is calculated using the following equation:

$$UV = \frac{C_r d}{d - C_r \Delta t} \tag{6.2}$$

Where $C_r$ is the velocity of ultrasound in water, $\Delta t$ is the arrival time difference between reference and sample wave and $d$ is the diameter of the bone sample. In this study, the first high peak of the fast wave is used as the landmark to calculate the time difference $\Delta t$.

#### 6.2.4.2 Reflection mode QUS measurement

The reflection mode ultrasound scan was utilized to measure the thickness of trabecular bone for each scanning angle. In this mode, the echo of the ultrasound wave off of the surface of the bone cylinder sample is picked up by the same transducer which emitted the ultrasound wave. The same measurement was repeated using both transducers to calculate the distance between the transducers and bone cylinder, $d_1$ and $d_2$:

$$d_1 = C_r t_1$$
$$d_2 = C_r t_2 \tag{6.3}$$

Where $C_r$ is the velocity of ultrasound in water, $t_1$ and $t_2$ are the time taken for the ultrasound pulses from both transducers to bounce back off the surface of the bone cylinder and return to the transducers. With $d_1$ and $d_2$, the thickness of the bone cylinder $d$ was calculated:

$$d = D - d_1 - d_2 \tag{6.4}$$

Where $D$ is the distance between the two transducers, 101.6 mm. Figure 22 (b) illustrates the relation of the measuring of the distances. Then, the calculated bone cylinder thickness $d$ was used in equation (6.2) to calculate the ultrasound velocity and normalize the ultrasound attenuation calculated using equation (6.1).

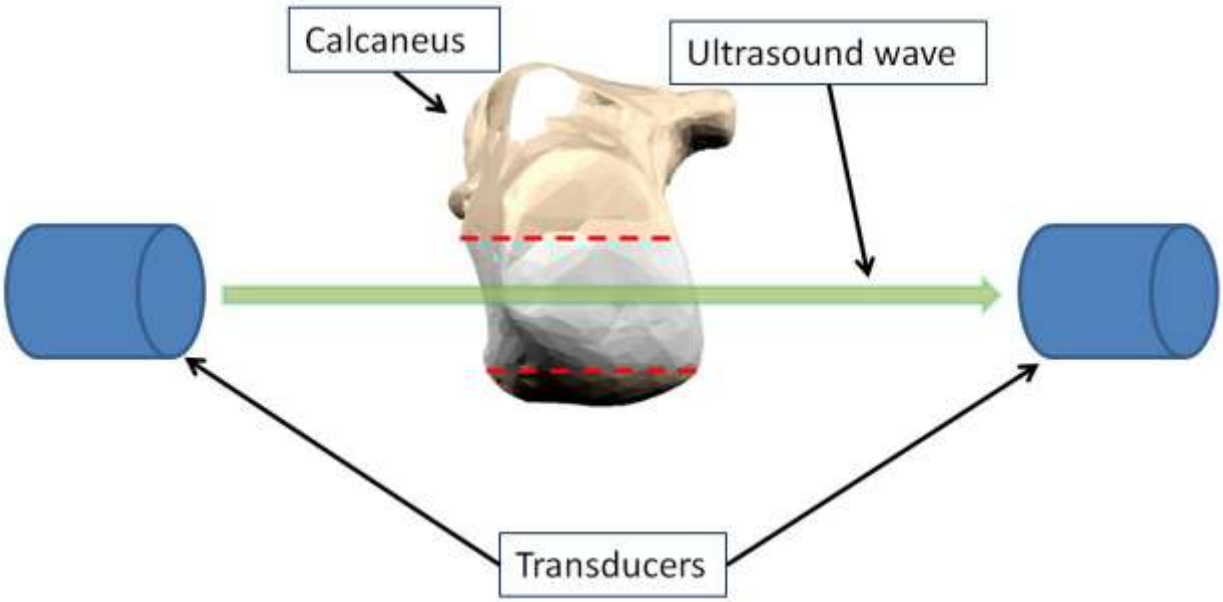


(a)

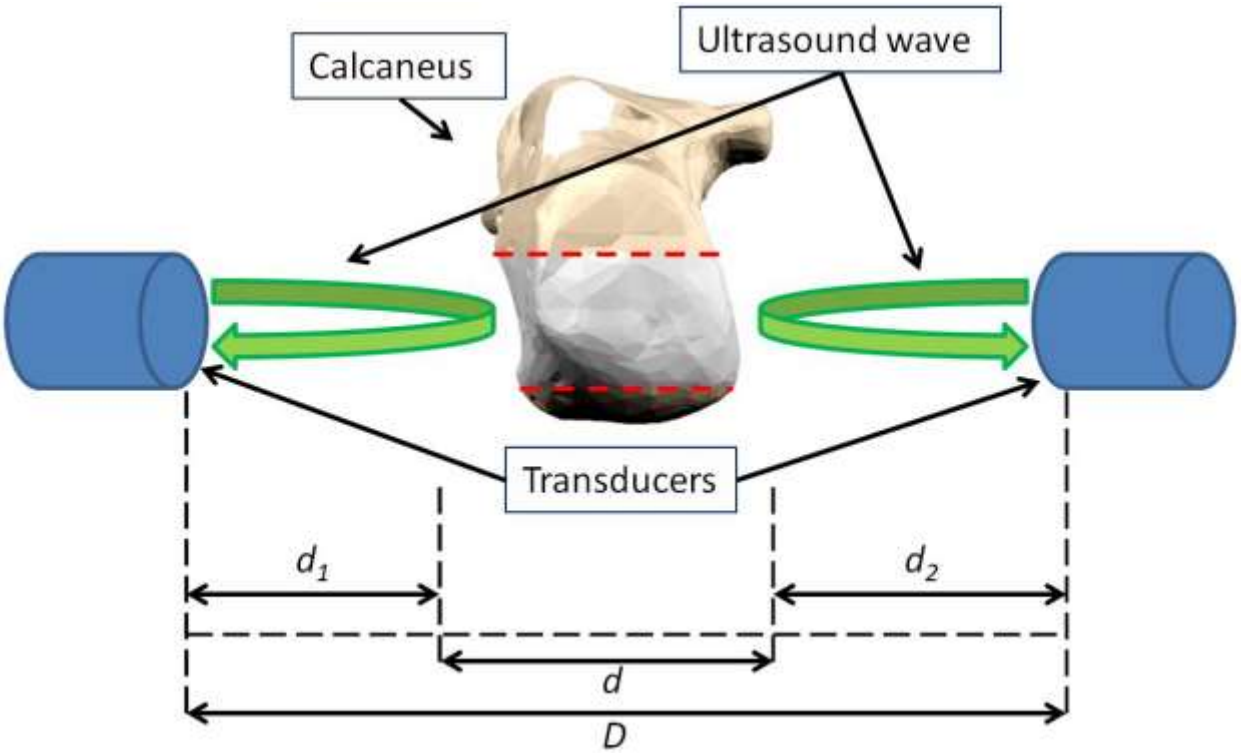


(b)

Figure 22 - Schematic representation of (a) transmission mode and (b) reflection mode QUS measurements. For transmission mode, ultrasound wave is emitted by one transducer and received by the other transducer on the side of the sample after propagating through the sample. For reflection mode, each transducer emits its own ultrasound wave signal and picks up the echo bounced back off the surface of the sample. Based on the time of flight of the echo, the distances between the sample surface and the transducer, $d_1$ and $d_2$, can be determined. The sample thickness can also be calculated, given the distance between two transducers $D$.

6.2.4.3 Combination of transmission and reflection modes of QUS measurement

The attenuation data from the transmission mode QUS measurement was normalized to the sample thickness in the corresponding scanning angle, which was obtained from the reflection mode QUS measurement. Ultrasound velocity in transmission mode was also calculated based on the sample thickness from reflection mode measurement. For attenuation, the angle with the highest normalized attenuation value was considered to be along the structural orientation of the trabecular architecture. The normalized attenuation value was denoted as $ATT_{T\text{-}R}$, while the conventional attenuation value in the medial-lateral orientation was denoted as $ATT_{M\text{-}L}$. The same calculation was also applied to the ultrasound velocity data. The highest

normalized velocity value among all scanning angles was denoted as $ATT_{T\text{-}R}$, and the velocity value in the medial-lateral orientation was denoted as $UV_{M\text{-}L}$.

### 6.2.5 Compressive mechanical loading

Compressive mechanical loading was performed on a Bose TestBench loading system (ElectroForce Group, Bose Corporation, Eden Prairie, MN) with a 100 lb load cell. A slow speed diamond saw (Microslice, Metals Research Limited, Cambridge, England) with constant water irrigation was used to cut off the uneven cortical end plates of the cylinder sample. The loading protocol began with a 10 N preload to make sure full contact between interfaces and eliminate effects caused by the surface conditions of the samples. The loading then proceeded at the rate of 0.005 mm/s to minimize the effect caused by the viscosity of bone material. The force and displacement data recorded by the system was then used to calculate the Young's modulus ($E$) of the bone cylinder using the following equation:

$$E = \frac{Fd}{lA} \tag{6.5}$$

Where $F$ is the loading force of the piston, $l$ is the displacement of the loading piston, $d$ is the thickness of the sample and $A$ is the cross section area perpendicular to the loading orientation.

### 6.2.6 Data analysis

Linear correlation analysis was performed between the ultrasound parameters and the structural parameters, and between the ultrasound parameters and the mechanical property. Further analysis of covariance (ANCOVA) was made between the correlations of conventional QUS scan in medial-lateral orientation and the combined transmission-reflection method to evaluate the improvement of adapting the new QUS method. ANCOVA was performed using SPSS, in which p-value less than 0.05 was considered significant.

## 6.3 Results

The mean, standard deviation, range and the 95% confidence interval of the structural, mechanical and QUS parameters are listed in Table 13. The transmission ATT data was normalized to the sample thickness obtained from reflection mode measurement. The average of $ATT_{M-L}$ was 0.68±0.17 dB/mm, 10.53% lower than the average of $ATT_{T-R}$, 0.76±0.19 dB/mm. The linear correlation between $ATT_{M-L}$ and $ATT_{T-R}$ was significant ($R^2$=0.89, $p<0.001$). For ultrasound velocity, the average of $UV_{M-L}$ 1539.62±55.55 m/s was 1.17% lower than the average of $UV_{T-R}$, 1557.88±63.47 m/s, and the linear correlation between them was also significant ($R^2$=0.87, $p<0.001$).

Table 13 - Mean, standard deviation, maximum, minimum and the 95% confidence interval of the measured structural, mechanical and QUS parameters.

| | Mean | SD | Maximum | Minimum | 95% CI |
|---|---|---|---|---|---|
| Structural | | | | | |
| Conn-Dens. ($1/mm^3$) | 2.05 | 0.79 | 3.5 | 0.47 | 1.84-2.25 |
| SMI | 1.42 | 0.54 | 2.8 | 0.66 | 1.28-1.56 |
| BV/TV | 0.22 | 0.08 | 0.36 | 0.05 | 0.19-0.24 |
| BS/BV (1/mm) | 10.28 | 2.28 | 16.63 | 5.84 | 9.68-10.89 |
| Tb.N (1/mm) | 1.03 | 0.26 | 1.41 | 0.37 | 0.96-1.09 |
| Tb.Th (mm) | 0.20 | 0.05 | 0.34 | 0.12 | 0.19-0.22 |
| Tb.Sp (mm) | 0.87 | 0.46 | 2.55 | 0.47 | 0.75-0.99 |
| DA | 1.70 | 0.08 | 1.91 | 1.47 | 1.68-1.72 |
| Mechanical | | | | | |
| Modulus (MPa) | 170.00 | 86.41 | 367.72 | 13.14 | 153.16-198.84 |
| Density | | | | | |
| BMD ($g/cm^2$) | 0.50 | 0.16 | 0.79 | 0.12 | 0.46-0.54 |
| QUS | | | | | |
| $ATT_{M-L}$ (dB/mm) | 0.68 | 0.17 | 1.10 | 0.26 | 0.64-0.73 |
| $ATT_{T-R}$ (dB/mm) | 0.76 | 0.19 | 1.18 | 0.34 | 0.71-0.81 |
| $UV_{M-L}$ (mm/s) | 1539.62 | 55.55 | 1667.93 | 1435.46 | 1524.94-1554.30 |
| $UV_{T-R}$ (mm/s) | 1557.88 | 63.47 | 1689.84 | 1437.28 | 1541.10-1574.65 |

The correlation between ultrasound parameters and both structural and mechanical parameters are listed in Table 14. No significant correlation was found between QUS parameters and degree of anisotropy, whereas all other structural or mechanical parameters had significant correlation with both ATT and UV. $ATT_{T-R}$ had significantly higher correlations with Conn-Dens. ($R^2$=0.17 to $R^2$=0.26, $p<0.05$), BV/TV ($R^2$=0.45 to $R^2$=0.54, $p<0.5$), Tb.N ($R^2$=0.35 to $R^2$=0.45, $p<0.05$), Tb.Sp ($R^2$=0.43 to $R^2$=0.49, $p<0.05$), Modulus ($R^2$=0.42 to $R^2$=0.54, $p<0.05$) and BMD ($R^2$=0.53 to $R^2$=0.63, $p<0.05$), when compared to $ATT_{M-L}$ (Table 15). As for ultrasound velocity measurement, $UV_{T-R}$ showed significantly improved prediction for Conn-Dens. ($R^2$=0.28 to $R^2$=0.38, $p<0.05$), BV/TV ($R^2$=0.52 to $R^2$=0.61, $P<0.05$), BS/BV ($R^2$=0.40 to $R^2$=0.57, $p<0.01$), Tb.Th ($R^2$=0.27 to $R^2$=0.47, $p<0.01$), Modulus ($R^2$=0.45 to $R^2$=0.57, $p<0.05$) and BMD ($R^2$=0.59 to $R^2$=0.65, $p<0.05$), when compared to $UV_{M-L}$ (Table 16).

Table 14 - Linear correlation coefficient (R) between QUS parameters on transverse plane and structural and mechanical parameters. All structural or mechanical parameters have significant correlations with at least one QUS parameters, except for DA. (* - $p<0.05$, ** - $p<0.01$, *** - $p<0.001$)

| | $ATT_{M-L}$ (dB/mm) | $ATT_{T-R}$ (dB/mm) | $UV_{M-L}$ (mm/s) | $UV_{T-R}$ (mm/s) |
|---|---|---|---|---|

| | | | | |
|---|---|---|---|---|
| Conn-Dens. ($1/mm^3$) | 0.41** | 0.51*** | 0.53*** | 0.62*** |
| SMI | -0.76*** | -0.77*** | -0.74*** | -0.79*** |
| BV/TV | 0.67*** | 0.73*** | 0.72*** | 0.79*** |
| BS/BV (1/mm) | -0.70*** | -0.72*** | -0.64*** | -0.75*** |
| Tb.N (1/mm) | 0.59*** | 0.67*** | 0.69*** | 0.74*** |
| Tb.Th (mm) | 0.60*** | 0.61*** | 0.52*** | 0.68*** |
| Tb.Sp (mm) | -0.65*** | -0.70*** | -0.69*** | -0.69*** |
| DA | 0.07 | 0.09 | 0.09 | 0.19 |
| Modulus (MPa) | 0.65*** | 0.73*** | 0.67*** | 0.76*** |
| BMD ($g/cm^2$) | 0.73*** | 0.79*** | 0.77*** | 0.81*** |

Table 15 - Comparison of the correlation coefficients (R) between ultrasound attenuation and structural and mechanical parameters shows that $ATT_{T-R}$ has significant better prediction for Conn-Dens., BV/TV, Tb.N, Tb.Sp, Modulus and BMD than $ATT_{M-L}$.

| | $ATT_{M-L}$ (dB/mm) | $ATT_{T-R}$ (dB/mm) | p |
|---|---|---|---|
| Conn-Dens. ($1/mm^3$) | 0.41 | 0.51 | <0.05 |
| SMI | -0.76 | -0.77 | N.S. |
| BV/TV | 0.67 | 0.73 | <0.05 |
| BS/BV (1/mm) | 0.70 | -0.72 | N.S. |
| Tb.N (1/mm) | 0.59 | 0.67 | <0.05 |
| Tb.Th (mm) | 0.60 | 0.61 | N.S. |
| Tb.Sp (mm) | -0.65 | -0.70 | <0.05 |
| DA | 0.07 | 0.09 | N.S. |
| Modulus (MPa) | 0.65 | 0.73 | <0.05 |
| BMD ($g/cm^2$) | 0.73 | 0.79 | <0.05 |

Table 16 - Comparison of the correlation coefficients (R) between ultrasound velocity on frontal plane and structural and mechanical parameters shows that $UV_{T-R}$ has significant better prediction for Conn-Dens., BV/TV, BS/BV, Tb.Th, DA, Modulus and BMD than $UV_{M-L}$.

| | $UV_{M-L}$ (mm/s) | $UV_{T-R}$ (mm/s) | p |
|---|---|---|---|
| Conn-Dens. ($1/mm^3$) | 0.53 | 0.62 | <0.05 |
| SMI | -0.74 | -0.79 | N.S. |
| BV/TV | 0.72 | 0.79 | <0.05 |
| BS/BV (1/mm) | -0.64 | -0.75 | <0.01 |
| Tb.N (1/mm) | 0.69 | 0.74 | N.S. |

| | | | |
|---|---|---|---|
| Tb.Th (mm) | 0.52 | 0.68 | <0.01 |
| Tb.Sp (mm) | -0.69 | -0.69 | N.S. |
| DA | 0.09 | 0.19 | <0.05 |
| Modulus (MPa) | 0.67 | 0.76 | <0.05 |
| BMD ($g/cm^2$) | 0.77 | 0.81 | <0.05 |

## 6.4 Discussion

QUS measurement for calcaneus had been performed in the current configuration for years. The relatively thin cortical cortex, flat and parallel geometry and richness of trabecular bone make it the most popular location for QUS measurement for prediction of bone health status (Chin and Ima-Nirwana, 2013, Floter et al., 2011). QUS for calcaneus provides a fast, non-radioactive and quantitative analysis of bone health status at low cost. However, this current configuration adopted by most commercial QUS devices only performs the measurement in medial-lateral orientation. This present study aims to design a combined transmission and reflection modes of QUS measurement for human calcaneus in an adjusted orientation, which is more relevant to the structural and mechanical properties of trabecular architecture.

Our previous works showed that the correlation between QUS measurement and mechanical strength of trabecular bone is highly orientation-dependent, in the manner that the orientation in which ultrasound attenuation and velocity peak has the highest mechanical strength (Lin et al., 2012, Lin et al., 2014). Other researchers have also demonstrated that reflection mode of QUS can also pick up the changes of structure of trabecular bone in different orientations (Liu et al., 2014). These previous results were obtained from ideal spherical or cylindrical trabecular bone specimens or models, of which sample thickness remained the same for all measuring orientations. For a bone sample with complex and irregular geometry, sample thickness in different orientation varies, which give rise to the need of taking this factor into the consideration of QUS measurement, for both *ATT* and *UV*. Reflection mode QUS is a well-established method of measuring the distance between an object and the ultrasound transducer, based on the time of flight of the reflected echo. This technique is proven to be very capable of doing surface topology and mapping even for biological samples with complex and irregular geometry, such as calcaneus (Xia et al., 2007).

In order to find the principal structural orientation of calcaneus, QUS was performed in multiple orientations in the frontal plane. Our previous QUS method included rotational QUS measurements in all 3 anatomical planes (Lin et al., 2012). Considering the physiological location of calcaneus and its surrounding structure, the frontal and transverse planes are the only feasible planes to perform QUS measurement in a confined range of angle. Furthermore, the

frontal plane is more aligned to the weight bearing orientation than the transverse plane and therefore was chosen as the measuring plane for this QUS configuration.

All structural and mechanical parameters have significant correlations with both QUS parameters, except for DA. Degree of anisotropy, defined as the ratio of the longest vector of the MIL tensor over the shortest vector, is based on the calculation of MIL tensor (Whitehouse, 1974). Therefore, to obtain a reliable prediction of degree of anisotropy using QUS, a complete 3-D measurement over the specimen is required. In this study, QUS measurement was only performed in the frontal plane and within a 40° angle range, not ensuring that the longest and shortest vectors of MIL tensor were included in the scanning orientations. While this confined scanning angle range is a limitation of this QUS technique, it is also realistic, given the fact that full 360° QUS is not feasible on any of the 3 anatomical planes for human calcaneus because of the existence of other bones like tibia and tarsal bones. Therefore, a confined 40° scanning angle range in the frontal plane is a practical approach to collect orientation-dependent QUS information in a physiologically feasible configuration.

The results show that combined transmission-reflection QUS significantly improves the ability to predict the structural and mechanical properties when compared to the conventional QUS measurement in medial-lateral orientation. This improvement is achieved by taking additional consideration of the different sample thickness in different scanning orientations and the fact that QUS information more aligned to the weight bearing orientation is more correlated with the mechanical strength. The longer sample thickness in these orientations contributed to the higher ultrasound attenuation values. As shown in Figure 23, normalizing the attenuation to the sample thickness significantly improved the correlation between ATT and BV/TV. The same mechanism applies to the ultrasound velocity analysis, in which sample thickness plays an intrinsically important role in the calculation process, as indicated in equation (6.2). It has been reported by Xia et al. (Xia et al., 2007) that a subtle change in sample thickness can cause significant difference in ultrasound velocity calculation, which implies that simply assume a uniform sample thickness for ultrasound measurement can cause error that leads to inaccurate prediction for bone strength and fracture risk. As shown in Table 13, even subtle difference between $ATT_{M\text{-}L}$ and $ATT_{T\text{-}R}$ and between $UV_{M\text{-}L}$ and $UV_{T\text{-}R}$ can cause significant difference in the correlations with density, structural and mechanical properties of trabecular bone.

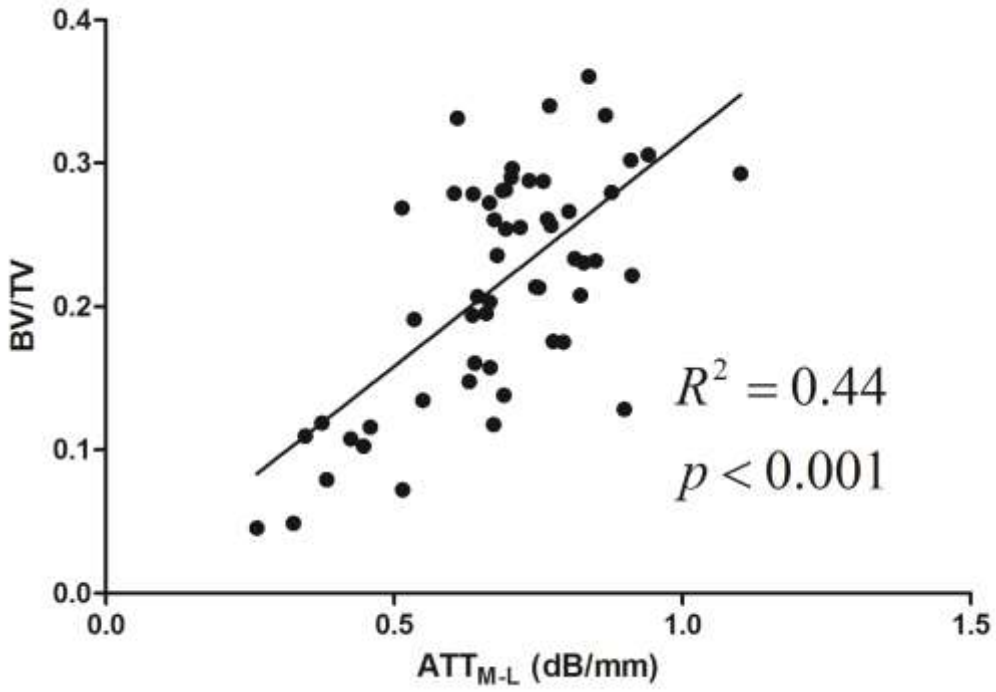


(a)

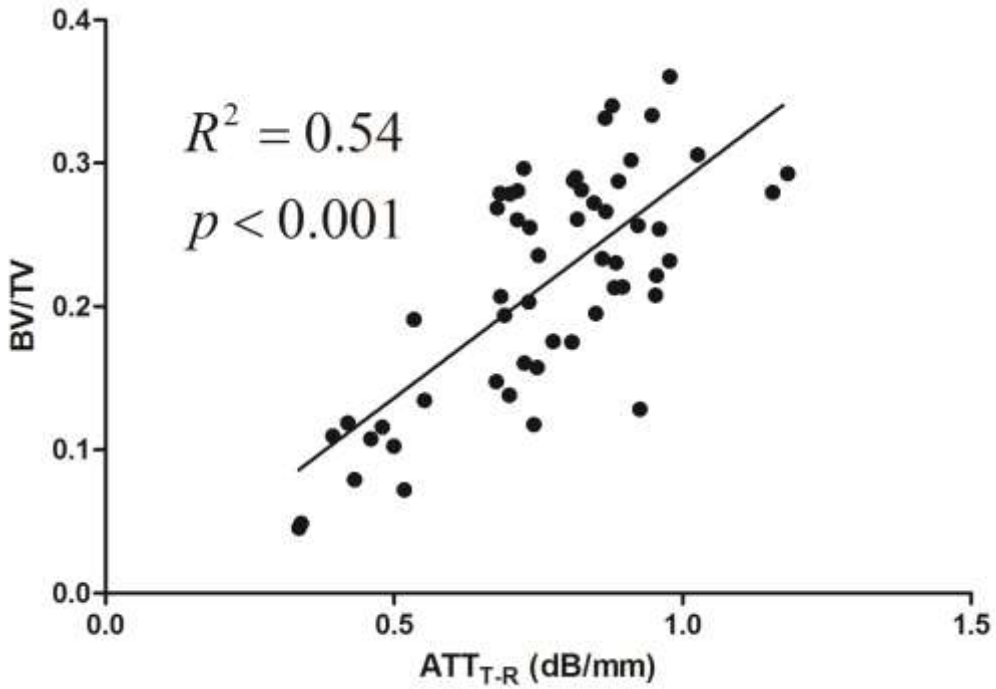


(b)

Figure 23 - Linear correlations between ultrasound attenuation (ATT) and bone volume fraction (BV/TV) using (a) traditional QUS ($ATT_{M-L}$) in medial-lateral orientation and (b) combined transmission-reflection QUS ($ATT_{T-R}$) in the frontal plane. Correlation of $ATT_{T-R}$ vs. BV/TV ($R^2$ = 0.54) is significantly higher than $ATT_{M-L}$ vs. BV/TV ($R^2$ = 0.44), $p<0.05$.

In conclusion, reflection mode QUS scanning can accurately measure the sample thickness in different scanning orientations; such sample thickness can be used to normalize the transmission mode QUS data, thus to determine the peak normalized QUS parameters. The normalized QUS values demonstrate significantly improved correlations with structural and mechanical properties of human calcaneus, when compared to the QUS values obtained from current QUS measurement protocol. This improvement indicates that better prediction for bone strength and fracture risk can be achieved by applying this combined transmission-reflection QUS measurement in proper clinical environment; it also pushes QUS one step further towards a more reliable and accurate imaging tool to replace DXA as the general standard for bone health status assessment.

# 7 Summary and discussion

Osteoporosis is a major public health threat for America, affecting eighteen million Americans and generating a financial burden of eighteen billion annually. Osteoporosis is usually characterized by a decrease in bone density and strength, which leads to high susceptibility of fracture. Therefore, early diagnosis of osteopenia or osteoporosis can result in timely treatment and intervention to avoid unnecessary financial lost and further complication in bone health status.

Currently gold standard of diagnosis for osteoporosis is dual-energy x-ray absorptiometry, namely DXA. By determining the amount of radiation energy absorption by different tissue, either soft tissue or bone, DXA can be used to measure the bone mineral density of the patient; and it is the most widely used technique to quantify bone content or bone density. Despite its widespread use, DXA has some inconvenient disadvantages, such as its immobility. The relatively big size of DXA makes it impossible to be used as a portal device in small clinics and increase the difficulty of operation. Secondly, DXA is too expensive to be used as a home screening tool for bone health status. Furthermore, DXA is intrinsically radioactive and therefore inconvenient for some application, such as bone health monitoring for astronauts in space-flight mission.

In light of the shortcomings of DXA, researchers have been looking for alternatives; and quantitative ultrasound is a very ideal candidate, because it is cheap, easy to operate, portable and non-radioactive. It has been 30 years since it was introduced to bone imaging field and has been widely used to monitor bone health status. Commercial QUS devices have been made available to assess the bone quality in hospitals and clinics. Over the past years, many researchers have been improving quantitative ultrasound technology to improve its accuracy to predict bone strength and fracture risk. With the current technology, it is estimated that nearly 80% of the variation of QUS parameters can be explained by bone quantity with an additional 8-17% contributed by bone architectural parameters.

According to the “Wolff’s Law”, as a living, vital and dynamic connective tissue, the structure and composition of bone is a product of adaptation to the mechanical loading

environment. The porosity of cortical bone ranges only 5-20%, while the porosity of trabecular bone ranges from 40% to 95%. Trabecular bone is usually found in the inner parts of bones. It looks like a porous sponge with a 3-dimensional network of rod- and plate-shape trabeculae surrounding an interconnected pore space filled with bone marrow. The most influential determinants of the material properties of trabecular bone are considered apparent density and the microstructural arrangement of the trabecular network. Besides the obvious influence of bone density to bone strength, researchers have also demonstrated that the alignment of trabecular structure can significantly affect the bone quality.

Many researchers have been investigating extensively on the interaction between ultrasound wave propagation and the anisotropic structure of trabecular bone and have clear evidence that ultrasound wave is sensitive to the structural alignment of trabecular bone. This gave rise to the possibility of including the microarchitecture information of trabecular bone in the ultrasound measurement to improve its accuracy. Given this challenge, the first problem we need to tackle is how to use ultrasound to measure the principal structural alignment, which is closely related to the anisotropic mechanical properties of trabecular bone.

The results shown in Chapter 3 gave a very clear answer to this question: ultrasound can be used to predict the principal structural orientation of trabecular bone. When compared to the current gold standard of measuring anisotropy, mean intercept length tensor calculated by μCT, the principal structural orientations predicted by ultrasound attenuation and velocity are very close, with about 5 ° difference between the PSO predicted by ultrasound velocity and mCT, and about 10° difference between the PSO predicted by ultrasound attenuation. This prediction is in agreement with the previous findings that the velocity of fast wave was shown to have a higher correlation with the MIL tensor than the ultrasound attenuation. This work not only proved the ability of QUS to predict the principal structural orientation of trabecular bone, but also provided a theoretical and technical foundation to the next stages of the study – to improve the accuracy of QUS by considering the microstructure of trabecular bone.

Although the result from this first stage of the study is promising, questions still remained to be answered: does trabecular bone has the highest mechanical strength in the PSO predicted by ultrasound? How different is the mechanical strength in such PSO from other orientations? Is

the angle difference between the PSO predicted by ultrasound and the longest vector of MIL tensor significant? To answer these questions, we performed the finite element analysis on a bone ball model in the second specific aim of the study, which is described in Chapter 4.

The finite element bone ball model used Chapter 4 made it feasible to evaluate the mechanical properties of the same structure in different orientations, including the PSOs predicted by QUS, longest vector of MIL tensor and 3 anatomical orientations. It is concluded from the results that the stiffness in the PSOs predicted by QUS are very close to the value in the MIL orientation, with no significant differences, while significantly higher than the stiffness in the anatomical orientations. These results suggested that although the PSOs predicted by QUS and μCT have certain angle differences, the mechanical properties measured in these PSOs are of the same level, having no significant differences.

At this point, the results from the first two aims showed a QUS method of predicting the principal structure orientation of trabecular bone in which the bone structure has the highest mechanical strength. It was hypothesized that ultrasound measurement in such orientation can improve the prediction of mechanical properties of trabecular bone, comparing to the conventional QUS measurement. The most popular anatomical location of QUS measurement is calcaneus, because of its richness of trabecular bone and relatively simple and parallel geometry. And traditionally, QUS measurement for human calcaneus is performed in the medial-lateral orientation.

To progress from an ideal bone ball model to a more realistic model, an interim trabecular bone cube model was introduced in Chapter 5 as a foundation to build the novel QUS measurement for whole calcaneus on. Reflection mode was first introduced to this study in this chapter. It was used to measure the different sample thickness in different QUS scanning orientations. It was shown in Chapter 5 that the combined transmission-reflection mode QUS measurement was able to translate the rotational measurement for spherical model to the more realistic bone cube model and improved the correlations between QUS parameters and mechanical properties, comparing to the traditional QUS measurement in medial-lateral orientations.

This novel combined transmission-reflection mode QUS measurement includes two stages of measurement: 1) use transmission and reflection modes of QUS to determine the principal structural orientation within a confined scanning angle range, 2) correlate the QUS parameters in that principal orientation with the mechanical and structural parameters obtained from mechanical test and μCT. Thorough evaluations were also performed to compare the measurements in the frontal and transverse planes. As expected, the QUS measurement in the frontal plane had better improvement than measurement in the transverse plane, whereas measurements in both planes showed improvement to the traditional measurement. This comparison further validated the rational of such combined mode measurement, because compared to transverse plane, trabecular structure in frontal plane is more aligned to the weight bearing orientation and has more variation in architecture induced by the mechanical loading condition.

With the significantly improved correlations between QUS and structural and mechanical properties, the next logical step would be to apply this measurement to a furthermore realistic model – whole human calcaneus. This stage of the study is considered the final step of validating the efficacy of such measurement technique before it could be applied to *in vivo* condition. By achieving the same improvement in correlations with mechanical and structural properties as shown in Chapter 6, it was concluded that such combined QUS measurement can be applied to critical anatomical sites, such as calcaneus, to better predict the mechanical strength and fracture risk than the conventional QUS measurement.

# 8 Clinical relevance and significance

This dissertation showcased a combined transmission-reflection mode ultrasonic measurement to improve the prediction for the mechanical and structural properties of trabecular bone by performing the ultrasound scanning in the principal structural orientation. This method is easy to incorporate to the current QUS measurement devices: an angular array ultrasound transducer could be employed to the measurement system to shorten the measuring time covering a wide angle range. Such addition to the current QUS system requires minimal technical upgrade or designing reconfiguration and could fit most of the available commercial QUS devices in the clinical market. Given the opportunity of large population clinical study, this combined transmission-reflection mode QUS measurement designed in this dissertation can be beneficial to millions of patients and senior people at risk of osteoporosis with more reliable and accurate measurement of bone strength and prediction of fracture risk.

# 9 List of references


AARON, J. E., SHORE, P. A., SHORE, R. C., BENETON, M. & KANIS, J. A. 2000. Trabecular architecture in women and men of similar bone mass with and without vertebral fracture: II. Three-dimensional histology. *Bone,* 27**,** 277-82.

ASHMAN, R. B., CORIN, J. D. & TURNER, C. H. 1987. Elastic properties of cancellous bone: measurement by an ultrasonic technique. *Journal of Biomechanics,* 20**,** 979-86.

ASHMAN, R. B. & RHO, J. Y. 1988. Elastic modulus of trabecular bone material. *J Biomech,* 21**,** 177-81.

BAUER, D. C., GLUER, C. C., CAULEY, J. A., VOGT, T. M., ENSRUD, K. E., GENANT, H. K. & BLACK, D. M. 1997. Broadband ultrasound attenuation predicts fractures strongly and independently of densitometry in older women. A prospective study. Study of Osteoporotic Fractures Research Group. *Arch Intern Med,* 157**,** 629-34.

BEVILL, G., ESWARAN, S. K., GUPTA, A., PAPADOPOULOS, P. & KEAVENY, T. M. 2006. Influence of bone volume fraction and architecture on computed large-deformation failure mechanisms in human trabecular bone. *Bone,* 39**,** 1218-1225.

BIEWENER, A. A., FAZZALARI, N. L., KONIECZYNSKI, D. D. & BAUDINETTE, R. V. 1996. Adaptive changes in trabecular architecture in relation to functional strain patterns and disuse. *Bone,* 19**,** 1-8.

BIOT, M. A. 1956a. Theory of Propagation of Elastic Waves in a Fluid-Saturated Porous Solid. I. Low-Frequency Range. *The Journal of the Acoustical Society of America,* 28**,** 168-178.

BIOT, M. A. 1956b. Theory of Propagation of Elastic Waves in a Fluid-Saturated Porous Solid. II. Higher Frequency Range. *The Journal of the Acoustical Society of America,* 28**,** 179-191.

BOUXSEIN, M. L. & RADLOFF, S. E. 1997. Quantitative ultrasound of the calcaneus reflects the mechanical properties of calcaneal trabecular bone. *Journal of bone and mineral research : the official journal of the American Society for Bone and Mineral Research,* 12**,** 839-46.

BURGHARDT, A. J., LINK, T. M. & MAJUMDAR, S. 2011. High-resolution computed tomography for clinical imaging of bone microarchitecture. *Clinical Orthopaedics and Related Research,* 469**,** 2179-93.

BURR, D. B., MILGROM, C., FYHRIE, D., FORWOOD, M., NYSKA, M., FINESTONE, A., HOSHAW, S., SAIAG, E. & SIMKIN, A. 1996. In vivo measurement of human tibial strains during vigorous activity. *Bone,* 18**,** 405-10.

BURR, D. B., TURNER, C. H., NAICK, P., FORWOOD, M. R., AMBROSIUS, W., HASAN, M. S. & PIDAPARTI, R. 1998. Does microdamage accumulation affect the mechanical properties of bone? *J Biomech,* 31**,** 337-45.

CARDOSO, L. & COWIN, S. C. 2011. Fabric dependence of quasi-waves in anisotropic porous media. *Journal of the Acoustical Society of America,* 129**,** 3302-16.

CARDOSO, L. & COWIN, S. C. 2012. Role of structural anisotropy of biological tissues in poroelastic wave propagation. *Mechanics of Materials,* 44**,** 174-188.

CARDOSO, L., TEBOUL, F., SEDEL, L., ODDOU, C. & MEUNIER, A. 2003. In vitro acoustic waves propagation in human and bovine cancellous bone. *Journal of Bone and Mineral Research,* 18**,** 1803-12.

CHIN, K. Y. & IMA-NIRWANA, S. 2013. Calcaneal quantitative ultrasound as a determinant of bone health status: what properties of bone does it reflect? *International journal of medical sciences,* 10**,** 1778-83.

CIARELLI, T. E., FYHRIE, D. P., SCHAFFLER, M. B. & GOLDSTEIN, S. A. 2000. Variations in three-dimensional cancellous bone architecture of the proximal femur in female hip fractures and in controls. *Journal of bone and mineral research : the official journal of the American Society for Bone and Mineral Research,* 15**,** 32-40.

CODY, D. D., GROSS, G. J., J. HOU, F., SPENCER, H. J., GOLDSTEIN, S. A. & P. FYHRIE, D. 1999. Femoral strength is better predicted by finite element models than QCT and DXA. *Journal of Biomechanics,* 32**,** 1013-1020.

CORTET, B., BOUTRY, N., DUBOIS, P., LEGROUX-GEROT, I., COTTEN, A. & MARCHANDISE, X. 2004. Does quantitative ultrasound of bone reflect more bone mineral density than bone microarchitecture? *Calcified Tissue International,* 74**,** 60-7.

COWIN, S. C. & CARDOSO, L. 2011. Fabric dependence of wave propagation in anisotropic porous media. *Biomechanics and Modeling in Mechanobiology,* 10**,** 39-65.

DROZDZOWSKA, B. & PLUSKIEWICZ, W. 2002. The ability of quantitative ultrasound at the calcaneus to identify postmenopausal women with different types of nontraumatic fractures. *Ultrasound in medicine & biology,* 28**,** 1491-7.

ESWARAN, S. K., FIELDS, A. J., NAGARATHNAM, P. & KEAVENY, T. M. 2009. Multi-scale modeling of the human vertebral body: comparison of micro-CT based high-resolution and continuum-level models. *Pacific Symposium on Biocomputing. Pacific Symposium on Biocomputing***,** 293-303.

FLOTER, M., BITTAR, C. K., ZABEU, J. L. & CARNEIRO, A. C. 2011. Review of comparative studies between bone densitometry and quantitative ultrasound of the calcaneus in osteoporosis. *Acta reumatologica portuguesa,* 36**,** 327-35.

FOUNDATION, N. O. 2010. Fast facts on osteoporosis. *In:* FOUNDATION, N. O. (ed.).

GEFEN, A. & SELIKTAR, R. 2004. Comparison of the trabecular architecture and the isostatic stress flow in the human calcaneus. *Med Eng Phys,* 26**,** 119-29.

GLUER, C. C. 1997. Quantitative ultrasound techniques for the assessment of osteoporosis: expert agreement on current status. The International Quantitative Ultrasound Consensus Group. *Journal of Bone and Mineral Research,* 12**,** 1280-8.

GRIMM, M. J. & WILLIAMS, J. L. 1997. Assessment of bone quantity and 'quality' by ultrasound attenuation and velocity in the heel. *Clin Biomech (Bristol, Avon),* 12**,** 281-285.

HADJI, P., HARS, O., GORKE, K., EMONS, G. & SCHULZ, K. D. 2000. Quantitative ultrasound of the os calcis in postmenopausal women with spine and hip fracture. *Journal of clinical densitometry : the official journal of the International Society for Clinical Densitometry,* 3**,** 233-9.

HA ÏAT, G., PADILLA, F., PEYRIN, F. & LAUGIER, P. 2008. Fast wave ultrasonic propagation in trabecular bone: Numerical study of the influence of porosity and structural anisotropy. *The Journal of the Acoustical Society of America,* 123**,** 1694.

HAIAT, G., SASSO, M., NAILI, S. & MATSUKAWA, M. 2008. Ultrasonic velocity dispersion in bovine cortical bone: an experimental study. *J Acoust Soc Am,* 124**,** 1811-21.

HAKULINEN, M. A., DAY, J. S., TOYRAS, J., TIMONEN, M., KROGER, H., WEINANS, H., KIVIRANTA, I. & JURVELIN, J. S. 2005. Prediction of density and mechanical properties of human trabecular bone in vitro by using ultrasound transmission and

backscattering measurements at 0.2-6.7 MHz frequency range. *Physics in Medicine and Biology,* 50**,** 1629-42.
HAN, S., MEDIGE, J., DAVIS, J., FISHKIN, Z., MIHALKO, W. & ZIV, I. 1997. Ultrasound velocity and broadband attenuation as predictors of load-bearing capacities of human calcanei. *Calcified Tissue International,* 60**,** 21-5.
HAN, S. M. & RHO, J. Y. 1998. Dependence of broadband ultrasound attenuation on the elastic anisotropy of trabecular bone. *Proceedings of the Institution of Mechanical Engineers. Part H, Journal of Engineering in Medicine,* 212**,** 223-7.
HEALTH, N. I. O. 2007. Osteoporosis: Handout on health. *Retrieved February,* 17**,** 2009.
HOSOKAWA, A. 2006. Ultrasonic pulse waves in cancellous bone analyzed by finite-difference time-domain methods. *Ultrasonics,* 44 Suppl 1**,** e227-31.
HOSOKAWA, A. 2009a. Effect of minor trabecular elements on fast and slow wave propagations through a stratified cancellous bone phantom at oblique incidence. *Jpn J Appl Phys,* 48**,** 07GK07-07GK07-7.
HOSOKAWA, A. 2009b. Numerical analysis of variability in ultrasound propagation properties induced by trabecular microstructure in cancellous bone. *IEEE transactions on ultrasonics, ferroelectrics, and frequency control,* 56**,** 738-47.
HOSOKAWA, A. 2010. Effect of porosity distribution in the propagation direction on ultrasound waves through cancellous bone. *IEEE transactions on ultrasonics, ferroelectrics, and frequency control,* 57**,** 1320-8.
HOSOKAWA, A. 2011a. Numerical investigation of ultrasound refraction caused by oblique orientation of trabecular network in cancellous bone. *IEEE Trans Ultrason Ferroelectr Freq Control,* 58**,** 1389-96.
HOSOKAWA, A. 2011b. Numerical investigation of ultrasound refraction caused by oblique orientation of trabecular network in cancellous bone. *IEEE Transactions on Ultrasonics, Ferroelectrics, and Frequency Control,* 58**,** 1389-96.
HOSOKAWA, A. & OTANI, T. 1997. Ultrasonic wave propagation in bovine cancellous bone. *The Journal of the Acoustical Society of America,* 101**,** 558-62.
HOSOKAWA, A. & OTANI, T. 1998. Acoustic anisotropy in bovine cancellous bone. *The Journal of the Acoustical Society of America,* 103**,** 2718-22.
HUOPIO, J., KROGER, H., HONKANEN, R., JURVELIN, J., SAARIKOSKI, S. & ALHAVA, E. 2004. Calcaneal ultrasound predicts early postmenopausal fractures as well as axial BMD. A prospective study of 422 women. *Osteoporosis international : a journal established as result of cooperation between the European Foundation for Osteoporosis and the National Osteoporosis Foundation of the USA,* 15**,** 190-5.
ISAKSSON, H., NAGAO, S., MAŁKIEWICZ, M., JULKUNEN, P., NOWAK, R. & JURVELIN, J. S. 2010. Precision of nanoindentation protocols for measurement of viscoelasticity in cortical and trabecular bone. *Journal of Biomechanics,* 43**,** 2410-2417.
KANIS, J. A., BORGSTROM, F., DE LAET, C., JOHANSSON, H., JOHNELL, O., JONSSON, B., ODEN, A., ZETHRAEUS, N., PFLEGER, B. & KHALTAEV, N. 2005. Assessment of fracture risk. *Osteoporosis International,* 16**,** 581-589.
KAUFMAN, J. J., LUO, G. & SIFFERT, R. S. 2007. A portable real-time ultrasonic bone densitometer. *Ultrasound in Medicine & Biology,* 33**,** 1445-52.
KEAVENY, T. M. 2010. Biomechanical computed tomography—noninvasive bone strength analysis using clinical computed tomography scans. *Annals of the New York Academy of Sciences,* 1192**,** 57-65.

KILAPPA, V., MOILANEN, P., XU, L., NICHOLSON, P. H., TIMONEN, J. & CHENG, S. 2010. Low-frequency axial ultrasound velocity correlates with bone mineral density and cortical thickness in the radius and tibia in pre- and postmenopausal women. *Osteoporos Int*.

KIM, D.-G., HUNT, C., ZAUEL, R., FYHRIE, D. & YENI, Y. 2007. The Effect of Regional Variations of the Trabecular Bone Properties on the Compressive Strength of Human Vertebral Bodies. *Annals of Biomedical Engineering,* 35**,** 1907-1913.

KOLSKY, H. 1963. *Stress waves in solids,* New York,, Dover Publications.

KRUG, R., BURGHARDT, A. J., MAJUMDAR, S. & LINK, T. M. 2010. High-resolution imaging techniques for the assessment of osteoporosis. *Radiologic clinics of North America,* 48**,** 601-21.

LANGTON, C. M., ALI, A. V., RIGGS, C. M., EVANS, G. P. & BONFIELD, W. 1990. A contact method for the assessment of ultrasonic velocity and broadband attenuation in cortical and cancellous bone. *Clin Phys Physiol Meas,* 11**,** 243-9.

LANGTON, C. M., NJEH, C. F., HODGSKINSON, R. & CURREY, J. D. 1996. Prediction of mechanical properties of the human calcaneus by broadband ultrasonic attenuation. *Bone,* 18**,** 495-503.

LANGTON, C. M., PALMER, S. B. & PORTER, R. W. 1984. The measurement of broadband ultrasonic attenuation in cancellous bone. *Engineering in Medicine,* 13**,** 89-91.

LAUGIER, P. 2006. Quantitative ultrasound of bone: looking ahead. *Joint Bone Spine,* 73**,** 125-128.

LAUGIER, P., DROIN, P., LAVAL-JEANTET, A. M. & BERGER, G. 1997. In vitro assessment of the relationship between acoustic properties and bone mass density of the calcaneus by comparison of ultrasound parametric imaging and quantitative computed tomography. *Bone,* 20**,** 157-65.

LAUGIER, P. & HAḶAT, G. 2011. *Bone Quantitative Ultrasound,* Springer Science+Business media B.V.

LEE, K. I., HUGHES, E. R., HUMPHREY, V. F., LEIGHTON, T. G. & CHOI, M. J. 2007. Empirical angle-dependent Biot and MBA models for acoustic anisotropy in cancellous bone. *Physics in Medicine and Biology,* 52**,** 59-73.

LEGRAND, E., CHAPPARD, D., PASCARETTI, C., DUQUENNE, M., KREBS, S., ROHMER, V., BASLE, M. F. & AUDRAN, M. 2000. Trabecular bone microarchitecture, bone mineral density, and vertebral fractures in male osteoporosis. *Journal of bone and mineral research : the official journal of the American Society for Bone and Mineral Research,* 15**,** 13-9.

LIN, L., CHENG, J., LIN, W. & QIN, Y. X. 2012. Prediction of trabecular bone principal structural orientation using quantitative ultrasound scanning. *Journal of Biomechanics,* 45**,** 1790-5.

LIN, L., OON, H., LIN, W. & QIN, Y.-X. 2014. Principal trabecular structural orientation predicted by quantitative ultrasound is strongly correlated with \upmu FEA determined anisotropic apparent stiffness. *Biomechanics and modeling in mechanobiology***,** 1-11.

LIN, W., MITTRA, E. & QIN, Y. X. 2006. Determination of ultrasound phase velocity in trabecular bone using time dependent phase tracking technique. *Journal of Biomechanical Engineering,* 128**,** 24-9.

LIN, W., XIA, Y. & QIN, Y. X. 2009. Characterization of the trabecular bone structure using frequency modulated ultrasound pulse. *J Acoust Soc Am,* 125**,** 4071-7.

LINK, T. M. 2012. Osteoporosis imaging: state of the art and advanced imaging. *Radiology,* 263**,** 3-17.

LINK, T. M., LOTTER, A., BEYER, F., CHRISTIANSEN, S., NEWITT, D., LU, Y., SCHMID, C. & MAJUMDAR, S. 2000. Changes in calcaneal trabecular bone structure after heart transplantation: an MR imaging study. *Radiology,* 217**,** 855-62.

LIU, C., TA, D., FUJITA, F., HACHIKEN, T., MATSUKAWA, M., MIZUNO, K. & WANG, W. 2014. The relationship between ultrasonic backscatter and trabecular anisotropic microstructure in cancellous bone. *Journal of Applied Physics,* 115**,** -.

LIU, X. S., BEVILL, G., KEAVENY, T. M., SAJDA, P. & GUO, X. E. 2009. Micromechanical analyses of vertebral trabecular bone based on individual trabeculae segmentation of plates and rods. *Journal of Biomechanics,* 42**,** 249-256.

MARCUS, R., FELDMAN, D., NELSON, D. A. & ROSEN, C. J. 2009. *Fundamentals of Osteoporosis,* Academic Press.

MARTIN, R. B., BURR, D. B. & SHARKEY, N. A. 1998. *Skeletal tissue mechanics,* New York, Springer.

MARTINI, F. H. & OBER, W. C. 2006. *Fundamentals of Anatomy & Physiology,* Pearson Benjamin Cummings.

MITTRA, E., RUBIN, C., GRUBER, B. & QIN, Y. X. 2008. Evaluation of trabecular mechanical and microstructural properties in human calcaneal bone of advanced age using mechanical testing, microCT, and DXA. *J Biomech,* 41**,** 368-75.

MIZUNO, K., MATSUKAWA, M., OTANI, T., LAUGIER, P. & PADILLA, F. 2009. Propagation of two longitudinal waves in human cancellous bone: an in vitro study. *The Journal of the Acoustical Society of America,* 125**,** 3460-6.

MIZUNO, K., MATSUKAWA, M., OTANI, T., TAKADA, M., MANO, I. & TSUJIMOTO, T. 2008. Effects of structural anisotropy of cancellous bone on speed of ultrasonic fast waves in the bovine femur. *IEEE Transactions on Ultrasonics, Ferroelectrics, and Frequency Control,* 55**,** 1480-7.

MIZUNO, K., SOMIYA, H., KUBO, T., MATSUKAWA, M., OTANI, T. & TSUJIMOTO, T. 2010. Influence of cancellous bone microstructure on two ultrasonic wave propagations in bovine femur: an in vitro study. *The Journal of the Acoustical Society of America,* 128**,** 3181-9.

NICHOLSON, P. F. 2008. Ultrasound and the biomechanical competence of bone. *IEEE Trans Ultrason Ferroelectr Freq Control,* 55**,** 1539-45.

NICHOLSON, P. H., HADDAWAY, M. J. & DAVIE, M. W. 1994. The dependence of ultrasonic properties on orientation in human vertebral bone. *Physics in medicine and biology,* 39**,** 1013-24.

NICHOLSON, P. H., MULLER, R., CHENG, X. G., RUEGSEGGER, P., VAN DER PERRE, G., DEQUEKER, J. & BOONEN, S. 2001. Quantitative ultrasound and trabecular architecture in the human calcaneus. *Journal of bone and mineral research : the official journal of the American Society for Bone and Mineral Research,* 16**,** 1886-92.

NIH 2000. Osteoporosis prevention, diagnosis, and therapy. *NIH consensus statement,* 17**,** 1-45.

NJEH, C., HANS, D., FUERST, T., GLÜER, C. & GENANT, H. 1999. *Quantitative Ultrasound: Assessment of Osteoporosis and Bone Status,* London, UK, Martin Dunitz.

NJEH, C. F., BOIVIN, C. M. & LANGTON, C. M. 1997. The role of ultrasound in the assessment of osteoporosis: a review. *Osteoporosis International,* 7**,** 7-22.

NJEH, C. F. & LANGTON, C. M. 1997. The effect of cortical endplates on ultrasound velocity through the calcaneus: an in vitro study. *Br J Radiol,* 70**,** 504-10.

PIDAPARTI, R. M. & TURNER, C. H. 1997. Cancellous bone architecture: advantages of nonorthogonal trabecular alignment under multidirectional joint loading. *J Biomech,* 30**,** 979-83.

QIN, Y.-X., XIA, Y., LIN, W., MITTRA, E., RUBIN, C. & GRUBER, B. 2007. Noninvasive Ultrasound Imaging for Bone Quality Assessment Using Scanning Confocal Acoustic Diagnosis, μCT, DXA Measurements, and Mechanical Testing. *In:* ZHANG, D. (ed.) *Medical Biometrics.* Springer Berlin / Heidelberg.

RUBIN, C. T. & LANYON, L. E. 1984. Dynamic strain similarity in vertebrates; an alternative to allometric limb bone scaling. *Journal of theoretical biology,* 107**,** 321-7.

SERRA-HSU, F., CHENG, J., LYNCH, T. & QIN, Y. X. 2011. Evaluation of a pulsed phase-locked loop system for noninvasive tracking of bone deformation under loading with finite element and strain analysis. *Physiological measurement,* 32**,** 1301-13.

SILVA, M. J. & GIBSON, L. J. 1997. Modeling the mechanical behavior of vertebral trabecular bone: effects of age-related changes in microstructure. *Bone,* 21**,** 191-9.

TABOR, Z. 2011. Equivalence of mean intercept length and gradient fabric tensors – 3d study. *Medical Engineering & Physics*.

TOMMASINI, S. M., TRINWARD, A., ACERBO, A. S., DE CARLO, F., MILLER, L. M. & JUDEX, S. 2012. Changes in intracortical microporosities induced by pharmaceutical treatment of osteoporosis as detected by high resolution micro-CT. *Bone,* 50**,** 596-604.

TOYRAS, J., NIEMINEN, M. T., KROGER, H. & JURVELIN, J. S. 2002. Bone mineral density, ultrasound velocity, and broadband attenuation predict mechanical properties of trabecular bone differently. *Bone,* 31**,** 503-7.

UNITS, I. C. O. R. & BETHESDA, M. 2009. Quantitative Aspects of Bone Densitometry.

WALD, M. J., MAGLAND, J. F., RAJAPAKSE, C. S., BHAGAT, Y. A. & WEHRLI, F. W. 2011. Predicting trabecular bone elastic properties from measures of bone volume fraction and fabric on the basis of micromagnetic resonance images. *Magnetic Resonance in Medicine***,** n/a-n/a.

WHITEHOUSE, W. J. 1974. The quantitative morphology of anisotropic trabecular bone. *Journal of Microscopy,* 101**,** 153-68.

WIRTZ, D. C., SCHIFFERS, N., PANDORF, T., RADERMACHER, K., WEICHERT, D. & FORST, R. 2000. Critical evaluation of known bone material properties to realize anisotropic FE-simulation of the proximal femur. *Journal of biomechanics,* 33**,** 1325-1330.

WOLFF, J. 1896. *The Law of Bone Remodeling,* Berlin Heidelberg New York, Springer.

XIA, Y., LIN, W. & QIN, Y. X. 2005. The influence of cortical end-plate on broadband ultrasound attenuation measurements at the human calcaneus using scanning confocal ultrasound. *Journal of the Acoustical Society of America,* 118**,** 1801-1807.

XIA, Y., LIN, W. & QIN, Y. X. 2007. Bone surface topology mapping and its role in trabecular bone quality assessment using scanning confocal ultrasound. *Osteoporosis International,* 18**,** 905-13.

YAMAMOTO, T., OTANI, T., HAGINO, H., KATAGIRI, H., OKANO, T., MANO, I. & TESHIMA, R. 2009. Measurement of human trabecular bone by novel ultrasonic bone densitometry based on fast and slow waves. *Osteoporosis International,* 20**,** 1215-24.

YENI, Y. N., ZELMAN, E. A., DIVINE, G. W., KIM, D.-G. & FYHRIE, D. P. 2008. Trabecular shear stress amplification and variability in human vertebral cancellous bone: Relationship with age, gender, spine level and trabecular architecture. *Bone,* 42**,** 591-596.

ZHENG, R., LE, L. H., SACCHI, M. D. & LOU, E. 2009. Broadband ultrasound attenuation measurement of long bone using peak frequency of the echoes. *IEEE Trans Ultrason Ferroelectr Freq Control,* 56**,** 396-9.

ZHENG, R., LE, L. H., SACCHI, M. D., TA, D. & LOU, E. 2007. Spectral ratio method to estimate broadband ultrasound attenuation of cortical bones in vitro using multiple reflections. *Phys Med Biol,* 52**,** 5855-69.

## 10 List of Abbreviations, Symbols, and their Definitions

| Abbr./ Symbol | Definition | Unit |
|---|---|---|
| *Ultrasound* | | |
| QUS | Quantitative ultrasound | |
| SCAD | Scanning confocal acoustic diagnostic system | |
| ATT | Ultrasound attenuation | dB |
| UV | Ultrasound velocity | m/s |
| BUA | Broadband ultrasound attenuation | dB/MHz |
| $ATT_{max}$ | Principal structural orientation predicted by ultrasound attenuation | |
| $UV_{max}$ | Principal structural orientation predicted by ultrasound velocity | |
| $ATT_{T-R}$ | Ultrasound attenuation measured by transmission-reflection combined method | dB/mm |
| $UV_{T-R}$ | Ultrasound velocity measured by transmission-reflection combined method | m/s |
| $ATT_{M-L}$ | Ultrasound attenuation in the medial-lateral orientation | dB/mm |
| $UV_{M-L}$ | Ultrasound velocity in the medial-lateral orientation | m/s |
| *Structural* | | |
| BV/TV | Bone volume fraction | % |
| SMI | Structural model index | |
| BS/BV | Bone surface density | 1/mm |
| Tb.N | Trabecular bone number | |
| Tb.Th | Trabecular thickness | mm |
| Tb.Sp | Trabecular spacing | mm |
| DA | Degree of anisotropy | |
| MIL | Mean intercept length | |
| *Mechanical* | | |
| Modulus | Young's modulus, the geometrically normalized stiffness. Usually calculated as the slope of the linear region of the stress/strain curve | Pa |
| *General* | | |
| BMD | Bone mineral density | $g/cm^2$ |
| DXA | Dual-energy X-ray absorptiometry | |
| μCT | Micro computed tomography | |
| R | Pearson product-moment correlation coefficient | |
| SD | Standard deviation | |
| FEA | Finite element analysis | |